The Evolution of Cosmological Density Fluctuations

by

Bhuvnesh Jain

Submitted to the Department of Physics
in partial fulfillment of the requirements for the degree of

Doctor of Philosophy

at the

MASSACHUSETTS INSTITUTE OF TECHNOLOGY

May 1994

Author .....Science.....
Department of Physics
May 13, 1994

Certified by .....
Edmund Bertschinger
Associate Professor
Thesis Supervisor

Certified by .....
Alan H. Guth
Professor
Thesis Supervisor

Accepted by .....
George F. Koster
Chairman, Departmental Committee on Graduate Students

The Evolution of Cosmological Density Fluctuations

by

Bhuvnesh Jain

Submitted to the Department of Physics
on May 13, 1994, in partial fulfillment of the
requirements for the degree of
Doctor of Philosophy

Abstract

We study two distinct aspects of the evolution of cosmological fluctuations. The first is the generation and evolution of quantum fluctuations in inflation with induced gravity. The spectrum of density perturbations, $\delta\rho/\rho$, is estimated in the extended inflationary model, in which the scalar curvature is coupled to a Brans-Dicke field. Through a conformal transformation and a redefinition of the Brans-Dicke field, the action of the theory is cast into a form with no coupling to the scalar curvature and a canonical kinetic term for the redefined field. Following Kolb, Salopek and Turner, we calculate $\delta\rho/\rho$ using the transformed action and the standard recipe developed for conventional inflation. The spectrum behaves as a positive power of the wavelength, a feature of relevance in building models to account for the observed large scale structure of the universe.

The second part of the thesis deals with the nonlinear evolution of density perturbations during the matter dominated era. In the weakly nonlinear regime we find that the dominant nonlinear contribution for realistic cosmological spectra is made by the coupling of long-wave modes and is well estimated by second order perturbation theory. For realistic spectra we find that due to the long-wave mode coupling, characteristic nonlinear masses are larger at higher redshifts than would be estimated using a linear extrapolation. For the cold dark matter model at $(1+z) = (20, 10, 5, 2)$ the nonlinear mass is about $(180, 8, 2.5, 1.6)$ times (respectively) larger than a linear extrapolation would indicate, if the condition rms $\delta\rho/\rho = 1$ is used to define the nonlinear scale. At high redshift the Press-Schechter mass distribution significantly underestimates the abundance of high-mass objects for the cold dark matter model. Finally, we investigate possible long-wave divergences in the evolution of scale free spectra, $P(k) \propto k^n$, using analytic techniques and N-body simulations. For $n < -1$, there are divergent terms in the evolution of the phases of the Fourier space density field. We give a kinematical interpretation of this divergence and demonstrate that the self-similar scaling of physically relevant measures of perturbation growth is preserved.

Thesis Supervisor: Edmund Bertschinger
Title: Associate Professor

Thesis Supervisor: Alan H. Guth
Title: Professor

Acknowledgments

It has been a pleasure and a privilege to have the guidance of Ed Bertschinger and Alan Guth for this thesis. The first part of the thesis was done in collaboration with Alan, though my association with him continued through all my research work. The extended, weekly meetings with him from my first months to the last have been one of my most fruitful experiences at MIT. Alan has also been a friend and mentor in every sense, and been unfailingly supportive through many difficult times. The major portion of this thesis is a collaborative effort with Ed Bertschinger. Most of what I have learned about research in large scale structure I owe to Ed. His energy and versatility have been a source of inspiration, and his personal concern and enthusiastic guidance of my work have been crucial at every stage.

I am grateful to Paul Schechter for useful comments on the thesis, persuasive advice through the years and for his entertaining company in the Common Room. My interest in theoretical physics and cosmology was initiated and shaped by Rajendra Popli, Richard Gott, Jim Peebles, Bharat Ratra and David Weinberg, with all of whom I have continued to have useful discussions. It is a pleasure to thank Simon White for his hospitality at the Institute of Astronomy and many stimulating discussions.

This thesis owes a lot to many others — I would especially like to thank: Priya who has made the years at MIT so special, for wonderful companionship and support at every stage; my parents and Bena for their constant support and encouragement over the years, in this and in every other venture I have undertaken; Shep Doeleman for the magic of imbuing Building 6 with warmth and humor, and for many memorable squash bruises; Chris Naylor for his help, concern and humor in handling all manner of problems and livening many a lunch hour; Mira, John Tsai and Ranga for their help and advice in the difficult first years at MIT; Janna for lessons in creative cosmology and timely reminders of life beyond Physics; Mark with whom I shared the long hours of the final month's writing, for pleasant company and for solving all my computer-related woes; Jim Frederic, Lam, Uros, Neal, John Blakeslee, Anand, Juliana, Chung-

Pei, Jim Gelb and Rosanne for entertaining company and unfailing support; Esko for enjoyable times while sharing an apartment, coffee breaks and Finnish licorice; Meenu for great company that livened many an evening, and for her thoughts on wave propagation; Sonit for sharing the ups and downs of the past year; Arunjot, Sowmya, Ranjan and Niranjan for their company and many culinary delights; and the Coffee Shop and its workers for cheap supplies and consistently jarring music which left me no choice but to get back to work.

This thesis is dedicated to my parents.

Contents

[1]Published in Phys. Rev. D **45**, 426 (1992)

[2]To be published in Ap. J., **431** (1994)

List of Figures

Chapter 1

Introduction

The first part of this thesis comprising Chapter 2 is a calculation of the density perturbation spectrum produced in the extended inflationary model. This work was done in collaboration with Alan Guth. The second part of the thesis comprising Chapters 3 and 4 is a study of the nonlinear evolution of density perturbations during the matter dominated era. This work was done in collaboration with Ed Bertschinger. In this Chapter I shall provide a brief introduction to both parts of the thesis. For details the reader is referred to the pedagogical review of inflation given by Blau & Guth (1987), and to Peebles (1980) for a review of theoretical approaches to large scale structure.

1.1 Fluctuations in Inflation

Inflation is a hypothetical period of rapid expansion of the universe in its very early history. It can arise quite naturally in Grand Unified Theories of particle physics at very high temperatures when the energy density of the universe is dominated by the potential energy density $[V(\phi)]$ of a scalar field ϕ. If $V(\phi)$ is constant, then the expansion scale factor $a(t)$ expands exponentially in time. This is known as de Sitter spacetime, and it provides the arena for calculating the detailed evolution of the inflationary universe.

One of the successes of inflationary cosmology is the generation of quantum fluc-

tuations which give rise to density fluctuations after the universe makes a transition to the radiation dominated, and subsequently, the matter dominated era. The predicted spectrum of density fluctuations is the scale-invariant spectrum in which the amplitude at horizon crossing is independent of scale. This spectrum has been popular in cosmology even before its origin was explained in the context of inflation. It is in approximate agreement with observations of the distribution of galaxies (after the spectrum at small scales is modified during the radiation dominated era), and with the microwave background fluctuations detected by the COBE satellite. In Chapter 2 we present a calculation of the density fluctuation spectrum in a recently proposed model of inflation known as extended inflation. This model is based on the Brans-Dicke theory of gravity. In extended inflation the scale factor expands as a power law in time, hence the background spacetime is no longer de Sitter. We find that the resulting density perturbation spectrum has slightly more power on large scales as compared to the scale-invariant spectrum. As a background to the calculation presented in Chapter 2 the standard calculation of the density fluctuation spectrum in inflation with de Sitter spacetime is qualitatively described here.

The goal of such a calculation is to compute the density perturbations in the post-inflationary era induced by the quantum fluctuations in ϕ which are generated during inflation on all scales within the event horizon. They rapidly cross outside the horizon due to the exponential expansion of space. After inflation when the horizon grows faster than the scale factor, these fluctuations enter the horizon as density perturbations. The scale invariance of the spectrum of standard inflation is related to the time-translation invariance of de Sitter spacetime: the physical size of the event horizon and the expansion rate are constant in time. Therefore scales which cross outside the horizon at different times do so under identical conditions, hence they have equal amplitude. Once outside the horizon causal processes cannot alter their growth, therefore when they enter the horizon after inflation they still have equal amplitude. This simple expectation is borne out by detailed calculations which are briefly outlined below.

The relevant wavelengths cross outside the horizon while the scalar field ϕ is still

very near the peak of the effective potential at $\phi = 0$, so during this period we can take $V(\phi) \approx V(0) =$ constant. The metric for the background de Sitter spacetime is then

$$ds^2 = -dt^2 + a(t)^2 d\vec{x}^2, \tag{1.1}$$

with $a(t) = e^{Ht}$, where H is a constant proportional to $\sqrt{V(\phi)}$. With this metric the classical equations of motion for $\phi(\vec{x}, t)$ can be obtained from its Lagrangian. Next ϕ is written as $\phi(\vec{x}, t) = \phi_0(t) + \delta\phi(\vec{x}, t)$, where $\delta\phi(\vec{x}, t)$ represents the quantum fluctuations in ϕ. With this substitution the following equation of motion for $\delta\phi(\vec{x}, t)$ is obtained:

$$\ddot{\delta\phi} + 3H\,\dot{\delta\phi} = e^{-2Ht}\,\nabla^2\delta\phi - \frac{\partial^2 V}{\partial\phi^2}(\phi_0)\,\delta\phi. \tag{1.2}$$

We proceed by observing that at very early times the term involving $V(\phi)$ on the right-hand side of equation (1.2) is negligible (since the first term on the right-hand side is exponentially large), so that ϕ can be approximated as a free, massless scalar field in de Sitter spacetime. For such a field the propagator is known, and can be used to estimate the root mean square fluctuations in ϕ, denoted by $\Delta\phi$. At late times on the other hand, the first term on the right-hand side becomes negligible, so $\delta\phi$ obeys the same equation as the homogeneous part $\phi_0(t)$. One of the two solutions to this differential equation is found to damp quickly, so the solution at large t is unique. In terms of this solution, $\delta\phi$ can be written as $\delta\phi(\vec{x}, t) \simeq \phi_0(t)\,\delta\tau(\vec{x})$, and to first order ϕ can be expressed as:

$$\phi(\vec{x}, t) \simeq \phi_0(t) - \dot{\phi}_0(t)\delta\tau(\vec{x}) \simeq \phi_0(t - \delta\tau(\vec{x})). \tag{1.3}$$

Hence at late times the effect of the fluctuations is to cause a position dependent time delay $\delta\tau(\vec{x})$ in the evolution of $\phi_0(t)$.

Thus one obtains the following simple physical picture of the generation of fluctuations. As $\phi(\vec{x}, t)$ approaches a minimum of $V(\phi)$, the energy density in the false vacuum gets converted into matter and radiation and provides the exit from the inflationary phase. The final expression in equation (1.3) indicates that different regions in

space follow the same history, but slightly offset in time due to the spatial dependence of $\delta\tau(\vec{x})$. Hence they exit the inflationary era at different times – this causes their temperatures at a given time early in the radiation dominated era to differ slightly, thus generating fluctuations in the post-inflationary epoch. These are calculated by introducing a new time variable t' which is the argument of ϕ in the final expression in equation (1.3). The perturbations are then recorded in the redefined metric which has t' as its time variable. By introducing the energy momentum tensor of a perfect fluid for the radiation dominated era the spectrum of the energy density perturbations is obtained in terms of $\delta\tau$. The latter is estimated by matching the early time expression for $\Delta\phi$ with the late time approximation of equation (1.3). The resulting spectrum depends on $H(\propto V(\phi))$, and therefore the parameters of the particle physics model, through $\Delta\phi$. The result for the rms density contrast smoothed on a given scale is $\delta\rho/\bar{\rho} \sim H^2/\dot{\phi}$, where the right-hand side is evaluated at the time that scale crossed outside the event horizon during inflation.

1.2 The Growth of Density Fluctuations

If the scale invariant spectrum were to remain unmodified on entering inside the horizon it would be of the form $P(k) \propto k$ for all k. This spectrum is scale invariant in the sense that the amplitude of the rms smoothed density contrast is independent of scale at the time of horizon crossing. The relation of the power spectrum at a given time to the spectrum of the rms $\delta\rho/\rho$ smoothed on the comoving length scale x at horizon crossing can be obtained by noting that $(\delta\rho/\rho)_x \sim a(t)x^{-1}$ for the scale invariant spectrum. Now consider a mode that enters the horizon in the radiation dominated era at time t_e, when its physical wavelength $\lambda = a(t_e)x = ct_e$. Since $a(t) \propto t^{1/2}$ during the radiation dominated era, $a(t_e) \propto x$. Hence it follows that at the time of horizon crossing, $(\delta\rho/\rho)_x \sim a(t_e)\,x^{-1}$ is independent of the length scale x.

The physical processes operating within the horizon in the radiation dominated era modify the spectrum at high k. Once a fluctuation scale enters the acoustic horizon during the radiation dominated era, it is acted on by processes that arise due to the

coupling of baryons to photons. The baryon-photon fluid oscillates like an acoustic wave due to radiation pressure, therefore fluctuations in this component cease to grow. Perturbations in non-relativistic dark matter also remain almost constant until the beginning of the matter dominated era due to the rapid expansion of the background. In addition, there are possible damping processes such as the Silk damping of adiabatic perturbations and neutrino free streaming which erase fluctuations on small scales. Hence the spectrum at small scales gets frozen or damped, while on scales outside the acoustic horizon it continues to grow.

Once the universe becomes matter dominated and recombination occurs, perturbations in the matter density grow as they are no longer coupled to photons and are Jeans unstable. The scales which enter the horizon during this epoch have remained virtually unaffected by the radiation dominated era. This causes the spectrum to retain the shape $P(k) \propto k$ on these large scales, while it approaches the asymptotic form $P(k) \propto k^{-3}$ on very small scales. The k^{-3} spectrum on small scales corresponds to density perturbations $(\delta\rho/\rho)_x$ which have equal amplitude as a function of scale at a given time. The scale that provides the transition between these asymptotic features is, to within an order of magnitude, the size of the horizon at matter-radiation equality, about $10(\Omega h^2)^{-1}$ Mpc for a Cold Dark Matter dominated universe (1 Mpc $\simeq 3 \times 10^{24}$ cm; h is the value of the Hubble parameter today in units of 100 km/s/Mpc). The detailed shape of the resulting post-recombination spectrum depends on assumptions made about the nature of dark matter. The basic features are evident in the power spectrum of the standard Cold Dark Matter (CDM) model (in which the matter density is taken to be dominated by pressureless, collisionless dark matter) studied in Chapter 3 and shown in Figure 3-1.

The CDM spectrum can be regarded as a model for the initial spectrum for the study of large scale structure in the universe. Since the mass density is taken to be dominated by collisionless dark matter, the dominant force responsible for the growth of perturbations is gravity. On scales sufficiently smaller than the horizon the Newtonian limit of general relativity is an adequate approximation for studying gravitational dynamics. Therefore the growth of density perturbations is well described by

Newtonian fluid equations in the expanding coordinates appropriate for cosmology.

At the time of recombination (redshift $z \simeq 1400$) the fluctuation amplitude on scales of interest to large scale structure (about 1–100 Mpc) is very small. Therefore at early times the growth of perturbations is accurately described by the linearized cosmological fluid equations which show that the fractional density contrast grows as $\delta\rho/\bar{\rho} \propto a(t)$. When the perturbation amplitude grows to be of order unity, nonlinear effects become significant and cause the perturbation to cease expanding and then to collapse. Such collapsed structures become the sites for the formation of galaxies, a process in which dissipative processes play an important role as well. Cosmological spectra like the CDM spectrum have increasing amounts of power on smaller length scales. Therefore the first scales to collapse are likely to be the smallest, and thereafter structure formation proceeds hierarchically on larger scales. This picture is a simplified version of the standard lore in large scale structure studies. It provides the context in which the work presented in Chapters 3 and 4 can be placed.

REFERENCES

Blau, S.K. & Guth, A.H. 1987, in 300 Years of Gravitation, eds. Hawking, S.W. & Israel, W. (Cambridge: Cambridge University Press)

Peebles, P. J. E. 1980, The Large-Scale Structure of the Universe, (Princeton: Princeton University Press)

Chapter 2

Density Fluctuations in Extended Inflation[1]

2.1 Introduction

Extended inflation is a new model of inflation, proposed by La and Steinhardt [1]. Its key feature is that the effective gravitational constant G varies with time due to the non-minimal coupling of a scalar field Φ to the scalar curvature R. As first proposed [1], it was based on the Brans-Dicke [2] theory of gravity, for which the action is given by [3]

$$S = \int d^4x\sqrt{-g}\left[-\frac{R}{16\pi}\Phi + \frac{\omega}{16\pi}g^{\mu\nu}\frac{\partial_\mu\Phi\partial_\nu\Phi}{\Phi} + \mathcal{L}_{\text{matter}}\right] . \tag{2.1}$$

With $\Phi \equiv 2\pi\phi^2/\omega$, the kinetic term for the scalar field can be written in the standard way:

$$S = \int d^4x\sqrt{-g}\left[-\frac{R}{8\omega}\phi^2 + \frac{1}{2}g^{\mu\nu}\partial_\mu\phi\partial_\nu\phi + \mathcal{L}_{\text{matter}}\right] . \tag{2.2}$$

We shall work with (2.1), the form originally introduced by Brans and Dicke.

The Brans-Dicke field Φ couples to gravity and is responsible for the time variation of G. The inflaton field σ contributes to $\mathcal{L}_{\text{matter}}$ and provides the nearly constant vacuum energy density that drives inflation. ω is a dimensionless parameter of the

[1]Published in Phys. Rev. D 45, 426 (1992)

theory: Brans-Dicke gravity becomes identical to Einstein gravity as ω approaches infinity.

In contrast to the exponential expansion of standard inflation, the time variation of G in extended inflation leads to a power law expansion of the scale factor $a(t)$. The Hubble parameter $H \equiv \dot{a}/a$ is therefore decreasing with time. Once H becomes sufficiently small, the transition to a radiation-dominated universe can be completed by bubble nucleation, providing the possibility of a graceful exit to the false vacuum phase. If H changes too slowly, however, then the problems of the original inflationary scenario remain— a nearly scale-invariant distribution of bubbles is formed, resulting in large inhomogeneities and distortions of the cosmic background radiation. These distortions are unacceptably large unless $\omega \lesssim 25$ [4, 5], whereas time-delay experiments constrain ω to be $\gtrsim 500$ [6]. This problem can be avoided by introducing a potential for the Φ field which has a minimum at $\Phi = G_{\rm N}^{-1}$, where $G_{\rm N}$ is the present value of the gravitational constant. Thus, a scalar field that couples to gravity can be used to construct an interesting cosmological model. The physics of this coupling is interesting in any case, because a number of particle theories—superstring, supergravity, and Kaluza-Klein theories, for example—involve such a coupling. In general, terms with higher order couplings of Φ to the scalar curvature are also possible. Steinhardt and Accetta [7] have studied a generalization of extended inflation, called hyperextended inflation, in which the consequences of such higher order coupling terms are explored.

In this paper we compute the density perturbation spectrum $\delta\rho/\rho$ in the context of La and Steinhardt's original model of extended inflation. Specifically, we compute the curvature fluctuations that arise from quantum fluctuations in the Φ field. We work with the simple Brans-Dicke action because it provides tractable equations of motion.

We begin in Section 2.2 by obtaining the equations of motion in the Jordan frame, i.e., the frame defined by the action (2.1). In Section 2.3, following Holman *et al.* [8], we make a conformal transformation that takes the action to the standard Einstein-Hilbert form. In this conformally rescaled frame, known as the Einstein frame, a

rescaled time variable is introduced and the equations of motion are derived. A new field Ψ, obeying the equations of motion of a minimally coupled scalar field, is defined in terms of Φ. As pointed out by Kolb, Salopek and Turner [9] (hereafter called KST), this form of the action allows us to directly apply the results for $\delta\rho/\rho$ obtained in standard inflation [10–13]. The calculation of $\delta\rho/\rho$ is carried out in Section2.4. We point out some subtleties in the application of the standard density perturbation results, but we leave the investigation of these subtleties to a future paper. We nonetheless argue that the present result should be acceptable as an order-of-magnitude estimate. In Section 2.5 our result is compared with that obtained by naively applying the standard formalism in the Jordan frame. A calculation similar to ours is carried out in KST, but our result differs from theirs by a factor that depends on ω. This discrepancy vanishes in the limit of large ω, a limit in which both results agree with the answer that would be obtained naively in the Jordan frame. We point out what we believe are the reasons for the discrepancy. We also demonstrate that the action for a more general class of gravity theories can in principle be transformed to the form for a minimally coupled scalar field with a canonical kinetic term. We summarize in Section 2.6.

2.2 Jordan Frame Results

In this section we summarize the homogeneous background solutions for $\Phi(t)$ and the scale factor $a(t)$ for the Jordan frame action (2.1), assuming a flat (*i.e.*, $k = 0$) Robertson-Walker metric. We follow the notation of KST to facilitate comparison of results.

From the action (2.1), the equations of motion for $\Phi(t)$ and $a(t)$ are given by

$$\ddot{\Phi} + 3H\dot{\Phi} = \frac{8\pi}{2\omega + 3}(\rho - 3p), \tag{2.3}$$

$$H^2 \equiv \left(\frac{\dot{a}}{a}\right)^2 = \frac{8\pi\rho}{3\Phi} + \frac{\omega}{6}\left(\frac{\dot{\Phi}}{\Phi}\right)^2 - H\frac{\dot{\Phi}}{\Phi}. \tag{2.4}$$

The energy density ρ and the pressure p are determined by $\mathcal{L}_{\text{matter}}$, which describes

the inflaton field σ and all other matter fields:

$$\mathcal{L}_{\text{matter}} = \frac{1}{2} g^{\mu\nu} \partial_\mu \sigma \partial_\nu \sigma - V(\sigma) + \cdots \ . \tag{2.5}$$

In extended inflation $V(\sigma)$ provides the nearly constant false vacuum energy density that dominates the energy density of the universe during inflation. Since the σ field stays anchored very near its false-vacuum value, its kinetic energy is negligible. Thus, during inflation we have $\rho \approx \rho_{\text{vac}}$ and $p \approx -\rho_{\text{vac}}$, where $\rho_{\text{vac}} \equiv M^4$ is the value of $V(\sigma)$ in the false vacuum. The desired solution can then be written

$$\Phi(t) = \Phi_0 (Bt)^2, \tag{2.6}$$

$$a(t) = a_0 (Bt)^{\omega + \frac{1}{2}}, \tag{2.7}$$

$$H(t) = \frac{\omega + \frac{1}{2}}{t}, \tag{2.8}$$

where

$$B \Phi_0^{1/2} = \frac{M^2}{q\omega} \quad , \text{ and } \quad q = \sqrt{\frac{(6\omega + 5)(2\omega + 3)}{32\pi\omega^2}} \ . \tag{2.9}$$

(Readers comparing with KST will note that we have chosen a different origin for the time variable t.) Unlike exponential inflation, the Hubble parameter H in this case is time-dependent.

2.3 Einstein Frame Results

In this section we make the conformal transformation [8] that defines the Einstein frame in terms of the Jordan frame described above. The Einstein frame quantities will be indicated by an overbar.

Define a new metric $\bar{g}_{\mu\nu}$ as

$$g_{\mu\nu}(\vec{x}, t) = \Omega^2(t) \bar{g}_{\mu\nu}(\vec{x}, t), \tag{2.10}$$

where

$$\Omega^2(t) = \frac{m_{pl}^2}{\Phi(t)} \ , \tag{2.11}$$

and $m_{pl} \equiv G_{\rm N}^{-1/2}$ is the present value of the Planck mass. Define a field Ψ in terms of Φ by

$$\Psi = \Psi_0 \ln\left(\frac{\Phi}{m_{pl}^2}\right), \tag{2.12}$$

where

$$\Psi_0 = \sqrt{\frac{2\omega+3}{16\pi}}\, m_{pl}\ . \tag{2.13}$$

The field Ψ is introduced so that the kinetic term also takes the canonical form. Carrying out the conformal transformation (2.10) (see, e.g., Birrel and Davies [14] for the transformation of $R[g_{\mu\nu}]$) yields

$$\begin{aligned}\bar{S} = \int d^4x\sqrt{-\bar{g}}\Bigg[&-\frac{\bar{R}}{16\pi G_{\rm N}} + \frac{1}{2}\bar{g}^{\mu\nu}\partial_\mu\Psi\partial_\nu\Psi \\ &+ \frac{1}{2}e^{-\Psi/\Psi_0}\bar{g}^{\mu\nu}\partial_\mu\sigma\partial_\nu\sigma - e^{-2\Psi/\Psi_0}M^4\Bigg],\end{aligned} \tag{2.14}$$

where we have used $V(\sigma) = M^4$. Notice that the gravitational part of $\bar{S}$ has the usual Einstein form, and that the kinetic term for Ψ also takes the canonical form. Since the kinetic energy of the σ field is negligible, $\bar{S}$ takes the form of the action for a minimally coupled scalar field Ψ with an exponential potential,

$$V(\Psi) = M^4 e^{-2\Psi/\Psi_0}. \tag{2.15}$$

In $\bar{S}$, Ψ plays the role of the inflaton field—this identification simplifies the calculation of $\delta\rho/\rho$ [15].

We write the equations of motion in terms of a rescaled time variable $\bar{t}$ so that the metric takes the Robertson-Walker form

$$d\bar{s}^2 = d\bar{t}^2 - \bar{a}(\bar{t})^2\, d\bar{x}^2 = \Omega^{-2}(t) ds^2\ , \tag{2.16}$$

where

$$d\bar{t} = \Omega^{-1}\, dt, \tag{2.17}$$

$$\bar{a}(\bar{t}) = \Omega^{-1} a(t), \tag{2.18}$$

$$d\bar{x} = dx\ . \tag{2.19}$$

In these coordinates the equations of motion are

$$\ddot{\Psi}(\bar{t}) + 3\bar{H}\dot{\Psi}(\bar{t}) + \frac{dV}{d\Psi} = 0, \tag{2.20}$$

$$\bar{H}^2 \equiv \left[\frac{\dot{\bar{a}}(\bar{t})}{\bar{a}(\bar{t})}\right]^2 = \frac{8\pi}{3m_{pl}^2}\left[\frac{1}{2}\dot{\Psi}^2(\bar{t}) + V(\Psi)\right]\ . \tag{2.21}$$

In (2.20) and (2.21) and in all subsequent equations, an overdot indicates a derivative with respect to $\bar{t}$.

Using Eqs. (2.11) and (2.15), one sees that the desired conformal transformation is given by

$$\Omega(t) = \frac{m_{pl}}{B\Phi_0^{1/2} t}\ . \tag{2.22}$$

The relation between $\bar{t}$ and t can then be found by integrating Eq. (2.17), yielding

$$C\bar{t} = (Bt)^2, \tag{2.23}$$

with

$$C = \frac{2Bm_{pl}}{\Phi_0^{1/2}}\ . \tag{2.24}$$

By combining Eqs. (2.6), (2.12), and (2.13), the Jordan frame solution for $\Phi(t)$ can be transformed to give

$$\Psi(\bar{t}) = \Psi_0 \ln\left(\frac{C\Phi_0\bar{t}}{m_{pl}^2}\right)\ . \tag{2.25}$$

Eqs. (2.18), (2.22), and (2.23) lead to

$$\bar{a}(\bar{t}) = \bar{a}_0 (C\bar{t})^{\frac{2\omega+3}{4}}\ , \tag{2.26}$$

where

$$\bar{a}_0 = a_0 \frac{\Phi_0^{1/2}}{m_{pl}}\ . \tag{2.27}$$

The time-dependence of the Hubble parameter can be obtained by differentiating

Eq. (2.26), yielding

$$\bar{H} = \frac{2\omega + 3}{4\bar{t}} \ . \tag{2.28}$$

It is straightforward to verify that the equations of motion (2.20) and (2.21) are satisfied by these transformed solutions.

2.4 Calculation of $\delta\rho/\rho$

The equation of motion (2.20) for Ψ is the same as that for a minimally coupled scalar field in standard inflation. This identification [9, 16] allows us to use the results [10–13] for density perturbations arising from quantum fluctuations of a minimally coupled scalar field. The density perturbation amplitude for a scale coming inside the Hubble length in the late universe is then given by

$$\left(\frac{\delta\rho}{\rho}\right)_{\text{Hubble}} \approx \left.\frac{\bar{H}(\bar{t})^2}{\dot{\Psi}(\bar{t})}\right|_{\bar{t}=\bar{t}_h} \ , \tag{2.29}$$

where the right-hand side is to be evaluated at the time $\bar{t}_h$ when the scale crossed outside the Hubble length during inflation.

While the conformal transformation has eliminated the coupling between the scalar field and gravity, we must still ask whether Eq. (2.29) is adequate for our problem. There are several issues that must be considered:

(i) Even in the original context of standard inflation, the formula is only an approximation. It can be obtained, as in Ref. [11], by matching together an approximate solution valid at early times and an approximate solution valid at late times. The matching is done at the time of Hubble length crossing, a time when neither solution is highly reliable. Alternatively, as in Ref. [10], it can be obtained by fixing the amplitude of the late time solution by using a rough estimate of quantum fluctuations at early times. The approximation is good enough for most purposes, but here we face the problem that the effects we will be studying are quite small— see, for example, Fig. 1-1 below. To properly justify the consideration of such small effects, one wants to know that the other uncertainties are even smaller. A rough estimate of the uncer-

tainty in formula (2.29) can be obtained by recognizing that the precise time at which the right-hand side is to be evaluated has not been carefully thought out. While the standard convention holds that it should be evaluated at $\lambda_{\rm physical} = H^{-1}$, one might just as well have decided to evaluate it when $\lambda_{\rm physical} = 2H^{-1}$. This modification of the rules, however, would produce an ω-dependent correction that is comparable to the size of the effects that will be considered below.

(ii) The standard derivations of Eq. (2.29) assumed that the $\ddot{\Psi}$ term of the equation of motion for Ψ is negligible, while we will find that this is not the case when ω is small. Again there is no problem if Eq. (2.29) is considered an approximation, but the accuracy that we desire will merit a more careful look at this approximation.

(iii) Eq. (2.29) was derived originally for exponential inflation, while here we are applying it to power-law inflation, with $a(t) \propto t^p$. The application to power-law inflation has been investigated by Lucchin and Matarrese [17], who conclude that the standard formula is correct. This conclusion, however, is valid only as an approximation. Abbott and Wise [18] have shown, for example, that the two-point function that is used to calculate the scalar field quantum fluctuations depends on the exponent p in a complicated way. Moreover, if H depends on time, any answer that depends on H must specify precisely the time at which it should be evaluated.

These issues, however, are separate from the question of evaluating the right-hand side of Eq. (2.29). In this paper we will carry out this evaluation, postponing the investigation of the subtle issues. We believe that the answer obtained below is a valid order-of-magnitude estimate (similar in its accuracy to the standard results [10–13] in conventional inflation), but it is not a precise calculation.

Since the equation of motion is obtained from the Einstein action with $\bar{t}$ as the time variable, we must be careful to evaluate the right-hand side of Eq. (2.29) by using $\bar{t}$ and the Einstein frame Hubble parameter $\bar{H}(\bar{t})$. In order to express $(\delta\rho/\rho)_{\rm Hubble}$ as a function of a present-day length scale, we use the ratio of the scale factors at the time of Hubble length crossing and the present time. In doing so we assume that the transition from inflation to radiation domination occurs instantaneously at a temperature $T \approx M$, and that the field $\Phi(t)$ does not vary significantly after the

end of inflation. Therefore we approximate

$$\Phi(t_e) \approx \frac{1}{G_{\rm N}} \equiv m_{pl}^2 \ , \tag{2.30}$$

where t_e denotes the time at the end of inflation. We assume that Eq. (2.30) holds also for all $t \gtrsim t_e$. Then $\Omega^2(t) = m_{pl}^2/\Phi(t) \approx 1$ for all $t \gtrsim t_e$, so after the end of inflation the Einstein and Jordan frames coincide. The evolution of the perturbation amplitude after inflation is therefore the same in both frames. We will need an expression for $\bar{t}_e$ (the rescaled time variable at the end of inflation), which can be found by combining Eqs. (2.6) and (2.23) to obtain $\Phi(\bar{t}_e) = C\Phi_0\bar{t}_e = m_{pl}^2$. Then using Eqs. (2.24) and (2.27), one has

$$\bar{t}_e = \frac{q\omega m_{pl}}{2M^2} \ . \tag{2.31}$$

To evaluate (2.29) we use (2.28) for $\bar{H}(\bar{t})$ and (2.25) for $\Psi(\bar{t})$ to obtain

$$\left(\frac{\delta\rho}{\rho}\right)_{\rm Hubble} \approx \left.\frac{\bar{H}^2(\bar{t})}{\dot{\Psi}(\bar{t})}\right|_{\bar{t}=\bar{t}_h} = \frac{(2\omega+3)^2}{16\Psi_0\bar{t}_h} \ . \tag{2.32}$$

To solve for $\bar{t}_h$, the rescaled time variable at the moment of Hubble length crossing, we use

$$\lambda_{\rm physical}(\bar{t}_h) = \bar{a}(\bar{t}_h)\lambda_c = \bar{H}(\bar{t}_h)^{-1} \ . \tag{2.33}$$

where λ_c denotes the comoving wavelength. This can be rewritten as

$$\frac{\bar{a}(\bar{t}_h)}{\bar{a}(\bar{t}_e)}\frac{\bar{a}(\bar{t}_e)}{\bar{a}(\bar{t}_0)}\lambda_c = \bar{H}(\bar{t}_h)^{-1} \ , \tag{2.34}$$

where we have set the present value of the scale factor $\bar{a}(\bar{t}_0) = 1$. Since $\bar{a}(\bar{t}) \propto T^{-1}$, $\bar{a}(\bar{t}_e)/\bar{a}(\bar{t}_0) = T_0/M$, where $T_0 \approx 2.9\,{\rm K}$ is the present photon temperature. Also, $\bar{a}(\bar{t}_h)/\bar{a}(\bar{t}_e) = (\bar{t}_h/\bar{t}_e)^{(2\omega+3)/4}$ from (2.26). We substitute these relations into (2.34) to get

$$\left(\frac{\bar{t}_h}{\bar{t}_e}\right)^{\frac{2\omega+3}{4}}\left(\frac{T_0}{M}\right)\lambda_c = \frac{4\bar{t}_h}{2\omega+3} \ . \tag{2.35}$$

Solving for $\bar{t}_h$ and substituting in (2.32) we obtain

$$\left(\frac{\delta\rho}{\rho}\right)_{\rm Hubble} \approx \frac{(2\omega+3)^2}{16\Psi_0}\left[\left(\frac{2\omega+3}{4}\right)\left(\frac{T_0}{M}\right)\lambda_c\right]^{\frac{4}{2\omega-1}} \times \left(\frac{1}{\bar{t}_e}\right)^{\frac{2\omega+3}{2\omega-1}} . \tag{2.36}$$

We now eliminate Ψ_0 and $\bar{t}_e$ by using Eqs. (2.13) and (2.31), obtaining $\delta\rho/\rho$ in terms of known quantities:

$$\left(\frac{\delta\rho}{\rho}\right)_{\rm Hubble} \approx \sqrt{2\pi}\left(\frac{2\omega+3}{2}\right)^{\frac{6\omega+5}{2(2\omega-1)}}\left(\frac{1}{q\omega}\right)^{\frac{2\omega+3}{2\omega-1}} \times \left(\frac{M}{m_{pl}}\right)^{\frac{2(2\omega+1)}{2\omega-1}} (\lambda_c\, T_0)^{\frac{4}{2\omega-1}} . \tag{2.37}$$

Since we set $\bar{a}(\bar{t}_0) = 1$, λ_c is the physical wavelength at the present time. Remembering that we are using units for which $\hbar = c = k = 1$, one has the conversion $\lambda_c T_0 = \lambda_{\rm Mpc} \times 1\ {\rm Mpc} \times 2.9\,{\rm K} = 3.64 \times 10^{25}\lambda_{\rm Mpc}$. Thus,

$$\left(\frac{\delta\rho}{\rho}\right)_{\rm Hubble} \approx \sqrt{2\pi}\left(\frac{2\omega+3}{2}\right)^{\frac{6\omega+5}{2(2\omega-1)}}\left(\frac{1}{q\omega}\right)^{\frac{2\omega+3}{2\omega-1}} \times \left(\frac{M}{m_{pl}}\right)^{\frac{2(2\omega+1)}{2\omega-1}} \left(3.64\times 10^{25}\lambda_{\rm Mpc}\right)^{\frac{4}{2\omega-1}} , \tag{2.38}$$

where q is defined in Eq. (2.9). This is our main result. Notice that beyond using $\delta\rho/\rho \approx \bar{H}^2(\bar{t})/\dot{\Psi}(\bar{t})$, the only approximation that we have made is to neglect the evolution of $\Phi(t)$ after the end of inflation.

In agreement with KST, we find that the perturbations are proportional to $\lambda^{4/(2\omega-1)}$. This means that extended inflation might be an attractive way to account for the astronomical observations that show evidence for increased power on large scales.

2.5 Comments

2.5.1 Comparison with the Naive Jordan Frame Result

To see the effect on this calculation of the transformation to the Einstein frame, it is interesting to compare our result (2.38) with the answer that would be obtained by naively applying the standard formalism in the Jordan frame. Using an asterisk to denote the naive calculation, we have

$$\left(\frac{\delta\rho}{\rho}\right)^*_{\rm Hubble} \equiv \left.\frac{H^2(t)}{d\phi(t)/dt}\right|_{t=t_h^*} , \tag{2.39}$$

where ϕ is the field defined canonically by the action (2.2), and t_h^* is the time of Hubble length crossing as seen in the Jordan frame. In the following we denote the time of Hubble length crossing as seen in the Einstein frame by $t = t_h$ (and $\bar{t} = \bar{t}_h$ for the rescaled time variable), while the time of Hubble length crossing in the Jordan frame is denoted by $t = t_h^*$ (and $\bar{t} = \bar{t}_h^*$). Our result for $(\delta\rho/\rho)_{\rm Hubble}$ differs from the naive result for two reasons:

(i) At a given time the quantities $H^2/(d\phi/dt)$ and $\bar{H}^2/(d\Psi/d\bar{t})$ are not equal. Using the formulas from Section 2.2, one easily finds that

$$\frac{H^2(t)}{d\phi(t)/dt} = \frac{\sqrt{2\pi\omega}(2\omega+1)^2 q}{4M^2 t^2} . \tag{2.40}$$

For comparison, the right-hand side of Eq. (2.32) can be expressed in terms of t by using Eq. (2.23). One then finds

$$\frac{\bar{H}^2(\bar{t})}{d\Psi(\bar{t})/d\bar{t}} = \sqrt{\frac{2\omega}{2\omega+3}}\left(\frac{2\omega+3}{2\omega+1}\right)^2 \left.\frac{H^2(t)}{d\phi(t)/dt}\right|_{t=t(\bar{t})} . \tag{2.41}$$

(ii) The time of Hubble length crossing itself is different in the two frames. In the Jordan frame this time is evaluated using

$$a(t_h^*)\lambda_c = H(t_h^*)^{-1} , \tag{2.42}$$

which is not equivalent to the Einstein frame relation (2.33). Using Eq. (2.23) to evaluate t_h in terms of $\bar{t}_h$, one finds the relation

$$\left(\frac{1}{t_h^2}\right) = \left(\frac{2\omega+3}{2\omega+1}\right)^{\frac{4}{2\omega-1}} \left(\frac{1}{t_h^{*2}}\right) \quad . \tag{2.43}$$

To put together the two sources of discrepancy, note that the correct expression for $(\delta\rho/\rho)_{\text{Hubble}}$ is obtained by evaluating the left-hand side of Eq. (2.41) at $\bar{t}_h$, which implies that the right-hand side is evaluated at t_h. According to Eq. (2.40) this expression is proportional to $1/t_h^2$, which can be replaced by the right-hand side of Eq. (2.43). The factors occurring in Eqs. (2.41) and (2.43) are then multiplied to give

$$\left(\frac{\delta\rho}{\rho}\right)_{\text{Hubble}} = F(\omega) \left(\frac{\delta\rho}{\rho}\right)^{*}_{\text{Hubble}} \quad , \tag{2.44}$$

where the correction factor is given by

$$F(\omega) = \sqrt{\frac{2\omega}{2\omega+3}} \left(\frac{2\omega+3}{2\omega+1}\right)^{\frac{2(2\omega+1)}{2\omega-1}} \quad . \tag{2.45}$$

The correction factor $F(\omega)$ is plotted in Fig. 1-1. It decreases monotonically with ω, approaching one as ω approaches infinity.

We emphasize again that in the Einstein frame the field Ψ behaves as a minimally coupled scalar field, and the rescaled time variable $\bar{t}$ and scale factor $\bar{a}(\bar{t})$ correspond to a Robertson-Walker metric; therefore *these* functions, not the original ones, must be used in applying the standard methods to calculate $(\delta\rho/\rho)_{\text{Hubble}}$.

2.5.2 Comparison with KST's Results

KST (Ref. [9]) have also worked with the Einstein frame action, but nonetheless their answer (Eq. (2.21) of their paper) differs from ours: it is equal to our answer (Eq. 2.38) times the factor

$$\sqrt{\frac{6\omega+5}{3(2\omega+3)}} \left(\frac{2\omega}{2\omega+3}\right)^{\frac{4}{2\omega-1}} \quad . \tag{2.46}$$

This discrepancy is due to the following reasons:

(i) They evaluate $\bar{H}^2(\bar{t})/\dot{\Psi}(\bar{t})$ at the time of Hubble length crossing in the Jordan frame, while we maintain that the time of Hubble length crossing must be evaluated in the Einstein frame. According to Eq. (2.43), this causes their result to contain an additional factor $[(2\omega+1)/(2\omega+3)]^{4/(2\omega-1)}$.

(ii) They use a "slow-rollover" approximation $\dot{\Psi}(\bar{t}) \approx -(dV/d\Psi)/3\bar{H}(\bar{t})$, while we evaluate $\dot{\Psi}(\bar{t})$ by differentiating the exact solution for $\Psi(\bar{t})$. This causes their result to contain the additional factor $\dot{\Psi}_{\rm exact}/\dot{\Psi}_{\rm approx} = 3(2\omega+3)/(6\omega+5)$.

(iii) They evaluate $\bar{H}$ by using $\bar{H}^2 \approx 8\pi V/3m_{pl}^2$ (neglecting the kinetic energy), while we used the exact expression. This causes their result to contain an additional factor $(\bar{H}_{\rm approx}/\bar{H}_{\rm exact})^3 = [(6\omega+5)\,/\,3(2\omega+3)]^{3/2}$.

(iv) They omit a factor $2\omega/(2\omega+1)$ that should appear on the top line of their Eq. (2.9). This causes their result to contain an additional factor $[2\omega/(2\omega+1)]^{4/(2\omega-1)}$.

Each of these discrepancy factors approaches one as ω approaches infinity, but in this limit the effect of transforming to the Einstein frame disappears altogether.

The discrepancy factor (2.46) carries over into the formula for the temperature fluctuations of the cosmic background radiation, $(\delta T/T)_{\theta>1^\circ} \simeq \bar{H}^2(\bar{t})/15\dot{\Psi}(\bar{t})$, given as Eq. (2.25) in KST. For the same reasons, we would differ with KST's results for graviton perturbations, Eqs. (2.13) and (2.16) in their paper. For the dimensionless amplitude of a gravitational-wave perturbation as it comes inside the Hubble length in the late universe, we obtain

$$h_\lambda \approx \frac{\bar{H}}{m_{pl}} = \left(\frac{M}{m_{pl}}\right)^{\frac{2(2\omega+1)}{2\omega-1}} \left(\frac{2\omega+3}{2q\omega}\right)^{\frac{2\omega+3}{2\omega-1}} \times \left(3.64\times 10^{25}\lambda_{\rm Mpc}\right)^{\frac{4}{2\omega-1}} . \qquad (2.47)$$

2.5.3 Application to Generalized Gravity Theories

We have obtained the density perturbation spectrum for a simple model of extended inflation. The method we have used, however, is applicable to a wide class of generalized gravity theories that involve a scalar field coupled to gravity. Suppose that the

action can be written as

$$S = \int d^4x\sqrt{-g} \quad \left[-f(\phi)R + \frac{1}{2}g^{\mu\nu}T(\phi)\partial_\mu\phi\partial_\nu\phi + \mathcal{L}_{\rm matter}\right] , \tag{2.48}$$

where $f(\phi)$ and $T(\phi)$ are arbitrary functions. From Eq. (2.2) it follows that for Brans-Dicke gravity $f(\phi) = \phi^2/8\omega$ and $T(\phi) = 1$. If $T(\phi) = 1$, then for all $f(\phi) > 0$ (the condition for a general $T(\phi)$ is given below) the conformal transformation to the Einstein frame can be performed and, through a redefinition of fields, the action can be cast in the form of the action for a minimally coupled scalar field. We first demonstrate this for a general $f(\phi)$, and then consider the analytically tractable case of $f(\phi) = \phi^4$.

We make the conformal transformation $g_{\mu\nu} = \Omega^2\bar{g}_{\mu\nu}$, where

$$\Omega^2 = \frac{m_{pl}^2}{16\pi}\frac{1}{f(\phi)} \quad . \tag{2.49}$$

The action (2.48) then takes the form (with $\mathcal{L}_{\rm matter} = 0$ for convenience)

$$\bar{S} = \int d^4x\sqrt{-\bar{g}}\left[-\frac{m_{pl}^2}{16\pi}R + \frac{1}{2}g^{\mu\nu}K(\phi)\partial_\mu\phi\partial_\nu\phi\right] . \tag{2.50}$$

where $K(\phi)$ is given by Salopek, Bond, and Bardeen [19] as

$$K(\phi) = \frac{m_{pl}^2}{16\pi}\frac{1}{f(\phi)^2}[3f'(\phi)^2 + f(\phi)T(\phi)] . \tag{2.51}$$

The first term on the right-hand side of (2.51) comes from the conformal transformation of the scalar curvature term in (2.48), and the second term comes from the original kinetic term. If we define a field $\Psi(\phi)$ such that $\Psi'(\phi) = \sqrt{K(\phi)}$, then

$$\partial_\mu\Psi(\phi)\partial_\nu\Psi(\phi) = \Psi'(\phi)^2\partial_\mu\phi\partial_\nu\phi = K(\phi)\partial_\mu\phi\partial_\nu\phi . \tag{2.52}$$

So in terms of $\Psi(\phi)$ the kinetic term is canonical and the action takes the form for a

minimally coupled scalar field. For $K(\phi) > 0$ the integral

$$\Psi(\phi) = \int \sqrt{K(\phi)} d\phi \tag{2.53}$$

is well defined and is a monotonically increasing function of ϕ, so there is a unique value of $\Psi(\phi)$ (up to an additive constant) for every value of ϕ. Therefore one expects that the quantum theory for Ψ gives the standard result, Eq. (2.29), for the density perturbation spectrum. In general the integral for $\Psi(\phi)$ and the solutions of the equations of motions must be obtained numerically.

For Brans-Dicke gravity, the integral for $\Psi(\phi)$ is simple and the result is given by (2.12). $\Psi(\phi)$ can also be obtained in closed form for the case $f(\phi) = \phi^4$, $T(\phi) = 1$. From Eq. (2.51) one has

$$K(\phi) = \frac{m_{pl}^2}{16\pi} \left(\frac{48\phi^2 + 1}{\phi^4} \right) , \tag{2.54}$$

which can be integrated according to Eq. (2.53) to give

$$\Psi(\phi) = \sqrt{\frac{3m_{pl}^2}{\pi}} \quad \left[-\sqrt{\frac{48\phi^2 + 1}{48\phi^2}} + \ln(\sqrt{48}\phi + \sqrt{48\phi^2 + 1}) \right] . \tag{2.55}$$

In hyperextended inflation a term of this form may dominate the $f(\phi)R$ coupling during a cosmologically important epoch, so it is of some interest to study its density perturbation spectrum [9].

A non-minimally coupled scalar field with $f(\phi) = 1 - \alpha\phi^2$ has been studied by Futamase and Maeda [20], who have obtained $\Psi(\phi)$ for all $\alpha > 0$.

2.6 Conclusion

We have estimated the density perturbation spectrum in the original model of extended inflation, with Brans-Dicke gravity. Curvature fluctuations arising from quan-

tum fluctuations in the Brans-Dicke field contribute a significant amplitude of density perturbations. They are a slowly increasing function of the scale, a feature that might be useful in building models to account for the observed large scale structure of the universe. We have performed the calculation by transforming to the Einstein conformal frame, then applying the standard procedures used in conventional inflationary models. We have pointed out some subtleties associated with this procedure, but we nonetheless believe that the result is valid as an order-of-magnitude estimate

We have compared our density perturbation amplitude to the answer that would be obtained by working naively in the Jordan frame— our answer is larger by a factor that is near unity, but which becomes large for very small values of the Brans-Dicke parameter ω. If the calculation is done correctly in both frames, however, one should of course expect to obtain the same answer. Indeed, part of our motivation was to lay some groundwork toward a consistent calculation in the two frames. The success of such a calculation would give us confidence that the field theory is being treated correctly, and that the conformal transformation method is valid at the quantum (or at least semiclassical) level as well as the classical level. The question of consistency between the two frames has been addressed in two recent preprints [21].

As pointed out earlier, the model we have studied must be modified if it is to satisfy experimental constraints. One possibility is to add a small mass term for the Brans-Dicke field— the evolution of Φ during the inflationary period would not be significantly affected, but the mass term could still freeze the value of the field in the present epoch so that the theory would be consistent with observation. As pointed out by KST, in this scenario the Φ particles would have to be unstable in order to prevent the mass density of the universe from becoming dominated by them. If the model is repaired in this fashion, then the calculation of density fluctuations presented in this paper would remain valid. One can also imagine more substantial modifications to the model, in which case our calculation would no longer be valid in detail. It would nonetheless serve as an illustration of a technique to compute $(\delta\rho/\rho)_{\rm Hubble}$ for models with a scalar field coupled to gravity.

The authors would like to thank Dalia Goldwirth and Tsvi Piran for interesting discussions. They are also extremely grateful to Robert Brandenberger for many valuable conversations.

The work of A.H.G. was supported in part by the U.S. Department of Energy (D.O.E.) under contract #DE-AC02-76ER03069, and the work of B.J. was supported in part by funds provided by the Karl Taylor Compton Fellowship.

REFERENCES

[1] D. La and P. J. Steinhardt, Phys. Rev. Lett. **62**, 376 (1989). An early paper describing some aspects of inflation in a Brans-Dicke theory is C. Mathiazhagan and V. B. Johri, Class. Quantum Grav. **1**, L29 (1984).

[2] C. Brans and R. H. Dicke, Phys. Rev. **24**, 925 (1961).

[3] See, for example, S. Weinberg, **Gravitation and Cosmology** (Wiley, New York, 1972).

[4] D. La, P. J. Steinhardt, and E. Bertschinger, Phys. Lett. **231B**, 231 (1989).

[5] E. J. Weinberg, Phys. Rev. D**40**, 3950 (1989).

[6] R. D. Reasenberg *et al.*, Ap. J. **234**, L219 (1979).

[7] P. J. Steinhardt and F. S. Accetta, Phys. Rev. Lett. **64**, 2740 (1990).

[8] R. Holman, E. W. Kolb, S. L. Vadas, Y. Wang, and E. J. Weinberg, Phys. Lett. **237B**, 37 (1990).

[9] E. W. Kolb, D. S. Salopek, and M. S. Turner, Phys. Rev. D**42**, 3925 (1990).

[10] J. M. Bardeen, P. J. Steinhardt, and M. S. Turner, Phys. Rev. D**28**, 679 (1983).

[11] A. H. Guth and S.-Y. Pi, Phys. Rev. Lett. **49**, 1100 (1982).

[12] A. A. Starobinski, Phys. Lett. **117B**, 175 (1982).

[13] S. W. Hawking, Phys. Lett. **115B**, 295 (1982).

[14] N. D. Birrell and P.C.W. Davies, **Quantum Fields in Curved Space** (Cambridge University Press, Cambridge, England, 1982).

[15] In the Jordan frame the effective gravitational constant $G_{\rm eff} = \Phi^{-1}$ is time-dependent, while the potential energy density $V(\sigma) \approx M^4$ is constant. In the Einstein frame the effective gravitational constant $G_{\rm eff} = m_{pl}^{-2}$ is time-independent, but here the potential energy density $V = M^4 e^{-2\Psi/\Psi_0} =$

$M^4 m_{pl}^4/\Phi^2$ varies with time. The ratio of the potential energy mass scale to the effective Planck scale, $V^{1/4}/G_{\rm eff}^{-1/2}$, has the value $M/\Phi^{1/2}$ in both frames. See Ref. [8].

[16] We learned after this paper was submitted that a similar calculation in a model with a single scalar field, with an $R\phi^2$ coupling, has been carried out by R. Fakir and W. G. Unruh, Phys. Rev. D **41**, 1783 (1990); Phys. Rev. D **41**, 1792 (1990).

[17] F. Lucchin and S. Matarrese, Phys. Rev. D**32**, 1316 (1985).

[18] L. F. Abbott and M. B. Wise, Nucl. Phys. **B244**, 541 (1984).

[19] D. S. Salopek, J. R. Bond, and J. M. Bardeen, Phys. Rev. D**40**, 1753 (1989).

[20] T. Futamase and K. Maeda, Phys. Rev. D**39**, 399 (1989).

[21] N. Makino and M. Sasaki (unpublished); R. Fakir and S. Habib (unpublished).

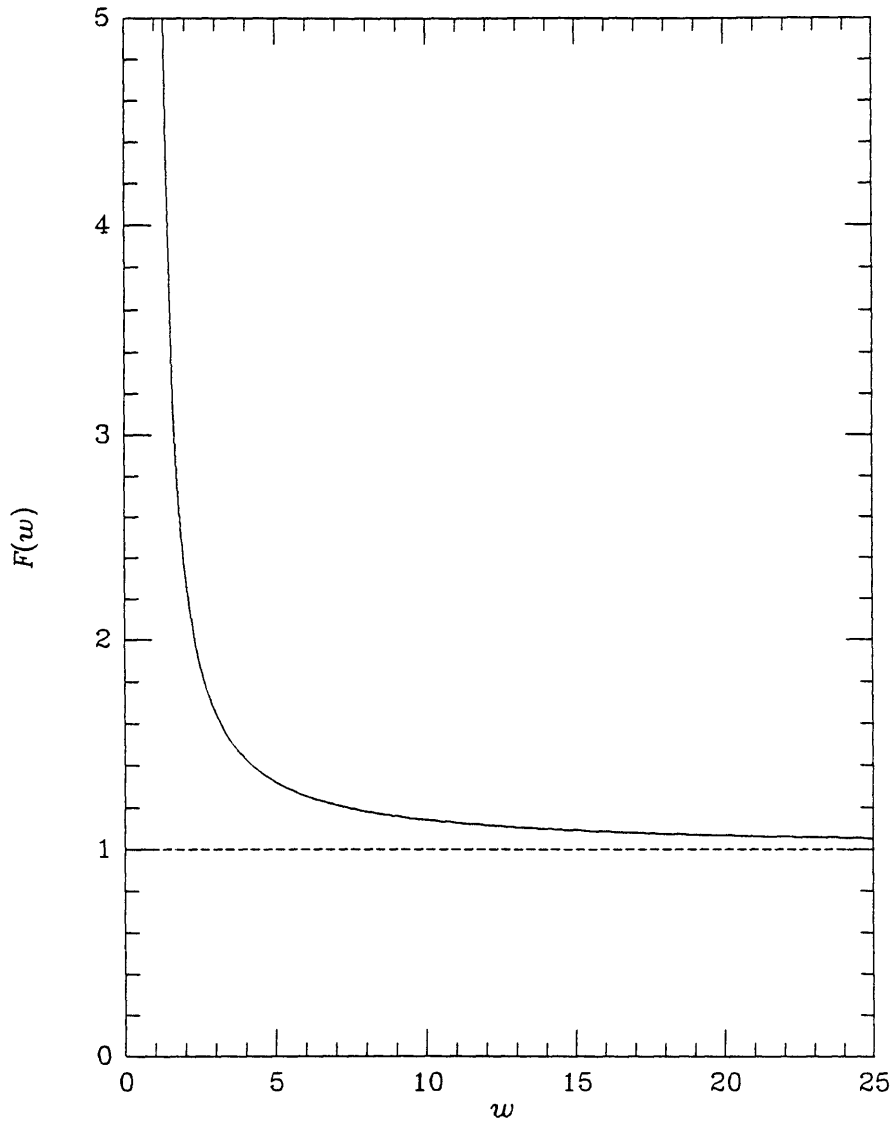

Figure 2-1 The effect of transforming to the Einstein frame. The correct answer for $\delta\rho/\rho$ is larger by the factor $F(\omega)$ than the answer that would be obtained by naively applying the standard formalism in the Jordan frame.

Chapter 3

Second Order Power Spectrum and Nonlinear Evolution at High Redshift[1]

3.1 Introduction

There exists a standard paradigm for the formation of cosmic structure: gravitational instability in an expanding universe. According to this paradigm, dark matter density fluctuations $\delta(\vec{x}) \equiv \delta\rho(\vec{x})/\bar{\rho}$ created in the early universe lay dormant until the universe became matter-dominated at a redshift $z = z_{\rm eq} \approx 2.5 \times 10^4\,\Omega h^2$ (where Ω is the present density parameter for nonrelativistic matter and the present Hubble parameter is $H_0 = 100\,h$ km s^{-1} Mpc^{-1}). After this time, the density fluctuations increased in amplitude as predicted by the well-known results of linear perturbation theory (e.g., Peebles 1980; Efstathiou 1990; Bertschinger 1992), until the fluctuations became nonlinear on some length scale. Bound condensations of this scale then collapsed and virialized, forming the first generation of objects (Gunn & Gott 1972; Press & Schechter 1974). Structure formation then proceeded hierarchically as density fluctuations became nonlinear on successively larger scales.

[1]To be published in Ap. J., **431** (1994)

At early times density fluctuations were small on the length scales of present day large-scale structure. Therefore, after the universe became matter dominated fluctuations on scales much larger than the scale of collapsed objects can be studied under the approximation of a pressureless, irrotational fluid evolving under the action of Newtonian gravity. A perturbative analysis of the fluid equations in Fourier space can then be used to study the effects of mode coupling between scales that are weakly nonlinear. This is the approach we shall follow in this paper. Nonlinear analyses in real and Fourier space are somewhat complementary in that real space analyses are best suited to studying the effect of nonlinearities on the collapse and shapes of individual objects (Bertschinger & Jain 1993), whereas Fourier space studies provide estimates of how different parts of the initial spectrum couple and influence the evolution of statistical quantities like the power spectrum. In principle of course, the two approaches are equivalent and should give the same information. For perturbative analyses in real space see, e.g., Peebles (1980), Fry (1984), Hoffman (1987), Zaroubi & Hoffman (1993), and references therein.

Although density fluctuations of different wavelengths evolve independently in linear perturbation theory, higher order calculations provide an estimate of some nonlinear effects. Preliminary second order analyses have led to the conventional view that in models with decreasing amounts of power on larger scales long-wavelength fluctuations have no significant effect on the gravitational instability occuring on small scales. On the other hand, it is known that under some circumstances small-scale, nonlinear waves can transfer significant amounts of power to long-wavelength, linear waves. If the initial spectrum is steeper than k^4 at small k (comoving wavenumber), then small-scale, nonlinear waves can transfer power to long wavelength linear waves so as to produce a k^4 tail in the spectrum. (Zel'dovich 1965; Peebles 1980, Section 28; Vishniac 1983; Shandarin & Melott 1990).

The question of whether power can be transfered from large to small scales was examined by Juszkiewicz (1981), Vishniac (1983), Juszkiewicz, Sonoda & Barrow (1984), and more recently by Coles (1990), Suto and Sasaki (1991) and Makino, Sasaki and Suto (1992). Their analyses involved writing down integral expressions for the

second order contribution to the power spectrum, examining their limiting forms and evaluating them for some forms of the initial spectrum. Juszkiewicz et al. (1984) examined the autocorrelation function and found that the clustering length decreases due to power transfer from large to small scales for the initial spectrum $P(k) \propto k^2$. However, for the cold dark matter (hereafter CDM) spectrum Coles (1990) found the opposite effect, though it is not significant unless σ_8 is taken larger than 1. Makino et al. (1992) have analytically obtained the second order contributions for power law spectra, and estimated the contribution for the CDM spectrum by approximating it as two power laws. Bond & Couchman (1988) have compared the second order CDM power spectrum to the Zel'dovich approximation evaluated at the same order. Some issues of mode coupling have recently been investigated through N-body simulations in 2-dimensions (see e.g., Beacom et al. 1991; Ryden & Gramann 1991; Gramann 1992).

We have used the formalism developed in some of the perturbative studies cited above, and especially by Goroff et al. (1986), to calculate second order contributions to the power spectrum (i.e., up to fourth order in the initial density) for the standard CDM spectrum. Second order perturbation theory has a restricted regime of validity, because once the density fluctuations become sufficiently large the perturbative expansion breaks down. For this reason N-body simulations have been used more extensively to study the fully nonlinear evolution of density fluctuations. However, perturbation theory is very well suited to address some specific aspects of nonlinear evolution and to provide a better understanding of the physical processes involved. Being less costly and time-consuming than N-body simulations, it lends itself easily to the study of different models. Perturbation theory should be considered a complementary technique to N-body simulations, for while its validity is limited, it does not suffer from the resolution limits that can affect the latter. Hence by comparing the two techniques their domains of validity can be tested and their drawbacks can be better understood. In this paper we shall make such comparisons for the CDM spectrum.

The most powerful use of perturbative calculations is in the study of weakly non-

linear evolution out to very high redshifts, spanning decades of comoving length scales in the spectrum. Since the formulation of the perturbative expansion allows for the time evolution of the spectrum to be obtained straightforwardly, we obtain the scaling in time of characteristic nonlinear mass scales ranging from the nonlinear scale today, about $10^{14}\,M_\odot$, to about $10^5\,M_\odot$, the smallest baryonic mass scale likely to have gone nonlinear after the universe became matter dominated. Such an analysis cannot be done by existing N-body simulations as the dynamic range required to cover the full range of scales with adequate spectral resolution exceeds that of the current state-of-the-art.

There are two principal limitations to our analytic treatment: the first arises from the general problem that the perturbative expansion breaks down when nonlinear effects become sufficiently strong. This drawback is particularly severe in our case because the regime of validity is difficult to estimate. It is reasonable to expect that second order perturbation theory ceases to be valid when the rms $\delta\rho/\rho \gtrsim 1$, but one cannot be more precise without explicitly calculating higher order contributions.

The second kind of limitation arises from the simplifying assumptions that pressure and vorticity are negligible. On small enough scales nonlinear evolution causes the intersection of particle orbits and thus generates pressure and vorticity. Through these effects virialization on small-scales can alter the growth of fluctuations on larger scales. It is plausible that the scales in the weakly nonlinear regime are large enough that this effect is not significant. This belief is supported by heuristic arguments as well as recent studies of N-body simulations (Little, Weinberg & Park 1991; Evrard & Crone 1992 and references therein). We conclude that the first kind of limitation, namely the neglect of higher order contributions, or worse still, the complete breakdown of the perturbative expansion, is likely to be more severe for our results. We shall address this where appropriate and accordingly attempt to draw conservative conclusions supported by our own N-body simulations.

The formalism for the perturbative calculation is described in Section 2. We describe the numerical results for CDM in Section 3.1 and compare them to N-body simulations in Section 3.2. The scaling of the nonlinear scale as a function of redshift is

presented in Section 3.3. The distribution of nonlinear masses is examined in Section 3.4 We discuss cosmological implications of the results in Section 4.

3.2 Perturbation Theory

In this section we describe the formalism for perturbative solutions of the cosmological fluid equations in Fourier space. Our approach is similar to that of Goroff et al. (1986). The formal perturbative solutions are then used to write down the explicit form of the second order contribution to the power spectrum.

3.2.1 General Formalism

We suppose for simplicity that the matter distribution after recombination may be approximated as a pressureless fluid with no vorticity. We further assume that peculiar velocities are nonrelativistic and that the wavelengths of interest are much smaller than the Hubble distance cH^{-1} so that a nonrelativistic Newtonian treatment is valid. Using comoving coordinates $\vec{x}$ and conformal time $d\tau = dt/a(t)$, where $a(t)$ is the expansion scale factor, the nonrelativistic cosmological fluid equations are

$$\frac{\partial \delta}{\partial \tau} + \vec{\nabla} \cdot [(1+\delta)\vec{v}] = 0 \ , \tag{3.1a}$$

$$\frac{\partial \vec{v}}{\partial \tau} + \left(\vec{v} \cdot \vec{\nabla}\right) \vec{v} = -\frac{\dot{a}}{a} \vec{v} - \vec{\nabla}\phi \ , \tag{3.1b}$$

$$\nabla^2 \phi = 4\pi G a^2 \bar{\rho} \delta \ , \tag{3.1c}$$

where $\dot{a} \equiv da/d\tau$. Note that $\vec{v} \equiv d\vec{x}/d\tau$ is the proper peculiar velocity, which we take to be a potential field so that $\vec{v}$ is fully specified by its divergence:

$$\theta \equiv \vec{\nabla} \cdot \vec{v} \ . \tag{3.1d}$$

We assume an Einstein-de Sitter ($\Omega = 1$) universe, with $a \propto t^{2/3} \propto \tau^2$. We will also assume that the initial (linear) density fluctuation field is a gaussian random field.

To quantify the amplitude of fluctuations of various scales it is preferable to work with the Fourier transform of the density fluctuation field, which we define as

$$\hat{\delta}(\vec{k},\tau) = \int \frac{d^3x}{(2\pi)^3}\, e^{-i\vec{k}\cdot\vec{x}}\, \delta(\vec{x},\tau)\ , \tag{3.2}$$

and similarly for $\hat{\theta}(\vec{k},\tau)$. The power spectrum (power spectral density) of $\delta(\vec{x},\tau)$ is defined by the ensemble average two-point function,

$$\langle \hat{\delta}(\vec{k}_1,\tau)\, \hat{\delta}(\vec{k}_2,\tau)\rangle = P(k_1,\tau)\, \delta_{\rm D}(\vec{k}_1+\vec{k}_2)\ , \tag{3.3}$$

where $\delta_{\rm D}$ is the Dirac delta function, required for a spatially homogeneous random density field. For a homogeneous and isotropic random field the power spectrum depends only on the magnitude of the wavevector. The contribution to the variance of $\delta(\vec{x},\tau)$ from waves in the wavevector volume element d^3k is $P(k,\tau)d^3k$.

Fourier transforming equations (3.1) gives

$$\frac{\partial\hat{\delta}}{\partial\tau} + \hat{\theta} = -\int d^3k_1 \int d^3k_2\, \delta_{\rm D}(\vec{k}_1+\vec{k}_2-\vec{k})\, \frac{\vec{k}\cdot\vec{k}_1}{k_1^2}\, \hat{\theta}(\vec{k}_1,\tau)\, \hat{\delta}(\vec{k}_2,\tau)\ , \tag{3.4a}$$

$$\frac{\partial\hat{\theta}}{\partial\tau} + \frac{\dot{a}}{a}\,\hat{\theta} + \frac{6}{\tau^2}\,\hat{\delta} = -\int d^3k_1 \int d^3k_2\, \delta_{\rm D}(\vec{k}_1+\vec{k}_2-\vec{k})\, \frac{k^2(\vec{k}_1\cdot\vec{k}_2)}{2k_1^2k_2^2}\, \hat{\theta}(\vec{k}_1,\tau)\, \hat{\theta}(\vec{k}_2,\tau)\ . \tag{3.4b}$$

In equations (3.4) the nonlinear terms constitute the right-hand side and illustrate that the nonlinear evolution of the fields $\hat{\delta}$ and $\hat{\theta}$ at a given wavevector $\vec{k}$ is determined by the mode coupling of the fields at all pairs of wavevectors whose sum is $\vec{k}$, as required by spatial homogeneity. This makes it impossible to obtain exact solutions to the equations, so that the only general analytical technique for self-consistently evaluating the nonlinear terms is to make a perturbative expansion in $\hat{\delta}$ and $\hat{\theta}$. The formalism for such an expansion has been systematically developed by Goroff et al. (1986) and recently extended by Makino et al. (1992). Following these authors we

write the solution to equations (3.4) as a perturbation series,

$$\hat{\delta}(\vec{k},\tau) = \sum_{n=1}^{\infty} a^n(\tau)\,\delta_n(\vec{k})\ , \quad \hat{\theta}(\vec{k},\tau) = \sum_{n=1}^{\infty} \dot{a}(\tau)a^{n-1}(\tau)\,\theta_n(\vec{k}) \tag{3.5}$$

It is easy to verify that for $n = 1$ the time dependent part of the solution correctly gives the linear growing modes $\hat{\delta}_1 \propto a(\tau)$ and $\hat{\theta}_1 \propto \dot{a}$ and that the time-dependence is consistent with equations (3.4) for all n. To obtain formal solutions for the $\vec{k}$ dependence at all orders we proceed as follows.

Substituting equation (3.5) into equations (3.4) yields, for $n > 1$,

$$n\delta_n(\vec{k}) + \theta_n(\vec{k}) = A_n(\vec{k})\ , \quad 3\delta_n(\vec{k}) + (1+2n)\theta_n(\vec{k}) = B_n(\vec{k})\ , \tag{3.6}$$

where

$$A_n(\vec{k}) \equiv -\int d^3k_1 \int d^3k_2\, \delta_{\rm D}(\vec{k}_1+\vec{k}_2-\vec{k})\,\frac{\vec{k}\cdot\vec{k}_1}{k_1^2}\sum_{m=1}^{n-1}\theta_m(\vec{k}_1)\,\delta_{n-m}(\vec{k}_2)\ , \tag{3.7a}$$

$$B_n(\vec{k}) \equiv -\int d^3k_1 \int d^3k_2\, \delta_{\rm D}(\vec{k}_1+\vec{k}_2-\vec{k})\,\frac{k^2(\vec{k}_1\cdot\vec{k}_2)}{k_1^2k_2^2}\sum_{m=1}^{n-1}\theta_m(\vec{k}_1)\,\theta_{n-m}(\vec{k}_2)\ . \tag{3.7b}$$

Solving equations (3.6) for δ_n and θ_n gives, for $n > 1$,

$$\delta_n(\vec{k}) = \frac{(1+2n)A_n(\vec{k}) - B_n(\vec{k})}{(2n+3)(n-1)}\ , \quad \theta_n(\vec{k}) = \frac{-3A_n(\vec{k}) + nB_n(\vec{k})}{(2n+3)(n-1)}\ . \tag{3.8}$$

Equations (3.7) and (3.8) give recursion relations for $\delta_n(\vec{k})$ and $\theta_n(\vec{k})$, with starting values $\delta_1(\vec{k})$ and $\theta_1 = -\delta_1$. The general solution may be written

$$\delta_n(\vec{k}) = \int d^3q_1 \cdots \int d^3q_n \delta_{\rm D}(\vec{q}_1+\cdots+\vec{q}_n-\vec{k})F_n(\vec{q}_1,\ldots,\vec{q}_n)\delta_1(\vec{q}_1)\cdots\delta_1(\vec{q}_n)\ , \tag{3.9a}$$

$$\theta_n(\vec{k}) = -\int d^3q_1 \cdots \int d^3q_n \delta_{\rm D}(\vec{q}_1+\cdots+\vec{q}_n-\vec{k})G_n(\vec{q}_1,\ldots,\vec{q}_n)\delta_1(\vec{q}_1)\cdots\delta_1(\vec{q}_n)\ . \tag{3.9b}$$

From equations (3.7)–(3.9) we obtain recursion relations for F_n and G_n:

$$F_n(\vec{q}_1,\ldots,\vec{q}_n) \;=\; \sum_{m=1}^{n-1}\frac{G_m(\vec{q}_1,\ldots,\vec{q}_m)}{(2n+3)(n-1)}\Bigg[(1+2n)\frac{\vec{k}\cdot\vec{k}_1}{k_1^2}F_{n-m}(\vec{q}_{m+1},\ldots,\vec{q}_n)$$

$$+\frac{k^2(\vec{k}_1\cdot\vec{k}_2)}{k_1^2k_2^2}G_{n-m}(\vec{q}_{m+1},\cdots,\vec{q}_n)\Bigg]\,, \tag{3.10a}$$

$$\begin{aligned} G_n(\vec{q}_1,\ldots,\vec{q}_n) &= \sum_{m=1}^{n-1}\frac{G_m(\vec{q}_1,\ldots,\vec{q}_m)}{(2n+3)(n-1)}\Bigg[3\frac{\vec{k}\cdot\vec{k}_1}{k_1^2}F_{n-m}(\vec{q}_{m+1},\cdots,\vec{q}_n) \\ &\quad +n\frac{k^2(\vec{k}_1\cdot\vec{k}_2)}{k_1^2k_2^2}G_{n-m}(\vec{q}_{m+1},\ldots,\vec{q}_n)\Bigg]\,, \end{aligned} \tag{3.10b}$$

where $\vec{k}_1 \equiv \vec{q}_1+\cdots+\vec{q}_m$, $\vec{k}_2 \equiv \vec{q}_{m+1}+\cdots+\vec{q}_n$, $\vec{k}\equiv\vec{k}_1+\vec{k}_2$ and $F_1 = G_1 = 1$. Equations (3.10) are equivalent to equations (3.6) and (A1) of Goroff et al. (1986), with $F_n = P_n$ and $G_n = (3/2)Q_n$ in their notation.

3.2.2 Power Spectrum at Second Order

To calculate the power spectrum we shall prefer to use symmetrized forms of F_n and G_n, denoted $F_n^{(s)}$ and $G_n^{(s)}$ and obtained by summing the $n!$ permutations of F_n and G_n over their n arguments and dividing by $n!$. Since the arguments are dummy variables of integration the symmetrized functions can be used in equations (3.9) without changing the result. The symmetrized second-order solutions of equations (3.10) are given by

$$F_2^{(s)}(\vec{k}_1,\vec{k}_2) = \frac{5}{7}+\frac{2}{7}\frac{(\vec{k}_1\cdot\vec{k}_2)^2}{k_1^2k_2^2}+\frac{(\vec{k}_1\cdot\vec{k}_2)}{2}\left(\frac{1}{k_1^2}+\frac{1}{k_2^2}\right)\,, \tag{3.11a}$$

$$G_2^{(s)}(\vec{k}_1,\vec{k}_2) = \frac{3}{7}+\frac{4}{7}\frac{(\vec{k}_1\cdot\vec{k}_2)^2}{k_1^2k_2^2}+\frac{(\vec{k}_1\cdot\vec{k}_2)}{2}\left(\frac{1}{k_1^2}+\frac{1}{k_2^2}\right)\,. \tag{3.11b}$$

Note that $F_2^{(s)}$ and $G_2^{(s)}$ have first-order poles as $k_1\to 0$ or $k_2\to 0$ for fixed $\vec{k}$: $F_2^{(s)} \sim G_2^{(s)} \sim (1/2)\cos\vartheta\,(k_1/k_2+k_2/k_1)$ where ϑ is the angle between $\vec{k}_1$ and $\vec{k}_2$. The expression for $F_3^{(s)}$ will also be required, but since it is very long we shall wait to write a simplified form below.

The recursion relations in equations (3.10) may be used to compute the power spectrum at any order in perturbation theory. Substituting equation (3.5) into equa-

tion (3.3), we have

$$\begin{aligned} P(k,\tau)\,\delta_{\rm D}(\vec{k}+\vec{k}') &= \langle \delta(\vec{k},\tau)\,\delta(\vec{k}',\tau)\rangle \\ &= a^2(\tau)\langle \delta_1(\vec{k})\,\delta_1(\vec{k}')\rangle + a^4(\tau)\Big[\langle \delta_1(\vec{k})\,\delta_3(\vec{k}')\rangle + \\ &\quad \langle \delta_2(\vec{k})\,\delta_2(\vec{k}')\rangle + \langle \delta_3(\vec{k})\,\delta_1(\vec{k}')\rangle\Big] + O(\delta_1^6)\,. \end{aligned} \tag{3.12}$$

Equation (3.12) explicitly shows all the terms contributing to the power spectrum at fourth order in the initial density field δ_1 (or second order in the initial spectrum), as the nth order field $\delta_n(\vec{k})$ involves n powers of $\delta_1(\vec{k})$. With the definition

$$\langle \delta_m(\vec{k})\,\delta_{n-m}(\vec{k}')\rangle \equiv P_{m,n-m}(k)\,\delta_{\rm D}(\vec{k}+\vec{k}') \tag{3.13}$$

the power spectrum up to second order (i.e., fourth order in δ_1) is given by equation (3.12) as

$$\begin{aligned} P(k,\tau) &= a^2(\tau)P_{11}(k) + a^4(\tau)[P_{22}(k) + 2P_{13}(k)] \\ &= a^2(\tau)P_{11}(k) + a^4(\tau)P_2(k)\,, \end{aligned} \tag{3.14}$$

where the net second order contribution $P_2(k)$ is defined as

$$P_2(k) = P_{22}(k) + 2P_{13}(k)\,. \tag{3.15}$$

To determine $P_2(k)$ we need to evaluate the 4-point correlations of the linear density field $\delta_1(\vec{k}\,)$. For a gaussian random field, all cumulants (irreducible correlation functions) of $\delta_1(\vec{k}\,)$ vanish aside from the 2-point cumulant, which is given by equation (3.3) for $m = n-m = 1$. All odd moments of $\delta_1(\vec{k}\,)$ vanish. Even moments are given by symmetrized products of the 2-point cumulants. Thus the 4-point correlation function of $\delta_1(\vec{k})$ is

$$\begin{aligned} \langle \delta_1(\vec{k}_1)\delta_1(\vec{k}_2)\delta_1(\vec{k}_3)\delta_1(\vec{k}_4)\rangle &= P(k_1)P(k_3)\delta_{\rm D}(\vec{k}_1+\vec{k}_2)\delta_{\rm D}(\vec{k}_3+\vec{k}_4) + \\ &\quad P(k_1)P(k_2)\delta_{\rm D}(\vec{k}_1+\vec{k}_3)\delta_{\rm D}(\vec{k}_2+\vec{k}_4) + \end{aligned}$$

$$P(k_1)P(k_2)\delta_{\rm D}(\vec{k}_1+\vec{k}_4)\delta_{\rm D}(\vec{k}_2+\vec{k}_3)\ . \qquad (3.16)$$

With the results and techniques described above, we can proceed to obtain the second order contribution to the power spectrum. The two terms contributing at second order simplify to the following 3-dimensional integrals in wavevector space:

$$P_{22}(k) = 2\int d^3q\, P_{11}(q)\, P_{11}(|\vec{k}-\vec{q}|)\left[F_2^{(s)}(\vec{q},\vec{k}-\vec{q})\right]^2\ , \qquad (3.17)$$

with $F_2^{(s)}$ given by equation (3.11a), and

$$2P_{13}(k) = 6P_{11}(k)\int d^3q\, P_{11}(q)\, F_3^{(s)}(\vec{q},-\vec{q},\vec{k})\ . \qquad (3.18)$$

The numbers in front of the integrals arise from the procedure of taking expectation values illustrated in equation (3.16). We write the integrals in spherical coordinates q, ϑ, and ϕ: the magnitude, polar angle and azimuthal angle, respectively, of the wavevector $\vec{q}$. Then with the external wavevector $\vec{k}$ aligned along the z-axis the integral over ϕ is trivial and simplifies $\int d^3q$ to $2\pi\int dq\, q^2\int d\cos\vartheta$. For P_{13}, the dependence on ϑ is also straightforward as it arises only through $F_3^{(s)}$ and not P_{11}. This allows the integral over $\cos\vartheta$ to be done analytically as well, giving (Makino et al. 1992)

$$\begin{aligned} 2P_{13}(k) \;=\; & \frac{2\pi}{252}P_{11}(k)\int dq\, P_{11}(q)\left[12\frac{k^2}{q^2}-158+100\frac{q^2}{k^2}-42\frac{q^4}{k^4}\right. \\ & \left.+\frac{3}{k^5q^3}(q^2-k^2)^3(7q^2+2k^2)\ln\left(\frac{k+q}{|k-q|}\right)\right]. \end{aligned} \qquad (3.19)$$

Thus with a specified initial spectrum $P_{11}(k)$ equations (3.17) and (3.19) give the second order contribution. Before evaluating these integrals for the CDM initial spectrum, we point out that the poles of F_2 and G_2 described after equations (3.11) give the leading order part of the integrand of equation (3.17) in (q/k) as:

$$P_{22}(k) \sim k^2 P_{11}(k)\int\frac{d^3q}{3q^2}\,P_{11}(q)\ . \qquad (3.20)$$

If $P_{11}(k)\sim k^n$ with $n\le -1$ as $k\to 0$, then P_{22} diverges. Vishniac (1983) showed that

the leading order part of $2P_{13}$ in (q/k) is negative and exactly cancels that of P_{22} — this can be demonstrated by examining the limiting form of $F_3^{(s)}$. In a future paper we will analyze the leading order behavior of perturbative integrals at higher orders and also calculate it using a nonperturbative approach in order to investigate whether there may exist divergences for some power spectra at higher orders in perturbation theory. For the purposes of the second order integration the cancellation of the leading order terms has no consequence other than requiring that each piece, P_{22} and P_{13}, be integrated very accurately to get the resultant. This is necessary because the cancelling parts cannot be removed before performing the integrals as the two integrands have different forms: P_{22} is symmetric in $\vec{q}$ and $(\vec{k}-\vec{q})$, whereas P_{13} is not. We will return to this point in the next section.

3.3 Results for CDM

The results obtained in the previous section will now be used to obtain the second order contributions to the CDM power spectrum. We will use the standard CDM spectrum with parameters $\Omega = 1$, $H_0 = 50$ km s^{-1}Mpc^{-1}, and $\sigma_8 = 1$. For the linear spectrum at $a = 1$ we use the fitting form given by Bardeen et al. (1986):

$$\begin{aligned} P_{11}(k) &= AkT^2(k)\ , \quad A = 2.19 \times 10^4 \mathrm{Mpc}^4\ , \\ T(k) &= \frac{\ln(1+9.36k)}{9.36k}[1 + 15.6k + (64.4k)^2 \\ &\quad +(21.8k)^3 + (26.8k)^4]^{-1/4}\ , \end{aligned} \tag{3.21}$$

where k is in units of Mpc^{-1}. With this initial spectrum equations (3.17) and (3.19) can be used to obtain the second order contribution $P_2(k)$, which can then be used to obtain the net power spectrum as a function of a and k from equation (3.14).

3.3.1 Nonlinear Power Spectrum

As pointed out in Section 2.2 the integrals for P_{22} and P_{13} contain large contributions which exactly cancel each other. For the CDM spectrum these contributions are finite

but care is still required in their numerical evaluation. Equal contributions from P_{22} are made as $\vec{q} \to 0$ and $\vec{q} \to \vec{k}$, whereas the cancelling contribution from $2P_{13}$ is made only as $\vec{q} \to 0$. The integrand for P_{22} is symmetric in $\vec{q}$ and $(\vec{k} - \vec{q})$ and is positive definite. For ease of numerical integration, we break up the integration range for P_{22} as follows:

$$\begin{aligned} \int \frac{d^3q}{2\pi} &= 2\int_0^{\epsilon} dq \int_{-1}^{1} dy + \int_{\epsilon}^{k-\epsilon} dq \int_{-1}^{1} dy + \int_{k-\epsilon}^{k+\epsilon} dq \int_{-1}^{(k^2+q^2-\epsilon^2)/2kq} dy \\ &\quad + \int_{k+\epsilon}^{k-k_c} dq \int_{-1}^{1} dy + \int_{k-k_c}^{k_c} dq \int_{(k^2+q^2-k_c^2)/2kq}^{1} dy \ , \end{aligned} \tag{3.22}$$

where $y \equiv \cos\vartheta$, and k_c is the upper limit required because at high q the spectrum has departed strongly from the linear spectrum causing the perturbative expansion to break down. Transfer of power from higher frequencies is suppressed by virialization. The first term on the right-hand side of equation (3.22) has a factor of 2 because we have used the symmetry between $\vec{q}$ and $(\vec{k}-\vec{q})$ in the integrand to exclude a small ball of radius ϵ around $\vec{q} = \vec{k}$ (where the integration becomes difficult) by restricting the limits on y in the third term, requiring us to double the contribution from a similar ball around $\vec{q} = 0$ to compensate. The limits on y in the last term are set to ensure that $|\vec{k} - \vec{q}| \leq k_c$ as required to consistently impose the upper limit, i.e., to exclude any contribution from P_{11} in equation (3.17) when its argument exceeds k_c. It is in principle important to scale k_c with time to reflect the growth of the nonlinear length scale with time, because that determines the range of validity of the perturbative expansion. We have done so using the linear scaling $k_c \propto a^{-2/(3+n)}$, although as explained below at early times the result is insensitive to the choice of k_c.

The results of performing the integrals in equations (3.17) and (3.19) for a large range of values of k are shown in Figure 3-1. We plot the linear spectrum $a^2 P_{11}(k)$, the net spectrum including second order contributions given by eqution (14), and the nonlinear spectrum computed from high-resolution N-body simulations described in Section 3.2 at four values of the expansion factor. The spectra have been divided by a^2 to facilitate comparison of the results at different times. The second order results at different values of a are obtained by simply multiplying P_{11} and P_2 by

different powers of a as shown in equation (3.14), so the integration of P_{22} and P_{13} needs to be done only once for a given k. The second order spectrum should be taken seriously only for the range of k for which $a^4 P_2(k) < a^2 P_{11}(k)$, as we do not expect the perturbative results to be valid for higher k. The interesting range of k, the regime where nonlinear effects set in, moves to lower k as one looks at larger a, reflecting the progress of nonlinearities to larger length scales (lower k) at late times. As expected we find that at a given time the second order contribution is not significant for small k where the rms $\delta\rho/\rho \ll 1$.

For small k up to just over the peak of the spectrum, the second order contribution is negative, causing the nonlinear spectrum to be lower than the linear one. At relatively high k the second order contribution enhances the growth of the spectrum. This has the effect of making the slope of the spectrum significantly shallower at high k than that of the linear spectrum. Thus, power is effectively transfered from long to short wavelengths, although the enhancement at short wavelengths exceeds the suppression at long wavelengths.

The two power law model of Makino et al. (1992) gives qualitatively similar results to those shown in Figure 3-1. Bond & Couchman (1988) also computed the second order contributions to the CDM spectrum with a view to checking the reliability of the Zel'dovich approximation at the same order. They found excellent agreement, in contrast to the results of Grinstein & Wise (1987) who found that in comparison to perturbation theory the Zel'dovich approximation significantly underestimated the magnitudes of the gaussian filtered, connected parts of the third and fourth moment of the real space density. In comparison to our results, Figure 3 of Bond & Couchman shows a larger enhancement over the linear spectrum, and does not appear to show the suppression at relatively low k at all. They do not give the explicit form of the term corresponding to our P_{13}, but state that it is negligible in comparison to P_{22}. This does not agree with our results at low k and is probably the source of the difference in our figures. It is difficult to make a more detailed comparison without knowing the explicit form of their second term.

In order to obtain a better understanding of the dynamics of the mode-coupling, we

have examined the relative contribution of different parts of the CDM initial spectrum to the second order results at a given k. Let $\vec{q}$ denote the integrated wavevector and $\vec{k}$ the external wavevector at which the second order contribution is calculated, as in equations (3.17) and (3.19). There is a two-fold ambiguity because wavevector $\vec{k}-\vec{q}$ contributes at the same time as $\vec{q}$. We have carefully examined different ways of associating second order contributions from different parts of the initial spectrum, and found that the second order contribution from $q \lesssim k$ tends to be positive and that from $q \gtrsim k$ negative. Indeed we also find this to hold for power law spectra with $-3 \leq n \leq 1$, independently of the value of n, thus indicating that it is a general feature of second-order mode-coupling. In Figure 3-2 we associate the second-order contributions, $dP_2(k)/d\ln q$, with the smaller of q and $|\vec{k}-\vec{q}|$.

There are two regimes in the CDM spectrum, divided roughly by the part where the logarithmic slope $n\,[\equiv d\ln P_{11})/d\ln k]$ falls below -1. For small k, where $n \gtrsim -1$, the positive second order contribution from $q \lesssim k$ is swamped by the negative contribution made by large q. The net effect is to decrease the growth of the spectrum compared to the linear growth. For relatively large k, where $n \lesssim -2$ the positive contribution from small q dominates, increasingly so as one goes to higher k. A comparison of the curves in Figure 3-2 for $k = 0.1\,\mathrm{Mpc}^{-1}$ and $k = 1\,\mathrm{Mpc}^{-1}$ shows how the relative strengths of the positive and negative contributions shift as one moves across the spectrum. This shift can be understood by observing that at higher k there is an increasing amount of power in the initial spectrum at $q < k$; the plot of the rms power on scale k in Figure 3-3 illustrates this point. The increased power at small q causes a larger nonlinear enhancement at higher k. Since the weakly nonlinear regime moves to higher k at earlier times, the enhancement at high k in turn leads to a stronger nonlinear growth at earlier times. We study the consequence of this fact in detail in Section 3.3. The dominance of the nonlinear contribution from long-wave modes also strengthens the consistency of the perturbative calculation, because the amplitude of the density fluctuations is small for these modes. As discussed in Section 3.2, this may be responsible for the second order results being valid for a much larger range of scales at earlier times.

We emphasize that the transition value $n \simeq -1$ for the change in sign of the second order contribution is only approximate, because it depends on the value of k taken as being representative of the weakly nonlinear regime. We have examined the second order contribution for power law spectra $P_{11}(k) \propto k^n$, for a range of values of n between -3 and 1 to verify this transition. We find that in the weakly nonlinear regime (defined by $k \lesssim k_{nl}$, where k_{nl} is the scale at which the rms $\delta\rho/\rho = 1$), the second order contribution for n sufficiently larger than -1 is negative and that for n sufficiently smaller than -1 is positive. For $n \simeq -1$, the contribution is negative for low k and positive for high k in the weakly nonlinear regime. These results are consistent with the results of Makino et al. (1992) who examined the second order contributions for $n = 1, 0, -1, -2$; they also found good agreement with N-body simulations.

A possible transition in the nature of nonlinear evolution at $n = -1$ has also been explored by studying the clustering in real space in N-body simulations by Klypin & Melott (1992). An examination of the origin of the term providing the dominant second order enhancement suggests that the advective $(\vec{v} \cdot \vec{\nabla})$ terms in the real space fluid equations cause the change in sign of the nonlinear contribution. This interpretation is consistent with the fact that for $n < -1$ there is an increasing amount of power in the rms velocity field on larger scales, and this appears to cause the nonlinear enhancement of the density from long-wave modes to dominate. These arguments are by no means rigorous, and merit further exploration.

It is worth noting that for the deeply nonlinear regime the stable clustering hypothesis (Peebles 1980, Section 73) predicts that the spectrum steepens below the linear theory spectrum for $n > -2$ and rises above it for $n < -2$. Consistency with the second order results would require that at least for $-2 \lesssim n \lesssim -1$, the nonlinear spectrum first rise above the linear one in the weakly nonlinear regime and then fall below it in the deeply nonlinear regime. This is indeed seen in N-body simulations; the results of Efstathiou et al. (1988) show only hints of this feature owing to limited resolution, but it is clearly evident in simulations with higher resolution (Bertschinger & Gelb 1991; White 1993).

The second order spectrum provides an estimate of the change in the fluctuation amplitude due to nonlinear effects in the weakly nonlinear regime. The conventional normalization is to set the rms $\delta\rho/\rho$ on a scale of $8h^{-1}$ Mpc, denoted σ_8, equal to 1. The rms value is computed from the power spectrum using a top-hat filter as described in Section 3.3. We find that with the linear spectrum normalized in this way, second order effects increase σ_8 by 10%. This is a smaller enhancement than found by Hoffman (1987) for the standard deviation of the density (without filtering) using the Zel'dovich approximation. The N-body spectrum shows an even smaller change in σ_8 than the second order spectrum, although it is difficult to estimate accurately in a box of length 50 h^{-1} Mpc.

3.3.2 Comparison with N-Body Simulations

The N-body results shown in Figure 3-1 are from two different particle-particle/particle-mesh simulations of the CDM model in a $(100\,\mathrm{Mpc})^3$ box normalized so that linear $\sigma_8 = 1$ at $a = 1/(1+z) = 1$. For $a > 0.1$ we have used the simulation with 144^3 particles and Plummer softening distance 65 kpc performed by Gelb & Bertschinger (1993). To obtain accurate results at higher redshifts we have performed a new simulation with 288^3 particles each of mass $2.9 \times 10^9\, M_\odot$ with Plummer softening distance 20 kpc. In both cases the energy conservation, as measured by integrating the Layzer-Irvine equation, was much better than 1 percent.

The comparison of power spectra in Figure 3-1 shows qualitative agreement between the second order and N-body results — in both the small dip in the spectrum at small k and the enhancement at high k. At early times the agreement of the two nonlinear spectra is excellent. This agreement extends beyond the naive regime of validity of the second order results. As suggested above, the dominance of the contribution from long-wave modes to the nonlinear enhancement at early times apparently extends the regime of validity of the second order results.

At late times ($0.5 \lesssim a \lesssim 1$) the second order results at high k show a larger enhancement of the spectrum in comparison to the N-body results. There is significant discrepancy in the two results even within the expected regime of validity of the sec-

ond order results. This discrepancy, coupled with the good agreement at early times, indicates that even in principle the second order spectrum could not have agreed with the N-Body spectrum shown in Figure 3-1 at all times. The simple dependence of the second order spectrum on a given in equation (3.14) is incompatible with the dependence of the N-Body spectrum on a for the full range of k lying in the nonlinear regime.

A part of the discrepancy at late times could arise from the dependence of the second order results on the upper cutoff imposed on the integrals. The cutoff dependence is indeed the largest at late times: for $a \geq 0.5$ reasonable variations in k_c can change the result typically by over 10%. Another source of disagreement could be that the N-body simulations are done in a finite size box, therefore they have a small-k cutoff. Since the contribution from long-wave modes is positive, excluding these modes could cause simulations to underestimate the nonlinear enhancement of power. On comparing CDM simulations in boxes of sides 100 and 640 Mpc we do find this to be true, but the difference is very small. Thus neither of the two reasons mentioned above explain the magnitude of the disagreement between the second order and N-body spectra. A possible explanation is an inadequate suppression of the second order spectrum due to collapse on small scales, i.e., "previrialization" (Davis & Peebles 1977; Peebles 1990). Indeed the second order contribution from $q > k$ is negative, in qualitative agreement with such a suppression, but it should not be surprising if the magnitude of the suppression is significantly underestimated. Higher order perturbative contributions may well include some of this suppression. Our analytic treatment neglects small-scale pressure and vorticity, which should also suppress the nonlinear enhancement of power. As we mention in Section 1, so far N-body studies designed to test this hypothesis have concluded that small scale effects are negligible. However these studies have not tested different initial spectra, and they have not examined the power spectrum itself with as much dynamic range as our simulations provide.

3.3.3 Scaling in Time

The nonlinear power spectrum can be used to construct statistical measures of density fluctuations in real space. These can then be used to study the most important consequence of the coupling of long-wave modes: a systematic change in the variation of characteristic nonlinear scales with time. We proceed to do this by first defining the rms $\delta\rho/\rho$ averaged on length scale R by integrating over the power spectrum with an appropriate window function W:

$$\delta_R^2(a) \equiv \left\langle \left(\frac{\delta\rho}{\rho}\right)^2 \right\rangle_R = \int d^3k\, P(a,k)\, W^2(kR)\ . \tag{3.23}$$

For W we shall use three different functions: a shell in k-space, the top-hat in real space, and the gaussian, given respectively by,

$$W_{\rm D}^2(kR) = \delta_{\rm D}(kR-1)\ , \tag{3.24a}$$

$$W_{\rm TH}(kR) = \frac{3\left[\sin(kR) - kR\cos(kR)\right]}{(kR)^3}\ , \tag{3.24b}$$

$$W_G(kR) = \exp\left[-\frac{(kR)^2}{2}\right]\ . \tag{3.24c}$$

In Figure 3-3 we plot $[4\pi k^3 P(a,k)]^{1/2}$, or $\delta_R(a)$ for $W_{\rm D}$ with $k = r^{-1}$, to illustrate what we expect for the time dependence of a characteristic nonlinear scale, denoted as $R_{\rm nl}(a)$. If the spectrum evolved self-similarly then one would expect that at all a, the onset of nonlinear effects occurs at a scale defined by setting $4\pi k^3 P(a,k) =$ constant for some value of the constant of order unity. This behavior is expected for power law spectra of the form $P(k) \propto k^n$, and has been verified in studies of N-body simulations (Efstathiou et al. 1988). Even though CDM-like spectra are not pure power laws, the simplest assumption would be that they show a similar behavior. However, Figure 3-3 shows that at early times (small a), the spectrum deviates from the linear one at progressively smaller values of $4\pi k^3 P(a,k)$. This trend is even stronger for the N-body spectra. Thus already there is a hint of a systematic departure of the nonlinear

scaling from the conventional expectation, due to the variation of the spectral index n with scale for the CDM spectrum.

This conclusion is confirmed by using the other window functions to define the nonlinear scale as follows. We calculate $\delta_R(a)$ using equations (3.24b,c) for a range of R and a. We then define $R_{\rm nl}(a)$ as follows:

$$\delta_R(a) = \delta_c \quad \text{for} \quad R = R_{\rm nl}(a) \ , \tag{3.25}$$

where δ_c is a constant of order unity. Since $R_{\rm nl}(a)$ is a comoving length scale, it can be used to define a nonlinear scale for the mass as: $M_{\rm nl}(a) = (4\pi/3)\bar{\rho}R_{\rm nl}^3(a)$, where $\bar{\rho}$ is the critical density today.

In Figure 3-4 we have plotted $M_{\rm nl}(a)$ from $a = 0.04$ to 1 for the gaussian and top-hat filters, with δ_c chosen to be 1 and 1.69 for each filter. The dependence of $M_{\rm nl}(a)$ confirms the impression conveyed by Figure 3-3: nonlinear enhancement is stronger at earlier times. While the quantitative results depend on the choice of the window function and δ_c, it is clear that in each of the figures the slope of the second order curve is different from the linear curve, and this causes the relative enhancement of $M_{\rm nl}(a)$ to be larger at earlier times. Indeed, if the normalization of the second order curves was changed (thus shifting them to the right) so that at $a = 1$ they predicted the same nonlinear mass as the linear curves, then all four panels would show very similar relative enhancements at early times.

In stating quantitative results for the time-dependence of nonlinear masses we shall focus on the gaussian filter with $\delta_c = 1$. This choice provides the most conservative estimates of second order effects. At $a^{-1} = (1+z) = (20, 10, 5, 2)$, $M_{\rm nl}(a)$ from the second order spectrum is about $(180, 8, 2.5, 1.6)$ times (respectively) larger than the linear case. Figure 3-4 can also be used to read off the change in the redshift of nonlinearity for the desired mass scale due to second order effects. (Here as in the preceding figures, the linear spectrum is normalized so that $\sigma_8 = 1$ at $z = 0$ and this fixes the normalization of the second-order spectrum.) For example, the mass scale $10^6\, M_\odot$ goes nonlinear at $(1+z) \simeq 25$ as opposed to 19 if only the linear spectrum

is used; and the mass scale $10^{11}\,M_\odot$ at $(1+z) \simeq 6$ as opposed to 5. This change in redshift is a more meaningful indicator of the nonlinear effect, as the change in $M_{\rm nl}(a)$ is amplified due to the steepening of the spectrum at high k.

In Figure 3-4 we have also shown results from the Press-Schechter model (Press & Schechter 1974, hereafter PS). The PS model is a widely used ansatz for predicting the distribution of bound objects of a given mass at different times (section 3.4). It relies on the linear growth of the power spectrum, hence it is no surprise that the shape of the PS curve is very similar to the linear curve. Here the PS nonlinear mass is defined as the mass for which a fixed fraction, 0.4, of the mass in nonlinear clumps belongs to clumps of mass $M_{\rm nl}$ or larger. The fraction 0.4 is chosen so that the normalization of the PS curves is close to that of the other curves at $a = 1$ — in the upper panels it is close to the nonlinear curves and in the lower panels to the linear curves.

The N-body simulations can be used to define a characteristic nonlinear mass in many different ways. The dashed curves in Figure 3-4 show nonlinear masses computed using the power spectrum from the simulation in the same way as for the second order and linear spectra above (i.e., using eq. 3.25). The results are in very good agreement with the second order results, as expected because of the good agreement of the second order and nonlinear power spectra. The relative enhancement of $M_{\rm nl}(a)$ over the linear prediction at $(1+z) = (10, 5, 2)$ is $(11, 2.4, 1.2)$. By examining all four panels it can be seen that, independent of the parameters used, the slopes of the curves using second-order and nonlinear power spectra are distincty different from those of the linear and PS curves. The filled triangles use a different definition of the N-body characteristic nonlinear mass and will be discussed in the next section.

Our results in Figure 3-4 indicate that linear scaling for $M_{\rm nl}(a)$ significantly underestimates nonlinear enhancement at high redshift. Consequently the characteristic masses predicted by the PS model are much smaller than the second order and N-body masses for $z > 4$, even for the choice of parameters for which they agree at late times. This conclusion may appear at odds with previous tests of the PS formalism made by others. However, no previous tests have examined the CDM model at high redshift

with as much dynamic range as we have. As we have emphasized, mode-coupling from long waves is strongest for small n; for the CDM spectrum n varies with scale and approaches -3 at high k. It is precisely in this limit, previously untested with high-resolution N-body simulations, that we find the greatest departures from linear theory and the Press-Schechter model.

3.3.4 Distribution of Nonlinear Masses

The characteristic nonlinear masses defined above do not fully characterize the distribution of dense clumps that form as a result of gravitational instability. A better comparison of theory and simulation can be made using the complete distribution of masses.

In the N-body simulation we have identified dense clumps at mean overdensity about 200 using the friends-of-friends (FOF) algorithm with linking distance 0.2 times the mean interparticle separation. (The $N = 288^3$ simulation was used at $1+z = 10$, while the $N = 144^3$ simulation was used for $1 + z = 5$, 2, and 1.) The distribution of nonlinear clump masses is very broad, so there is no unique nonlinear mass. We have chosen to define the characteristic nonlinear mass $M_{\rm nl}$ for this distribution as the median clump mass defined so that half of the mass in clumps of at least 5 particles is contained in clumps more massive than $M_{\rm nl}$. The 5 particle limit corresponds to $M = 1.16 \times 10^{11}\,M_\odot$ and $1.45 \times 10^{10}\,M_\odot$ for the $N = 144^3$ and 288^3 simulations, respectively. The resulting nonlinear masses are denoted by the filled triangular symbols in the upper-left panel of Figure 3-4; for other panels these points would be at the same locations as in this panel. (If the PS curves were defined with the same lower limit for clump masses and the same value of the mass fraction, instead of having no lower limit and a mass fraction 0.4, they would agree more closely with the N-body FOF points.) It is coincidental that this definition of N-body nonlinear mass yields such close agreement with the analytic predictions at $z = 0$, because the broad range of clump masses would allow us to vary $M_{\rm nl}$ by factors of a few. The relative variations as a function of redshift are more meaningful. It is clear from Figure 3-4 that the variation of these N-body masses with a departs from the

linear scaling even more strongly than the curve computed from the N-body power spectrum. Thus, nonlinear effects on the formation of high-redshift objects appear to be even more significant than they are on the power spectrum. However, the 5 particle limit affects the FOF characteristic mass (no lower limit is imposed on the PS curve), so we should make a more detailed comparison with the mass distribution before reaching firm conclusions.

The PS model makes the ansatz that the formation of bound objects is determined by the overdensity in the linear density field. Using the gaussian distribution of the linear density field, this ansatz gives the comoving number density, $n(M,a)$, of nonlinear objects of mass M in the mass interval dM at expansion factor a as (Press & Schechter 1974):

$$n(M,a)\,dM = \bar{\rho}\left(\frac{2}{\pi}\right)^{1/2}\frac{\delta_c}{\sigma}\exp\left(-\frac{\delta_c^2}{2\sigma^2}\right)\frac{1}{\sigma}\left(\frac{d\sigma}{dM}\right)\frac{dM}{M}\,. \tag{3.26}$$

In this equation δ_c is a free parameter which can be taken to be a constant, with the linear rms density smoothed on the mass scale M, $\sigma(M,a)$, growing in proportion to a. A popular choice for δ_c is 1.69, the value of the linear density at which a spherical top-hat perturbation collapses to infinite density. The PS mass distribution $n(M,a)$ has been tested against N-body simulations and found by other workers to work very well. Efstathiou et al. (1988) tested it for scale-free simulations, and several authors have tested it for the CDM spectrum (e.g., Carlberg & Couchman 1989). The weaknesses of such tests — particularly, the finite resolution of the simulations — have been recognized by these authors, but even so the agreement has been surprisingly good for the range of masses and redshift probed. Consequently, the PS model has been widely used in predicting the number density of objects at high redshift, or in estimating the redshift at which a given mass scale goes nonlinear.

Figure 3-5 shows the cumulative mass fraction (CMF) as a function of clump mass from the N-body simulation and the PS prediction. The CMF is defined by

$$\mathrm{CMF}(M,a) = \bar{\rho}^{-1}\int_M^\infty n(M,a)M\,dM\ , \tag{3.27}$$

i.e., the fraction of mass in objects of mass M or larger. In Figure 3-4 we defined the PS nonlinear mass using the condition CMF = 0.4. For the PS prediction of Figure 3-5 we have chosen the top-hat filter with $\delta_c = 1.69$. At late times, this choice gives fairly good agreement for the high-mass end of the mass distribution. However, we see that at early times the N-body mass distribution lies systematically above the PS prediction. This is in qualitative agreement with the results shown in Figure 3-4 and supports our conclusion that nonlinear effects on the formation of nonlinear clumps are even stronger than they are for the power spectrum.

Because coupling of long waves modifies the power spectrum and therefore the rms density $\sigma(M, a)$, the failure of Press-Schecter theory to match the N-body results exactly does not surprise us. As an experiment we replaced $\sigma(M, a)$ in equation (3.26) using the second-order and N-body power spectra instead of linear theory. The resulting CMF(M) falls too rapidly at large M, even after δ_c is increased to compensate for the nonlinear enhancement of density fluctuations. If the nonlinear power spectrum is used the PS formula gives the wrong shape for $n(M, a)$ because it assumes a gaussian distribution of densities, while the nonlinear density field has a broader distribution. We have found no simple modification of the PS formula that can account for the systematic departures evident in Figure 3-5. Expressing an optimistic view, we note that the PS formula is accurate to about a factor of 2 for the CMF over the entire range shown in Figure 3-5. On the other hand, the deviations are larger for rarer objects (smaller CMF) and the sign and magnitude of the deviation changes systematically with a. Therefore one should use the PS formula, especially at high redshift and for rare objects, only with caution after calibration by high-resolution N-body simulations.

3.4 Discussion

We have calculated the second order contribution to the evolution of the standard CDM power spectrum. We believe that our results capture the dominant nonlinear contribution in the weakly nonlinear regime. They are consistent with N-body results

in this regime from $z = 9$ to $z \simeq 1$, but show a larger enhancement of the spectrum than the N-body results from $z \simeq 1$ to $z = 0$. The bulk of the second order enhancement in the growth of the power spectrum is provided by the mode coupling of long-wave modes, especially for the onset of nonlinearities at high redshift.

By analyzing the perturbative integrals we have studied the sensitivity of nonlinear evolution to different parts of the spectrum, and thus have probed the dynamics of the mode-coupling at work. We find that on scales of interest to large-scale structure in the universe, the dominant contribution to the weakly nonlinear evolution of most realistic power spectra comes from the mode-coupling of long-wave modes. Perturbation theory is quite adequate for estimating this contribution since the amplitude of density fluctuations is small for the long-wave modes.

An important consequence of nonlinear evolution is to change the time dependence of the nonlinear scale $M_{\rm nl}(a)$ from linear scaling: it is found to be significantly larger at high z. Thus objects of a given scale go nonlinear at higher redshifts than indicated by the standard linear extrapolation. As discussed in Section 3, this is a consequence of the variation with scale of the spectral index, with $n \gtrsim -1$ on the scales of interest for large-scale structure and $n \simeq -3$ on the smallest scales. We have given quantitative estimates of this effect for the standard CDM spectrum for different window functions and definitions of nonlinear scale. For a gaussian window function and $\delta_c = 1$, which provides the most conservative estimates, the change in the redshift factor of nonlinearity, $(1 + z_{nl})$, is about 20% for $10^{11}\,M_\odot$ objects (with linear extrapolation $1 + z_{nl} = 5$) and increases to about 33% for $10^6\,M_\odot$ objects $(1 + z_{nl} = 19)$. We have also computed nonlinear corrections using high resolution N-body simulations, using the power spectrum from the simulations as well as directly identifying bound objects. The results are in very good agreement with the second order predictions, especially between $z \simeq 4$ and 10. Quantitative comparisons are provided in Sections 3.3 and 3.4 and in Figure 3-4.

Thus the most striking implications of second order effects are for the formation of nonlinear objects at high z. Theoretical studies of, for example, the first generation of collapsed objects, the redshift of galaxy-formation, and reionization at high-z (see

e.g., Couchman & Rees 1986; Efstathiou & Rees 1988; Tegmark & Silk 1993) — all require as an input the scale of nonlinearity as a function of z. For analytical estimates this is invariably obtained using linear extrapolation, as for example in the Press-Schechter mass distribution. We have shown (Figure 3-5) that the Press-Schechter theory leads to a systematic underestimate of the abundance of high-mass nonlinear clumps at high redshift in the CDM model, but have not succeeded in suggesting a simple modification that works better. While nonlinear coupling to long waves increases the amplitude of small-scale density fluctuations, it also changes the probability distribution from the gaussian distribution appropriate in the linear regime.

Most realistic cosmological spectra steepen to $n \simeq -3$ at the smallest scales and have $n \gtrsim -1$ on the largest scales of interest. This is a generic feature arising from the sluggish, logarithmic growth of fluctuations during the radiation dominated era, thus causing the scale invariant spectrum with spectral index $n = 1$ initially to approach $n = -3$ on the smallest scales while retaining the primeval slope on scales much larger than the size of the horizon at the end of the radiation dominated era. Hence for different cosmological models the basic features of nonlinear gravitational evolution that we have studied should hold, although the quantitative details would depend on the values of parameters such as σ_8, δ_c, Ω and H_0.

The increase in redshift of collapse relative to linear theory that we have calculated for CDM should also occur in all realistic spectra provided that on the scales of interest n decreases sufficiently rapidly with increasing k. Our results will not apply if the dark matter is hot, but the qualitative implications should be the same for the evolution of the baryonic component in a CDM- or baryon-dominated model until dissipational effects become important. For spectra with a very steep slope at small scales (such as in the hot dark matter model), second order effects may lead to a strong nonlinear enhancement which would drive the spectrum to a shallower slope.

In the near future second order power spectra from theoretical models could be related to the power spectrum calculated from observational surveys. Indeed the shape of the best fit three-dimensional power spectrum computed from results of

the APM survey (Baugh & Efstathiou 1993) shows two characteristic features of the second order CDM spectrum: a relatively shallow slope at small scales and a flattening of the peak of the spectrum at large scales. The power spectrum computed from the CfA redshift survey (Vogeley et al. 1992) and from the 1.2Jy IRAS redshift survey (Fisher et al. 1993) had also shown the first feature of a shallow slope with n just below -1 at high k, but these surveys lacked the depth required to determine the shape of the spectrum near the peak. It will be interesting to see if the extended peak of the APM spectrum is a robust feature.

It is a pleasure to thank Alan Guth for many stimulating discussions. We also acknowledge useful discussions with Carlton Baugh, George Efstathiou, Yehuda Hoffman, Roman Juszkiewicz, David Weinberg and Simon White. We thank John Bahcall for his hospitality at the Institute for Advanced Study, where this work was completed. Supercomputing time was provided by the Cornell National Supercomputer Facility and the National Center for Supercomputing Applications. This work was supported by NSF grant AST90-01762.

REFERENCES

Bardeen, J.M., Bond, J.R., Kaiser, N., & Szalay, A.S. 1986, ApJ, 304, 15

Baugh, C. & Efstathiou, G. 1993, MNRAS, 265, 145

Beacom, J. F., Dominik, K. G., Melott, A. L., Perkins S. P. & Shandarin, S. F. 1991, ApJ, 372, 351

Bertschinger, E. 1992, in New Insights into the Universe, ed. Martinez, V. J., Portilla, M. & Saez, D. (Berlin: Springer-Verlag), p. 65

Bertschinger, E. & Gelb, J. 1991, Comp. in Physics, 5, 164

Bertschinger, E. & Jain, B. 1993, submitted to ApJ

Bond, J.R. & Couchman, H.M.P. 1988, in Proceedings of the Second Canadian Conference on General Relativity and Relativistic Astrophysics, ed. Coley, A.A. & Dyer, C. (Singapore: World Scientific), p. 385

Coles, P. 1990, MNRAS, 243, 171

Carlberg, R.G. & Couchman, H.M.P. 1989, ApJ, 340, 47

Couchman, H. M. P. & Rees, M. J. 1986, MNRAS, 221, 53

Davis, M. & Peebles, P. J. E. 1977, ApJS, 34, 425

Efstathiou, G. 1990, in Physics of the Early Universe, , ed. Peacock, J. A., Heavens, A. F. & Davies, A. T. (Bristol: IOP), p. 361

Efstathiou, G. & Rees, M. J. 1988, MNRAS, 230, 5P

Efstathiou, G., Frenk, C. S., White, S. D. M., & Davis, M. 1988, MNRAS, 235, 715

Evrard, A. E., & Crone, M. M. 1992, ApJ, 394, L1

Fisher, K. B., Davis, M., Strauss, M. A., Yahil, A., & Huchra, J. P. 1993, ApJ, 402, 42

Fry, J. N. 1984, ApJ, 279, 499

Gelb, J. M., & Bertschinger, E. 1993, submitted to ApJ

Goroff, M. H., Grinstein, B., Rey, S.-J. & Wise, M. B. 1986, ApJ, 311, 6

Grinstein, B. & Wise, M.B. 1987, ApJ, 320, 448

Gramann, M. 1992, ApJ, 401, 19

Gunn, J. E. & Gott, J. R. 1972, ApJ, 176, 1

Hoffman, Y. 1987, ApJ, 318, L7

Juszkiewicz, R. 1981, MNRAS, 197, 931

Juszkiewicz, R., Sonoda, R. H. & Barrow, J. D. 1984, MNRAS, 209, 139

Klypin, A. A. & Melott, A. A. 1992, ApJ, 399, 397

Little, B., Weinberg, D. H. & Park, C. 1991, MNRAS, 253, 307

Makino, N., Sasaki, M. & Suto, Y. 1992, Phys.Rev.D, 46, 585

Peebles, P. J. E. 1980, The Large-Scale Structure of the Universe, (Princeton: Princeton University Press)

Peebles, P. J. E. 1990, ApJ, 365, 207

Press, W. H. & Schechter, P. 1974, ApJ, 187, 425

Ryden, B. S. & Gramann, M. 1991, ApJ, 383, L33

Shandarin, S. F. & Melott, A. L. 1990, ApJ, 364, 396

Suto, Y. & Sasaki, M. 1991, Phys. Rev. Lett., 66, 264

Tegmark, M. & Silk, J. 1993, preprint

Vishniac, E. T. 1983, MNRAS, 203, 345

Vogeley, M. S., Park, C., Geller, M. J. & Huchra, J. P. 1992, ApJ, 391, L5

White, S. D. M. 1993, private communication

Zaroubi, S. & Hoffman, Y. 1993, ApJ, 414, 20

Zel'dovich, Ya. B. 1965, Adv. Astron. Ap., 3, 352

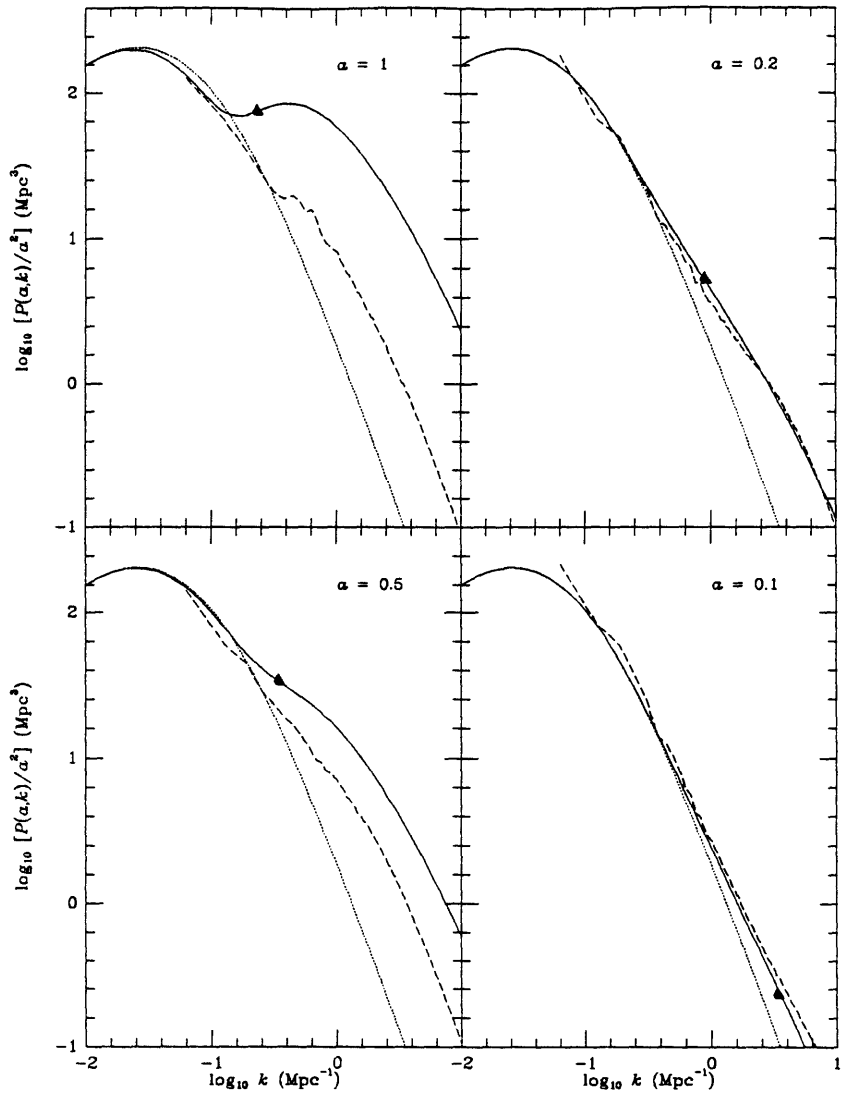

Figure 3-1 Linear and nonlinear power spectra at expansion factors $a = 0.1, 0.2, 0.5,$ and 1, where $a = 1$ corresponds to linear $\sigma_8 = 1$. The linear spectrum is given by the dotted curves, the corresponding second order spectrum $[P(k) = a^2 P_{11}(k) + a^4 P_2(k)]$ by the solid curves and the spectrum from high resolution N-body simulations by the dashed curve. The spectra are all divided by a^2 to facilitate better comparison of the nonlinear effects at different values of a. The triangles marked on the second order spectra indicate the point at which $a^4 P_2(k) = a^2 P_{11}(k)$: this indicates the approximate limit of validity of the second order results.

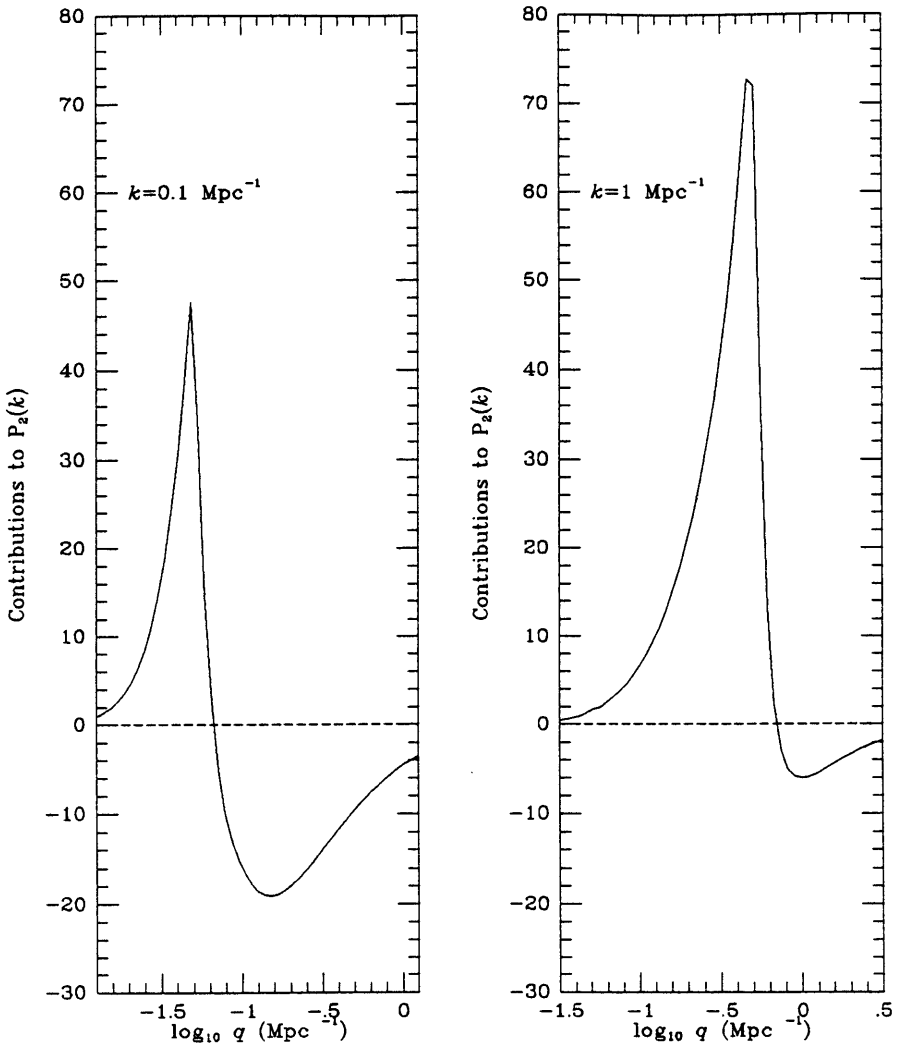

Figure 3-2 Contributions to $P_2(k)$ vs. $\log q$, where q is the magnitude of the integrated wavevector. The two panels are for different choices of k. $P_2(k)$ is defined in equation (3.15) and is the sum of the contributions $P_{22}(k)$ and $2P_{13}(k)$. The integrand of $P_{22}(k)$ is symmetric in $\vec{q}$ and $(\vec{k}-\vec{q})$; we have chosen to associate the contribution from such a pair of wavevectors with the wavevector with smaller magnitude. Other choices do not alter the basic trend seen here, namely, that the contribution from $q < k$ is generally positive and peaked at $q = k/2$, while that from $q > k$ is generally negative. Moreover, a comparison of the plots for the two values of k shown illustrates that at higher k the positive contribution from small q dominates, leading to a net enhancement of small-scale power. This is due to the increasing amount of power at $q < k$ for higher k, as can be seen in Figure 3-3.

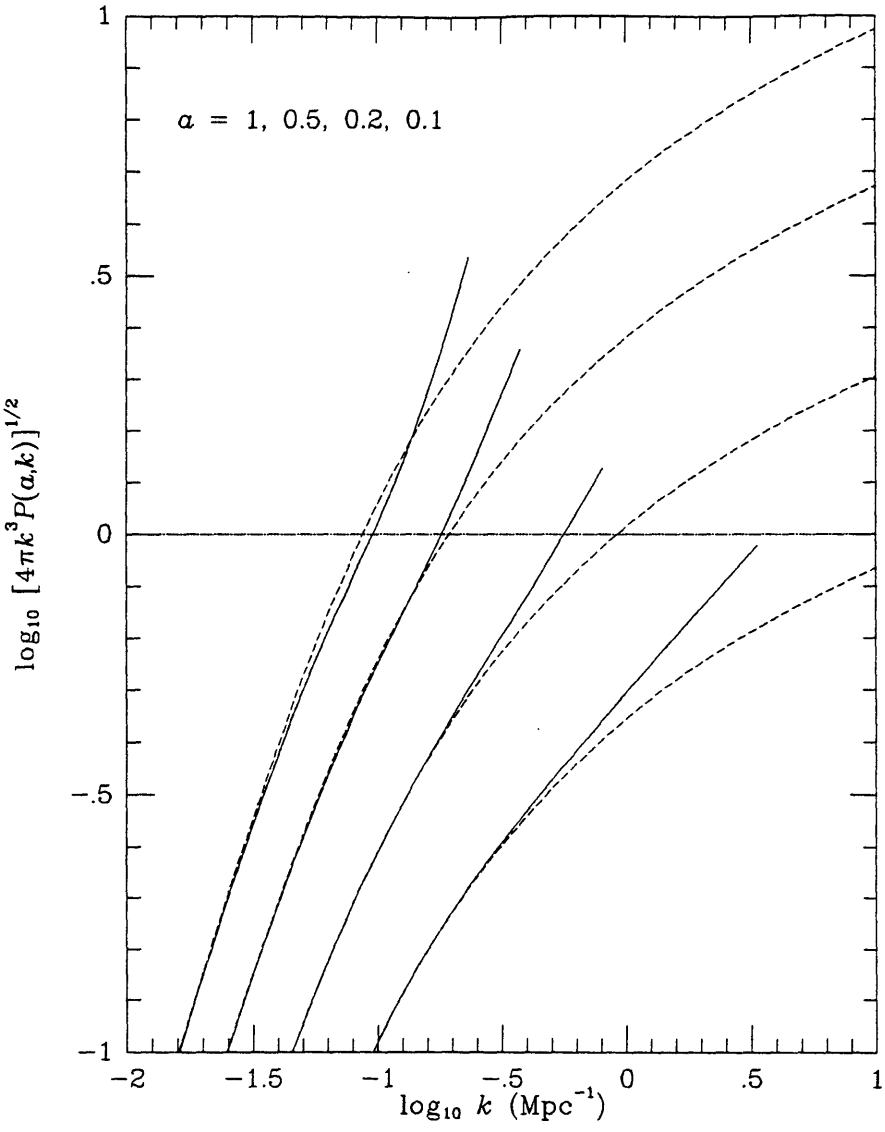

Figure 3-3 RMS amplitude of density fluctuations vs. scale k for several expansion factors. The lower curves correspond to smaller a. Solid (dashed) curves are used for the second order (linear) results. The second order curves are shown only for the estimated regime of validity shown in Figure 3-1. It is clear from the results at different a that the nonlinear contribution becomes significant at earlier a for successively smaller values of $[4\pi k^3 P(a,k)]^{1/2}$.

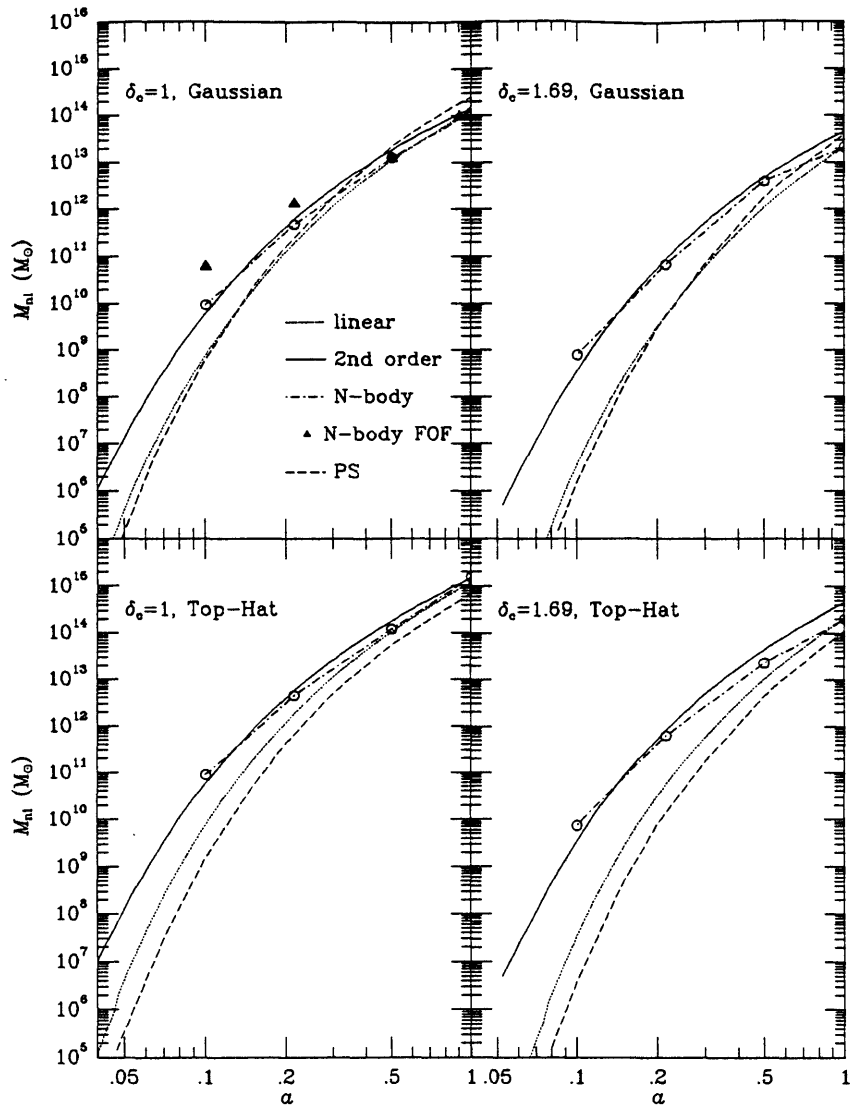

Figure 3-4 Growth of characteristic nonlinear mass with time. The mass scale $M_{\rm nl}(a)$ at which the rms $\delta\rho/\rho$ reaches a fixed value (denoted by δ_c in the figures) is plotted vs. the expansion factor $a = 1/(1+z)$. For each δ_c the rms $\delta\rho/\rho$ is computed with a gaussian window function for the upper panels, and with a real space top-hat for the lower panels. The dotted curves show $M_{\rm nl}(a)$ computed using the linear spectrum $P_{11}(k)$; the solid curves include the second order contribution for the same normalization of the linear spectrum. The dot-dashed curves have been computed from the N-body power spectrum shown in Figure 3-1. The dashed curves are computed using the Press-Schechter model, with the characteristic nonlinear mass defined as that at which a fixed fraction, 0.4, of the mass in nonlinear clumps is in clumps more massive than $M_{\rm nl}$. In the top-left panel the symbols labelled "N-body FOF" are obtained from the N-body simulation by using the friends-of-friends algorithm.

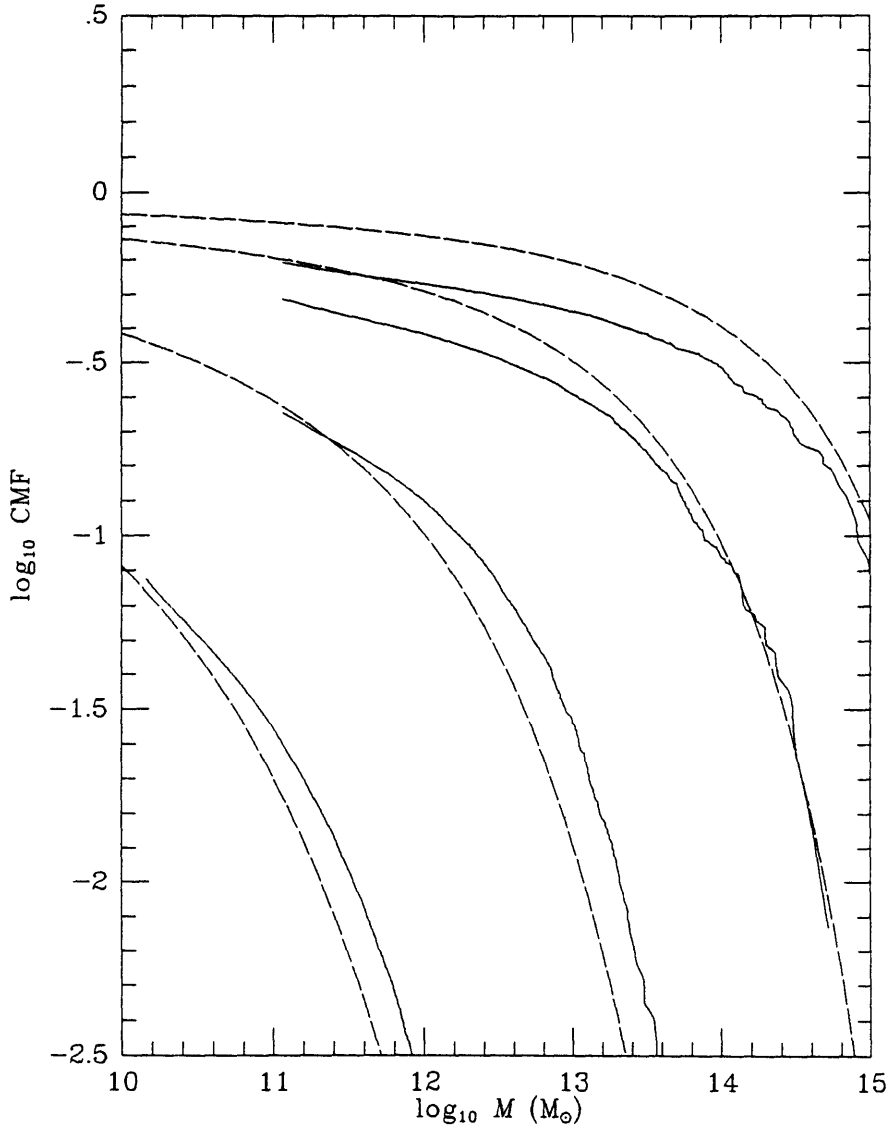

Figure 3-5 Cumulative mass fraction (CMF) vs. clump mass M at $a = 0.1, 0.2, 0.5, 1$. The dashed curves represent the predictions of the Press-Schechter model, while the solid curves are obtained from N-body simulations. The curves are shown at different times, with the higher curves representing larger values of a. The N-body curves are obtained using the friends-of-friends algorithm with linking parameter = 0.2.

Chapter 4

Self-Similar Scaling of Density Fluctuations

4.1 Introduction

A physical system is expected to display self-similar evolution if there is no preferred scale (in a sense to be clarified below) in the system, either in the initial conditions or in its dynamical behavior. The differential equations governing the evolution of such a system then admit of a self-similar solution. Suppose the basic evolution equation is a partial differential equation for the phase space density $f(\vec{x}, \vec{p}, t)$, where $\vec{x}$ is the spatial position, $\vec{p}$ is the momentum, and t is the time variable. In a self-similar system it is possible to re-cast the equation in a form with a solution $f = t^{\alpha}\, \hat{f}(\vec{x}/t^{\beta}, \vec{p}/t^{\gamma})$, where $\hat{f}$ is in general an unknown function. If α, β, and γ are known then the time dependence of f is present only through the rescaled $\vec{x}$ and $\vec{p}$ coordinates, aside from the overall factor of t^{α}. This special form of the solution is defined to be self-similar: the phase space density at time t_2 is related to that at time t_1 as

$$f(\vec{x}_2, \vec{p}_2, t_2) = \left(\frac{t_2}{t_1}\right)^{\alpha} f(\vec{x}_1, \vec{p}_1, t_1), \tag{4.1}$$

where $\vec{x}_1 = \vec{x}_2\,(t_1/t_2)^{\beta}$, and $\vec{p}_1 = \vec{p}_2\,(t_1/t_2)^{\gamma}$. Equation (4.1) explicitly demonstrates that the phase space density for any $(\vec{x}, \vec{p})$ at all times t_2 can be obtained merely by

re-scaling from some chosen time t_1. Clearly self-similarity is a powerful constraint because any statistical measure constructed from the the phase space density should be described by the appropriate scaling of coordinates consistent with equation (4.1).

We now consider the similarity properties of gravitational dynamics in a zero-pressure Einstein-de Sitter cosmology. An Einstein-de Sitter universe refers to the model with the cosmological density parameter $\Omega = \Omega_{matter} = 1$ and zero cosmological constant, so that the universe is spatially flat. The gravitational interaction also does not pick a special length scale. Further let the initial power spectrum be a power law, $P(k) \propto k^n$, over length scales of interest. Thus so far there is no preferred length scale in the system. However, the amplitude of the power spectrum can be used to define a characteristic physical length scale: the scale at which the rms smoothed density contrast equals unity is the conventional choice. To within an order of magnitude it is the scale at which over-densities collapse out of the background expansion. Hence it forms the boundary between two qualitatively different regimes in the universe. As we shall see below, it provides the reference scale required for scaling the spatial variable according to the similarity solution.

The explicit similarity transformation for the single particle phase space density $f(\vec{x}, \vec{p}, t)$ is described in Section 73 of Peebles (1980). It is also shown that knowing the linear solution is sufficient to fix the indices α, β and γ in terms of the spectral index n of the initial spectrum. The resulting self-similar scaling of spatial length scales x, and wavenumber scales k is:

$$x_{ss}(t) \propto a(t)^{2/(3+n)} \;\; ; \;\; k_{ss}(t) \sim x_{ss}(t)^{-1} \propto a(t)^{-2/(3+n)}. \tag{4.2}$$

The similarity solution for f is obtained by dimensional analysis of the differential equation describing its evolution. Whether or not the solution applies depends on the initial conditions. The initial fluctuations in cosmology are believed to be generated by a stochastic process which is statistically homogeneous and isotropic in space. For a given realization, the stochasticity of the initial distribution in space precludes the similarity solution for f from being valid. For all practical purposes, however, it is

sufficient that the ensemble averages (averages across different independent realizations) of f, or products of f for more than one particle, evolve self-similarly. This does happen because ensemble averaging removes the stochastic character of the initial conditions. Consequently statistical measures such as the correlation function ($\xi(x,t) \propto \int d^3p_1 \int d^3p_2 \langle f(1)f(2)\rangle$, where the indices 1 and 2 refer to two different particles) evolve self-similarly. The self-similar solution for ξ is obtained from the formal solution for f. The solution can be verified by dimensional analysis of the evolution equation for ξ that is obtained by taking moments of the BBGKY hierarchy equations (e.g., equation (71.1) of Peebles (1980)). The solution for the power spectrum is obtained by Fourier transforming $\xi(x,t)$, and is $P(k,t) = a^{3\alpha} k_0^{-3} \hat{P}(ka^\alpha/k_0)$, where $\alpha = 2/(3+n)$, k_0 is a constant which must be determined from the initial conditions, and $\hat{P}$ is an unspecified dimensionless function. It is easy to verify that the linear spectrum $P_{11}(k,\tau) \propto a^2 k^n$ is consistent with this functional form.

Likewise the scaling of all statistical measures defined as ensemble averages of products of f (and of their momentum moments), can be straightforwardly determined. Using the ergodic theorem the solutions for ensemble averages can then be applied to averages over sufficiently large volumes in space. A spatial statistic which follows the self-similar solution is a function of the spatial variable scaled by a power of time, rather than of time and space separately. This provides for a self-similarity in time (in this statistical sense) in the evolution of structure.

As discussed above, at every epoch there is a scale which demarcates the linear and nonlinear regimes. In wavenumber space this scale, denoted by k_δ, is given by the condition $k_\delta^3 P(k_\delta, t) \sim 1$ for $-3 < n < 1$. If the linear power spectrum, $a^2 P_{11}(k)$ is used as an approximation to $P(k,t)$, then it can be checked that the self-similar scaling of equation (4.2) is recovered for $k_\delta(t)$ as follows: $k^3 P(k,t) \sim k_\delta^3 a^2 k_\delta^n \sim 1$, or $k_\delta \propto a^{-2/(3+n)}$. By applying this condition at the initial time t_i, the constant k_0 can be related to the nonlinear wavenumber at the initial time $k_\delta(t_i)$. For most realistic cosmological spectra the density contrast increases with decreasing length scale; hence even at the initial time, on sufficiently small length scales [or wavenumber scales $k \gg k_\delta(t_i)$], the density contrast is larger than unity. Therefore in order to use self-

similar scaling to determine the complete future evolution, the initial conditions have to be such that a sufficient amount of nonlinear evolution has already occurred. One usually imagines a hierarchy of nonlinear structures on small length scales, and linear structures on the largest length scales. Then the system is believed to evolve such that by scaling the transition scale k_δ from the linear to the nonlinear regime (and all other scales as well) via equation (4.2), its complete evolution can be obtained. Clearly, to implement such a self-similar scaling, the full range of nonlinear clustering must be present on small enough scales from the outset. In practice, N-body simulations show that even though such conditions are not implemented (they would require knowing the full nonlinear solution), the system relaxes to self-similar behavior inclusive of fully nonlinear structures.

The discrete nature of particles introduces a scale, namely the mean interparticle separation, which breaks the idealized self-similar scaling of a perfect fluid. Such a departure from perfect self-similarity is typical of all realistic physical systems. The notion of intermediate asymptotic self-similarity, i.e., self-similar scaling over a restricted range of parameters, is used in such situations (Barenblatt 1979). In the cosmological context it simply means that the range of length scales over which self-similar scaling is accurately followed are restricted to be sufficiently larger than the interparticle separation (and in the case of N-body simulations, other scales introduced for numerical reasons).

Intermediate asymptotic self-similarity is a useful property even for realistic cosmological spectra like the CDM spectrum which are not scale free. As described in Chapter 1 the physical processes at work in the radiation dominated era imprint characteristic length scales on the spectrum. These spectra are nevertheless approximate power laws on a restricted range of k, over which their evolution may be well described by the similarity solution for the corresponding scale free spectrum. Thus the CDM spectrum has $n \simeq -2$ on galactic scales and $n \simeq -1$ on cluster/supercluster scales; therefore the study of scale free spectra with $-1 \lesssim n \lesssim -2$ is relevant for understanding the development of large scale structure in a CDM-like model. Another important practical application of similarity solutions is to use them to check the

validity of N-body simulations even in the deeply nonlinear regime.

An aspect of self-similarity which merits attention is the range of n, the spectral index of the initial spectrum, for which the statistics characterizing the growth of perturbations are well defined. More precisely, n must be restricted from below and above to prevent statistical measures of interest from diverging as the size of the system is made infinitely large and the interparticle spacing made infinitesimally small, respectively. In a finite system such a divergence is manifested by the influence of the largest (smallest) scales on the evolution of all intermediate scales of the system. This influence increases as the size of the system is made larger (smaller), and thereby breaks any possible self-similar scaling. This occurs (in spite of the initial conditions being scale free) if either the statistic is ill defined even in the initial configuration, or the dynamical influence of increasingly large or small scales is unbounded. If the former is true in an otherwise reasonable initial configuration, then it must mean that the particular statistic is not a suitable measure of the properties of the system (similar to the case of well behaved probability distributions having ill-defined moments). However, if the breaking of self-similarity is due to a divergent dynamical effect in a statistic of interest then it bears closer examination. The goal of this work is to examine the possible breaking of self-similar evolution for power law initial spectra with a view to assessing its influence on the formation of structre.

Early studies of self-similar evolution in cosmology include those of Peebles (1974); Press & Schechter (1974); Davis & Peebles (1977); and Efstathiou & Eastwood (1981). Davis & Peebles (1977) made a detailed analysis of the BBGKY hierarchy equations and presented solutions for the deeply nonlinear regime based on the stable clustering ansatz. Efstathiou et al. (1988) tested self-similar scaling in N-body simulations of scale free spectra with $n = -2, -1, 0, 1$. They examined the scaling of the correlation function $\xi(x,t)$, and of the multiplicity function describing the distribution of bound objects. They verified the predicted scaling for both statistics, and found consistency with the picture of hierarchical formation of nonlinear structure on increasingly large length scales. Their results for $n = -2$ did not match with the self-similar scaling as well as the other cases. Bertschinger & Gelb (1991) used better resolution simulations

to address these questions and also found similar results. These authors concluded that the reason for the weakness of the $n = -2$ results was the finite size of their simulation box, as the $n = -2$ case has the more power on large scales and therefore requires a larger box-size to approximate the infinite volume limit with the same accuracy as larger values of n.

The N-body results of Ryden & Gramann (1991), and Gramann (1992) suggested that the $n = -2$ case was different for a more fundamental reason. They studied $n = -1$ simulations in two dimensions, which are the analog of $n = -2$ in three dimensions, and examined the scaling of the phase (Ryden & Gramann 1991), and then both phase and amplitude (Gramann 1992) of the Fourier transform of the density field. The scaling was found to be different from the standard self-similar scaling. Characteristic wavenumber scales, instead of following the self-similar scaling, given in two dimensions by, $k_{ss}(t) \propto a(t)^{-2/(2+n)} \propto a(t)^{-2}$, showed the scaling $k \propto a(t)^{-1}$. They pointed out that this scaling would be obtained if the linear bulk velocity field were used to define characteristic scales, as opposed to the conventional choice of using the rms $\delta\rho/\rho$. Other studies in two dimensions also suggest that a transition in nonlinear evolution occurs at $n = -1$ (Klypin & Melott 1992).

It has been noted all along in the literature that the bounds on n for the self-similar solution to be applicable are $-1 < n < 1$. The requirements of an upper (lower) limit are made to prevent the single particle velocity dispersion from diverging due to contributions from small (large) length scales. These bounds on n are clearly stated as the domain of applicability of self-similar scaling in Peebles & Davis (1977), Efstathiou et al. (1988), and in the recent review of Efstathiou (1990). However, it appears to be implicitly believed that self-similar scaling is applicable for $n > -3$, rather than $n > -1$. This is because the divergence of the peculiar velocity field need not be an indication of unbounded growth of perturbations. The primary quantity that measures perturbation growth is the rms density contrast which is indeed convergent in linear theory for $n > -3$ as $k \to 0$ ($\delta\rho/\rho \sim a^2 k^{3+n}$). Thus Peebles (1993, p. 545) presents the standard self-similar scaling as being applicable for $-3 < n < 4$ (increasing the upper limit from $n = 1$ to $n = 4$ relies on the asymptotic behavior of

second order contributions to the density). Efstathiou (1990) is more cautious, but nevertheless hopes that: "If n lies outside this range (i.e., $-1 < n < 1$), the clustering may still approximate self-similar evolution over restricted ranges of length and time, although $n > -3$ is required to ensure that clustering proceeds from small to large scales."

To summarize, there is no clear answer on the issue of self-similar scaling for $-3 < n < -1$, in part due to conflicting results from N-body simulations: while three dimensional simulations have arguably shown consistency with standard self-similar scaling, the results of some two dimensional studies (which are numerically more convincing) point to a breaking of this scaling. Aside from the observation that the linear peculiar velocity field diverges but the linear density contrast does not, there are no analytical analyses of this issue. Our goal is to analyze the dynamics of the coupling of long wave modes by analytical and N-body techniques to address this question. One must bear in mind that the answer can depend on the particular statistic used to pose the question. For the purposes of structure formation the question of real interest concerns the self-similar growth of the density contrast. Therefore our attempt will be to identify the statistical measures that relate to the growth of density perturbations and examine their scaling behavior.

Section 4.2 provides a more detailed assessment of whether $-3 < n < -1$ is expected to yield self-similar evolution on the basis of simple dynamics. We argue that the issue can only be settled by a full consideration of the dynamical coupling of long wave modes, rather than by studying the convergence of particular statistics using linear solutions. In our analysis we shall work with the Fourier space density field as it quantifies the relative amounts of power on different scales most directly. In Section 4.3 we use perturbation theory to study self-similar scaling. We begin in Section 4.3.1 by formulating perturbation theory in a way that obeys this scaling at every order provided there are no long wave divergences. Next, in Section 4.3.2 we demonstrate that there are potentially divergent perturbative terms, but the leading order contributions exactly cancel out. Section 4.4 presents an alternative, non-perturbative approximation to estimate the coupling of long wave modes. The analytical results

obtained in this section are compared with results of N-body simulations in Section 4.5. Using high resolution simulations the scaling of the phase and amplitude is studied and kinematical effects which do not affect perturbation growth are distinguished from dynamical ones which do. In the light of this, the questions of good and bad statistics in the context of self-similar scaling are addressed. Some general aspects of the study of nonlinear phases are also explored. We conclude in Section 4.6.

4.2 Long Wave Divergences for $n < -1$

We suppose for simplicity that the matter distribution after recombination may be approximated as a pressureless fluid with no vorticity. We further assume that peculiar velocities are nonrelativistic and that the wavelengths of interest are much smaller than the Hubble distance cH^{-1} so that a nonrelativistic Newtonian treatment is valid. We shall work with comoving coordinates $\vec{x}$ and conformal time $d\tau = dt/a(t)$, where $a(t)$ is the expansion scale factor. The proper peculiar velocity, $\vec{v} \equiv d\vec{x}/d\tau$ is taken to be a potential field, so that, up to an arbitrary constant, it is fully specified by its divergence, $\theta \equiv \vec{\nabla} \cdot \vec{v}$. We assume an Einstein-de Sitter universe, with $a(\tau) = (H_0\tau/2)^2$, where H_0 is the present day value of the Hubble parameter. We will also assume that the initial density fluctuation field, $\delta(\vec{x}) \equiv \delta\rho(\vec{x})/\bar{\rho}$, is a Gaussian random field. Its Fourier transform is defined as $\delta(\vec{k},\tau) = \int d^3x/(2\pi)^3\, e^{-i\vec{k}\cdot\vec{x}}\, \delta(\vec{x},\tau)$, and similarly for $\theta(\vec{k},\tau)$. The power spectrum (spectral density) of $\delta(\vec{x},\tau)$ is defined by $\langle \delta(\vec{k},\tau)\, \delta(\vec{k}',\tau) \rangle = P(k,\tau)\, \delta_{\rm D}(\vec{k}+\vec{k}')$, where $\delta_{\rm D}$ is the Dirac delta function.

These approximations and the cosmological fluid equations for a self-gravitating fluid that follow are described in detail in Section 3.2.1. Fourier transforming equations (3.1) gives:

$$\frac{\partial \delta}{\partial \tau} + \theta = -\int d^3k_1\, \frac{\vec{k}\cdot\vec{k}_1}{k_1^2}\, \theta(\vec{k}_1,\tau)\, \delta(\vec{k}-\vec{k}_1,\tau)\ , \tag{4.3a}$$

$$\frac{\partial \theta}{\partial \tau} + \frac{\dot{a}}{a}\,\theta + \frac{6}{\tau^2}\,\delta = -\int d^3k_1\, k^2 \frac{\vec{k}_1\cdot(\vec{k}-\vec{k}_1)}{2k_1^2|\vec{k}-\vec{k}_1|^2}\, \theta(\vec{k}_1,\tau)\, \theta(\vec{k}-\vec{k}_1,\tau)\ . \tag{4.3b}$$

The fields on the left-hand side are all functions of $\vec{k}$ and τ. The nonlinear terms on the right-hand side of the above equations represent the coupling of modes at all pairs of wavevectors $(\vec{k}_1,\ \vec{k}-\vec{k}_1)$, which influence the evolution of δ and θ at the fixed external wavevector $\vec{k}$.

In order to study the limiting behavior as one of the pair of wavevectors $(\vec{k}_1, \vec{k}-\vec{k}_1)$ approaches 0 in magnitude (i.e., as the wavelength $\lambda = 2\pi/k$ is made infinitely large), consider the variance of the nonlinear terms. For simplicity we take $k_1 \rightarrow 0$ in the integral on the right-hand side of equation (4.3a). Approximating $(\vec{k}-\vec{k}_1)$ by $\vec{k}$, dropping the dependence on τ, and denoting the resulting variance by $\psi(k)$ we obtain:

$$\begin{aligned}\psi(k) \ &\simeq \ \left\langle \int d^3k_1 \, \frac{\vec{k}\cdot\vec{k}_1}{k_1^2}\,\theta(\vec{k}_1)\,\delta(\vec{k}) \ \int d^3k_2 \, \frac{\vec{k}\cdot\vec{k}_2}{k_2^2}\,\theta^*(\vec{k}_2)\,\delta^*(\vec{k}) \right\rangle , \\ &= \int d^3k_1 \int d^3k_2 \, \frac{\vec{k}\cdot\vec{k}_1}{k_1^2}\,\frac{\vec{k}\cdot\vec{k}_2}{k_2^2}\,\left\langle \theta(\vec{k}_1)\,\theta^*(\vec{k}_2)\,\delta(\vec{k})\delta^*(\vec{k}) \right\rangle . \qquad (4.4)\end{aligned}$$

Now we make the further approximation of taking k_1 small enough that the linear solutions are valid, thus giving:

$$\delta(\vec{k}_1,\tau) \simeq a(\tau)\delta_1(\vec{k}_1) \ ; \ \theta(\vec{k}_1,\tau) \simeq -\dot{a}(\tau)\delta_1(\vec{k}_1) . \qquad (4.5)$$

Substituting the expression for $\theta(\vec{k}_1,\tau)$ in equation (4.5) into equation (4.4) and evaluating the ensemble average using the properties of Gaussian random fields we finally obtain:

$$\psi(k) \simeq \dot{a}^2\delta_{\rm D}(0)P(k)\int d^3k_1 \left(\frac{\vec{k}\cdot\vec{k}_1}{k_1^2}\right)^2 P_{11}(k_1) \simeq \dot{a}^2\delta_{\rm D}(0)P(k)\,k^2\int dk_1 P_{11}(k_1) . \quad (4.6)$$

Note that in expressing the 4−point moment of equation (4.4) in terms of $P(k)$ and $P_{11}(k_1)$ we have assumed that $\delta(\vec{k})$ is a Gaussian random field as well. It is straightfoward to demonstrate that the right-hand side of equation (4.3b) takes the limiting form shown in equation (4.6) as well.

Equation (4.6) indicates that if $P_{11}(k_1) \propto k_1^n$ with $n < -1$, then the right-hand side

diverges due to contributions from low k_1. Thus a simple examination of the nonlinear terms in the cosmological fluid equations by substituting the initial distribution of the density and velocity field demonstrates the possibility of long wave divergences. These divergences can potentially be present in solutions for $\delta(\vec{k},\tau)$ and $\theta(\vec{k},\tau)$ obtained from these equations. It is not possible to make any definitive statements, however, because these are two coupled differential equations — it is necessary to first separate the equations for δ and θ, and then identify the nonlinear terms that affect the amplitude and phase of each quantity (since they are complex variables) to determine whether the divergent terms affect a particular statistic of interest. This is done in two different ways in Sections 4.3 and 4.4.

Before proceeding with a formal analysis of the divergent nonlinear pieces, we make the connection between the divergent nonlinear terms to the advective $(\vec{v}\cdot\vec{\nabla})$ terms in the real space equations. By tracing back the nonlinear terms on the right-hand side of equations (4.3) to the fluid equations in real space it can be seen that the terms which contribute to equation (4.4) arise from the $\vec{v}\cdot\vec{\nabla}\delta$ and $\vec{v}\cdot\vec{\nabla}\vec{v}$ terms. It is easy to see why such terms should diverge by examining the relation of the power spectrum of the peculiar velocity to that of the density in linear theory. Using the linear solutions of equation (4.5) and the definition $\theta(\vec{x},\tau)=\vec{\nabla}\cdot\vec{v}(\vec{x},\tau)$, gives,

$$P_{11\,v}(k,\tau)=\dot{a}^2P_{11}(k)/k^2, \tag{4.7}$$

where $P_{11\,v}(k)$ is the linear power spectrum of the peculiar velocity. The rms bulk velocity on a scale $x\sim k^{-1}$, $v_b(x,\tau)$, is given by integrating $P_v(k)$ over k with a window function $W(kx)$ (just as one integrates over $P(k)$ for the rms smoothed density contrast):

$$v_b(x,\tau)^2=\int d^3kP_{11\,v}(k,\tau)W^2(kx)=\dot{a}^2\,4\pi\int dkP_{11}(k)W^2(kx). \tag{4.8}$$

Since $W(kx)\rightarrow 1$ as $k\rightarrow 0$ (see for example the top-hat window function in equation (3.24b)), the integral on the right-hand side of equation (4.8) diverges at low k for $n<-1$ in the same manner as the integral in equation (4.6). Thus via the advective

$(\vec{v}\cdot\vec{\nabla})$ terms in the fluid equations, the divergence of the nonlinear terms demonstrated in equation (4.6) can be traced to the bulk velocity field on a given scale receiving divergent contributions from $k \to 0$, i.e., from the long wavelength modes.

We can now understand why this divergence may not affect self-similar scaling: the bulk velocity field does not in general have any influence on the growth of perturbations on small scales. In particular, large contributions to the bulk velocity field from long wave modes correspond to an almost uniform translation of the fluid, and therefore should not couple to the evolution of δ at all. This reasoning, and indeed the entire analysis of this section, relies on making plausible connections of linearized statistics for δ and $\vec{v}$ to their nonlinear dynamics. Therefore, while it provides a useful guide to one's intuition, it does not substitute for a rigorous examination of the nonlinear dynamics.

4.3 Self-Similarity and Perturbation Theory

4.3.1 Formalism

The basic formalism for perturbation theory has been developed in Section 3.2. Here we use that formalism to explicitly show that, in the absence of long wave divergences, perturbative contributions to the power spectrum preserve the standard self-similar scaling of equation (4.2). At sufficiently small scales $\delta\rho/\rho > 1$ even at the earliest times — hence the perturbative expansion breaks down at these scales. This means that even in the absence of a divergence as $k \to \infty$, a high-k cutoff, k_u, must be used to truncate the perturbative integrals. The requirement of a cutoff restricts the nonlinear effects that can be studied perturbatively. Nonlinear contributions *from* wavenumbers $q > k_u$ cannot be evaluated, but the contribution *to* any k (from all $q < k_u$) are calculable.

It is interesting to note that provided the contributions to $P(k)$ from low q are convergent, a perturbative expansion can be consistently defined such that the self-similar scaling of equation (4.2) is obeyed. This is achieved by defining the high-

k cutoff k_u to be time dependent such that: $k_u(\tau) \propto k_{ss}(\tau) \propto a^{-2/(3+n)}$. With this scaling, we now show that at all orders in perturbation theory the nonlinear contribution to the power spectrum takes a self-similar form with characteristic scales, denoted by $k_c(\tau)$, obeying $k_c(\tau) \propto a^{-2/(3+n)}$. This should not be surprising since, once $k_u(\tau)$ is chosen to scale with $k_{ss}(\tau)$, there is no other scaling in the problem. We proceed by obtaining the functional dependence of perturbative contributions on k and τ, without needing to know them explicitly. Without loss of generality, consider the contribution to $P(k,\tau)$ from the term $\langle \delta_m(\vec{k},\tau)\, \delta_{l-m}(\vec{k}',\tau)\rangle$, with $0 < m < l$, and l being even. This contribution is denoted $P_{m,l-m}(k,\tau)$ and is defined in equation (3.13). We substitute for δ_l and δ_m in equation (3.13) to obtain:

$$P_{m,l-m}(k,\tau) = a^l \int d^3q_1 \ldots d^3q_{(l-2)}\, \langle \hat{\delta}_1(\vec{q}_1) \ldots \delta_1(\vec{k} - \vec{q}_1 - \ldots - \vec{q}_{m-1})\, \delta_1(\vec{q}_m) \ldots \delta_1(\vec{k} - \vec{q}_m - \ldots - \vec{q}_{(l-2)}) \rangle\, M_1(\vec{q}_1, \ldots, \vec{q}_{(l-2)}, \vec{k}), \qquad (4.9)$$

where M_1 is a dimensionless function of $F_m^{(s)}$ and $F_{l-m}^{(s)}$, which are defined in equations (3.10). Note that we have already set the arguments of the two δ's opposite to each other, so that the expression on the right-hand side above has dimensions of a power spectrum. On taking the ensemble average, the $(l-2)$ independent phase factors contained in the functions $\delta_1(q_i)$ must cancel pairwise for the result to be non-zero (recall that the δ_1's are taken to be independent Gaussian random variables). Thus we obtain $(l-2)/2$ Dirac-delta functions which reduce the number of integration variables to $(l-2)/2$. $l/2$ powers of $P_{11}(q_i) = Aq_i^n$ are also present. Collecting the relevant factors which provide the k and τ dependence, and imposing the high-k cutoff $k_u(\tau)$, we obtain

$$P_{m,l-m}(k,\tau) = a^l\, k^{3(l-2)/2+nl/2}\, M_2(k_u(\tau)/k), \qquad (4.10)$$

where M_2 is another dimensionless function. Taking $k_u(\tau) = \eta a^{-2/(3+n)}$, where η is a constant, and introducing a new dimensionless function M_3, we finally obtain

$$P_{m,l-m}(k,\tau) = a^{6/(3+n)}\, M_3(k\,\eta a^{2/(3+n)}). \qquad (4.11)$$

Equation (4.11) gives the desired self-similar form for characteristic scales $k_c(\tau)$ defined by setting $k^3P(k,\tau) = 1$: $k_c(\tau) \propto a^{-2/(3+n)}$ in agreement with equation (4.2).

Thus at every order in perturbation theory the self-similar scaling of the power spectrum, and therefore of physical measures of perturbation growth such as the smoothed density contrast in real space constructed from it, is preserved. However, this scaling is broken if the perturbative integrals diverge as $k \to 0$, thus requiring a low-k cutoff. This possibility is considered next.

4.3.2 Long Wave Divergences in Perturbative Contributions

We showed in Section 3.2 that at second order in the power spectrum there are terms that are divergent for $n < -1$ due to the contribution from $k \to 0$. The two however cancel each other. This cancellation does not prove there is no divergence in the power spectrum. We must investigate higher-order terms $\delta_l(\vec{k})$. It is tedious to evaluate the full expressions for δ_l for $l > 2$ and then to form the power spectrum contributions $P_{m,l-m}(k)$. However, we do not need the exact nonlinear power spectrum if we are interested only in determining whether leading-order long wave divergences are canceled. In this case, it is sufficient to work from the outset with only the leading-order divergent parts of $\delta_l(\vec{k})$.

Iterating equations (3.7) and (3.8), one finds that the leading-order divergences arise from the term with $m = 1$ in equations (3.7), with the contribution doubled in equation (3.7b) because of the term $m = l - 1$. The leading-order divergent contributions are then

$$A_l(\vec{k}) \sim \delta_{l-1}(\vec{k})\,\zeta(\vec{k})\,, \quad B_l(\vec{k}) \sim 2\theta_{l-1}(\vec{k})\,\zeta(\vec{k})\,, \quad \zeta(\vec{k}) \equiv \int d^3q\,\frac{\vec{k}\cdot\vec{q}}{q^2}\,\delta_1(\vec{q})\,. \tag{4.12}$$

The leading-order divergence appears at $q = 0$ in the function $\zeta(\vec{k})$. Using equation (3.8) and iterating we now get the leading-order divergences of δ_l and θ_l:

$$\delta_l(\vec{k}) \sim \theta_l(\vec{k}) \sim \frac{\zeta^{l-1}(\vec{k})}{(l-1)!}\,\delta_1(\vec{k})\,. \tag{4.13}$$

From equations (3.13) and (4.13) we arrive at the leading-order divergent part of $P_{m,l-m}$:

$$P_{m,l-m}(\vec{k}) \sim \frac{(-1)^{m-1}\left\langle \zeta^{l-2} \right\rangle}{(m-1)!\,(l-m-1)!}\, P_{11}(k)\,, \tag{4.14}$$

where

$$\left\langle \zeta^{l-2} \right\rangle = (l-3)!!\, k^{l-2} \left[-\int \frac{d^3q}{3q^2}\, P_{11}(q) \right]^{(l-2)/2} . \tag{4.15}$$

The net contribution to the leading-order divergent part of the nonlinear power spectrum (3.12) is

$$P(k,\tau) \sim a^2(\tau)\, P_{11}(k) \sum_{m=2}^{\infty} \frac{a^{l-2}(\tau)\left\langle \zeta^{l-2} \right\rangle}{(l-2)!} \sum_{m=1}^{l-1} \frac{(-1)^{m-1}(l-2)!}{(m-1)!\,(l-m-1)!} . \tag{4.16}$$

Now, the sum over m is just the binomial expansion of $(1-1)^{l-2}$. Therefore, the sum vanishes for $n > 2$ and the leading-order divergences cancel at every nonlinear order of perturbation theory!

This surprising result does not prove that $P(k,\tau)$ is finite, however. Equation (4.13) gives only the most divergent contribution to $\delta_l(\vec{k})$, ζ^{l-1}. Terms diverging as ζ^{l-2} or more slowly have been neglected. The nonlinear power spectrum may still have an n-point contribution that diverges as $\langle \zeta^{l-4} \rangle$. The lowest order at which such sub-dominant divergences would appear is $l = 6$: $P = a^6(P_{15} + P_{24} + P_{33} + P_{42} + P_{51})$.

Let us gather together the ingredients needed for evaluating the nonlinear 6-point contribution to the power spectrum. Using equations (3.9a) and (3.13), we get

$$P_{15}(k) = 15 P_{11}(k) \int d^3q_1\, P_{11}(q_1) \int d^3q_2\, P_{11}(q_2)\, F_5^{(s)}(\vec{q}_1, -\vec{q}_1, \vec{q}_2, -\vec{q}_2, \vec{k})\,, \tag{4.17}$$

$$\begin{aligned} P_{24}(k) = 12 \int d^3q_1 \;\; & P_{11}(q_1) \int d^3q_2 P_{11}(q_2)\, P_{11}(|\vec{k} - \vec{q}_2|)\, F_4^{(s)}(\vec{q}_1, -\vec{q}_1, \vec{q}_2, \vec{k} - \vec{q}_2) \\ & \times F_2^{(s)}(-\vec{q}_2, \vec{q}_2 - \vec{k})\,, \end{aligned} \tag{4.18}$$

$$P_{33}(k) \;\; = \;\; 9 P_{11}(k) \int d^3q_1\, P_{11}(q_1) \int d^3q_2\, P_{11}(q_2)\, F_3^{(s)}(\vec{q}_1, -\vec{q}_1, \vec{k})\, F_3^{(s)}(\vec{q}_2, -\vec{q}_2, -\vec{k})$$

$$+6\int d^3q_1 P_{11}(q_1)\int d^3q_2\, P_{11}(q_2)\, P_{11}(|\vec{k}-\vec{q}_1-\vec{q}_2|)$$
$$\times F_3^{(s)}(\vec{q}_1,\vec{q}_2,\vec{k}-\vec{q}_1-\vec{q}_2)\, F_3^{(s)}(-\vec{q}_1,-\vec{q}_2,\vec{q}_1+\vec{q}_2-\vec{k})\ . \qquad (4.19)$$

The factors of 15, 12, 9 and 6 in equations (4.17)–(4.19) come from the number of equivalent graphs obtained by relabeling the internal wavevectors, assuming that $F^{(s)}$ and $G^{(s)}$ are fully symmetric in all their arguments.

To make further progress we must evaluate F_3, F_4, and F_5. With increasing l, the full expression for $F_l(\vec{q}_1,\ldots,\vec{q}_l)$ rapidly becomes unwieldy. We have attempted to evaluate some of the divergent terms in equations (4.17)–(4.19). By examining the form of the sub-dominant divergent parts of the contributing terms, it appears that the second term in P_{33} must cancel with the divergent part of P_{24} as $q_1 \to 0$ (and the other terms shown must cancel separately), if the net contribution at this order is to be convergent. We evaluated these divergent pieces using the "Maple" package for symbolic mathematics, and had tentatively concluded that the two terms did not cancel. However we were not able to check our calculations, and due to the computational complexity involved, did not pursue them further.

The results from the analysis of perturbation theory are therefore not conclusive. The cancellation of leading divergences is certainly suggestive of an underlying kinematical effect which appears in the power counting assessment of the divergence, but cancels out on computing the net dynamical influence on the power spectrum. We will interpret this cancellation by examining the phase of $\delta(\vec{k})$ in Section 4.4. However it is not feasible to evaluate all the divergent terms at arbitrary order in perturbation theory, therefore we pursue a somewhat different approximation to evaluate long wave mode coupling in the next section.

4.4 Analytic Approximation for Long Wave Mode Coupling

The approach in this section relies on assuming that the nonlinear terms in the Fourier space cosmological fluid equations (4.3) are dominated by the coupling of long wave modes. With this ansatz the mode coupling contribution is estimated and then checked for self-consistency. This allows us to obtain a leading order solution for the phase shift as described in Section 4.4.1. To make further progress we need to make the additional assumption that at low k, the Fourier space density and velocity fields are continuous and therefore amenable to a Taylor series expansion. This analysis is presented in Section 4.4.2, and its limitations are discussed.

4.4.1 Solution for the Phase Shift

In equations (4.3) the integrands on the right-hand side involve products of δ and θ evaluated at $\vec{k}_1$ and $(\vec{k}-\vec{k}_1)$. Let

$$\delta(\vec{k}-\vec{k}_1) = \delta(\vec{k}) + \epsilon(\vec{k},\vec{k}_1) \;\; ; \;\; \theta(\vec{k}-\vec{k}_1) = \theta(\vec{k}) + \omega(\vec{k},\vec{k}_1)\,, \tag{4.20}$$

where ϵ and ω are unknown functions. In this section we shall use "function" to refer to random valued fields as well. We shall also suppress the time dependence of $\delta(\vec{k},\tau)$ and of $\theta(\vec{k},\tau)$ for convenience (though when we introduce the linear solutions the τ dependent part will be explicitly written). Substituting equation (4.20) into equations (4.3) gives,

$$\frac{\partial\delta(\vec{k})}{\partial\tau} + \theta(\vec{k}) = -\int d^3k_1\,\theta(\vec{k}_1)\,\frac{\vec{k}_1\cdot\vec{k}}{k_1^2}\,\left[\delta(\vec{k}) + \epsilon(\vec{k},\vec{k}_1)\right] \equiv A(\vec{k}), \tag{4.21a}$$

$$\frac{\partial\theta(\vec{k})}{\partial\tau} + \frac{\dot{a}}{a}\,\theta(\vec{k}) + \frac{6}{\tau^2}\,\delta(\vec{k}) = -\int d^3k_1\,k^2\frac{\vec{k}_1\cdot(\vec{k}-\vec{k}_1)}{2k_1^2|\vec{k}-\vec{k}_1|^2}\theta(\vec{k}_1)\,\left[\theta(\vec{k}) + \omega(\vec{k},\vec{k}_1)\right] \equiv B(\vec{k}). \tag{4.21b}$$

In order to estimate the nonlinear effects of long wave modes we assume that the

integrands on the right-hand side of equations (4.21) are dominated by the contribution from $k_1 \ll k$. We then approximate $\theta(\vec{k}_1)$ by the linear solutions given in equation (4.5): $\theta_1(\vec{k}_1, \tau) = -\dot{a}\delta_1(\vec{k}_1)$, because for $k_1 \ll k$ the amplitude of the density perturbations is taken to be very small. Thus we write the right-hand side of equations (4.21) as

$$A(\vec{k}) = \dot{a}\,\delta(\vec{k}) \int d^3k_1 \frac{\vec{k}_1 \cdot \vec{k}}{k_1^2}\delta_1(\vec{k}_1) \; + \dot{a} \int d^3k_1 \frac{\vec{k}_1 \cdot \vec{k}}{k_1^2}\delta_1(\vec{k}_1)\,\epsilon(\vec{k}, \vec{k}_1), \tag{4.22a}$$

$$B(\vec{k}) = \dot{a}\,\theta(\vec{k}) \int d^3k_1 \frac{\vec{k}_1 \cdot \vec{k}}{k_1^2}\delta_1(\vec{k}_1) \; + \dot{a} \int d^3k_1 \frac{\vec{k}_1 \cdot \vec{k}}{k_1^2}\delta_1(\vec{k}_1)\,\omega(\vec{k}, \vec{k}_1). \tag{4.22b}$$

In the expression for $B(\vec{k})$ we have multiplied the right-hand side by 2 to include the contribution from $(\vec{k} - \vec{k}_1) \rightarrow 0$ as required by the symmetry of the integrand. We have also explicitly written out the τ dependence of $\theta(\vec{k}_1)$, so that $\delta_1(\vec{k}_1)$ does not depend on τ. We now define the integrals:

$$\vec{\alpha} = -i \int d^3k_1 \frac{\vec{k}_1}{k_1^2}\delta_1(\vec{k}_1)\,, \tag{4.23}$$

where $i = \sqrt{-1}$; and,

$$E(\vec{k}) = \dot{a} \int d^3k_1 \frac{\vec{k} \cdot \vec{k}_1}{k_1^2}\delta_1(\vec{k}_1)\epsilon(\vec{k}, \vec{k}_1) \;;\; W(\vec{k}) = \dot{a} \int d^3k_1 \frac{\vec{k} \cdot \vec{k}_1}{k_1^2}\delta_1(\vec{k}_1)\omega(\vec{k}, \vec{k}_1)\,. \tag{4.24}$$

Using these definitions equations (4.21) can be written as:

$$\frac{\partial\delta(\vec{k})}{\partial\tau} + \theta(\vec{k}) = i\,\dot{a}\,\vec{k} \cdot \vec{\alpha}\,\delta(\vec{k}) + E(\vec{k})\,, \tag{4.25}$$

$$\frac{\partial\theta(\vec{k})}{\partial\tau} + \frac{\dot{a}}{a}\theta(\vec{k}) + \frac{6}{\tau^2}\delta(\vec{k}) = i\,\dot{a}\,\vec{k} \cdot \vec{\alpha}\,\theta(\vec{k}) + W(\vec{k})\,. \tag{4.26}$$

The above equations are exact aside from using the linear solutions for $\theta(\vec{k}_1)$ in the right-hand side of equations (4.21). We have defined $\vec{\alpha}$ in equation (4.23) so that it is purely real. This can be verified by using the relation of δ_1 to its complex conjugate: $\delta_1(\vec{k}_1) = \delta_1^*(-\vec{k}_1)$, which is required to ensure that $\delta(\vec{x})$ is real. The reason

for introducing $\vec{\alpha}$ is that it is independent of $\vec{k}$ and τ, therefore, given the initial density δ_1, it can be treated as a numerical constant.

We now turn to the issue of long wave divergences. The variance of $\vec{\alpha}$ is:

$$\langle \alpha^2 \rangle \equiv \langle \vec{\alpha} \cdot \vec{\alpha} \rangle = \int d^3k_1 \frac{P_{11}(k_1)}{k_1^2} = 4\pi \int dk_1 P_{11}(k_1). \tag{4.27}$$

Thus $\langle \alpha^2 \rangle$ is a divergent integral for $n < -1$. To proceed further we need to estimate the degree of divergence of the integrals $E(\vec{k})$ and $W(\vec{k})$. We do so by using equation (4.20) to substitute for ϵ and ω in E and W. The resulting expression for the variance of E is:

$$\begin{aligned} \langle |E(\vec{k})|^2 \rangle &= \dot{a}^2 \int d^3k_1 \int d^3k_2 \left(\frac{\vec{k} \cdot \vec{k}_1}{k_1^2} \right) \left(\frac{\vec{k} \cdot \vec{k}_2}{k_2^2} \right) \\ &\quad \times \left\langle \delta_1(\vec{k}_1)\, \delta_1^*(\vec{k}_2) \left[\delta(\vec{k} - \vec{k}_1) - \delta(\vec{k}) \right] \left[\delta^*(\vec{k} - \vec{k}_2) - \delta^*(\vec{k}) \right] \right\rangle . \end{aligned} \tag{4.28}$$

To simplify this expression we assume that for the purposes of assessing the degree of divergence, all the fields involved are well approximated by the linear solution. Then the expectation values can be evaluated using the properties of Gaussian random fields. Of the twelve terms that result, the leading contribution in the long wave limit arises from the term with $\langle \delta_1(\vec{k}_1) \delta_1^*(\vec{k}_2) \rangle \langle \delta(\vec{k} - \vec{k}_1) \delta^*(\vec{k} - \vec{k}_2) \rangle$ in the integrand. This contribution is:

$$\langle |E(\vec{k})|^2 \rangle \sim \frac{1}{3} \dot{a}^2 \, P(k) \, \delta_D(0) \, k^2 \alpha^2. \tag{4.29}$$

The variance of the first term on the right-hand side of equation (4.25), $i\dot{a}\vec{\alpha} \cdot \vec{k}\delta(\vec{k})$ is exactly the same as the above result for $\langle |E(\vec{k})|^2 \rangle$, hence both terms must be retained at the same order in evaluating the long wave contribution. Likewise, it is easy to show that W in equation (4.26) is of the same order as the first term on the right-hand side, and is also proportional to α in its degree of divergence.

Equations (4.25) and (4.26) can be re-written as a pair of second order differential equations in τ for δ and θ. For δ the result is (with $\tilde{\alpha} \equiv \vec{k} \cdot \vec{\alpha}$),

$$\ddot{\delta} + \dot{\delta} \left(-2i\dot{a}\,\tilde{\alpha} + \frac{\dot{a}}{a} \right) + \delta \left(-\dot{a}^2 \tilde{\alpha}^2 - 3i\ddot{a}\tilde{\alpha} - \frac{6}{\tau^2} \right) - \frac{\dot{a}}{a} E + i\dot{a}\tilde{\alpha} E + W - \dot{E} = 0 . \tag{4.30}$$

Since, to leading order, we know the degree of divergence of the variances of all the terms involved in this equation, we are now in a position to evaluate the effect of long wave divergences. The variables in equation (4.30) are complex, hence it can be simplified further by separating the real and imaginary parts. To this end we express δ in terms of its amplitude and phase as:

$$\delta(\vec{k},\tau) = \Delta(\vec{k},\tau)\, e^{i\phi(\vec{k},\tau)}\,. \tag{4.31}$$

For convenience, we further define $\bar{E} \equiv Ee^{-i\phi}$, $\bar{W} \equiv We^{-i\phi}$, and $\bar{\dot{E}} \equiv \dot{E}e^{-i\phi}$. With these substitutions equation (4.30) separates into its real and imaginary parts (respectively) as:

$$\ddot{\Delta} + \frac{\dot{a}}{a}\dot{\Delta} + \Delta\left(-\dot{\phi}^2 + 2\dot{\phi}\dot{a}\tilde{\alpha} - \dot{a}^2\tilde{\alpha}^2 - \frac{6}{\tau^2}\right) + \mathrm{Re}\left[\frac{\dot{a}}{a}\bar{E} + i\dot{a}\tilde{\alpha}\bar{E} + \bar{W} - \bar{\dot{E}}\right] = 0\,, \tag{4.32a}$$

$$\dot{\Delta}\left(2\dot{\phi} - 2\dot{a}\tilde{\alpha}\right) + \Delta\left(\ddot{\phi} + \frac{\dot{a}}{a}\dot{\phi} - 3\ddot{a}\tilde{\alpha}\right) + \mathrm{Im}\left[\frac{\dot{a}}{a}\bar{E} + i\dot{a}\tilde{\alpha}\bar{E} + \bar{W} - \bar{\dot{E}}\right] = 0\,. \tag{4.32b}$$

"Re" and "Im" denote the real and imaginary parts, respectively, of the expressions in the square brackets.

We now make the ansatz that $\phi \sim O(\alpha)$, and that $\Delta \sim O(\alpha^p)$, where $0 \leq p < 1$. Since $E \sim W \sim O(\alpha)$ (in an rms sense) from equation (4.29), keeping terms of $O(\alpha^2)$ in equation (4.32a) gives,

$$\Delta\left(-\dot{\phi}^2 + 2\dot{\phi}\dot{a}\tilde{\alpha} - \dot{a}^2\tilde{\alpha}^2\right) + \mathrm{Re}\left[i\dot{a}\tilde{\alpha}\bar{E} - \bar{\dot{E}}\right] = 0\,. \tag{4.33}$$

As we shall see below, retaining the term $\bar{\dot{E}}$ is required for consistency. We make the assumption that at leading order in α the two parts of equation (4.33) in brackets vanish separately (this will also be justified below). The first part gives a quadratic equation for $\dot{\phi}$,

$$\dot{\phi}^2 - 2\dot{\phi}\dot{a}\tilde{\alpha} + \dot{a}^2\tilde{\alpha}^2 = 0\,, \tag{4.34}$$

which has the solution, $\dot{\phi} = \dot{a}\tilde{\alpha} = \dot{a}\vec{k}\cdot\vec{\alpha}$. Thus the leading order solution for ϕ is:

$$\phi(\vec{k},\tau) = a(\tau)\,\vec{k}\cdot\vec{\alpha} + \phi_i(\vec{k}), \tag{4.35}$$

where $\phi_i(\vec{k})$ is the value of the phase at the initial time.

The solution of equation (4.35) can be used to justify the assumptions that have been made. Firstly, ϕ is indeed of $O(\alpha)$, as assumed at the outset. Further, equations (4.24) and (4.35) can be used to simplify the expression for $\dot{\bar{E}}$ and thereby justify setting the first part of equation (4.33) to 0 separately. To start with let us write E in terms of Δ and ϕ:

$$E = \dot{a}\int d^3k_1 \frac{\vec{k}\cdot\vec{k}_1}{k_1^2}\Delta_1(\vec{k}_1)e^{i\phi(\vec{k}_1)}\left[\Delta(\vec{k}-\vec{k}_1)e^{i\phi(\vec{k}-\vec{k}_1)} - \Delta(\vec{k})e^{i\phi(\vec{k})}\right]. \tag{4.36}$$

Differentiating equation (4.36) with respect to τ and multiplying by $e^{-i\phi(\vec{k})}$ gives,

$$\begin{aligned}\dot{\bar{E}} \;=\; & \frac{\ddot{a}}{\dot{a}}\bar{E} + \dot{a}\int d^3k_1 \frac{\vec{k}\cdot\vec{k}_1}{k_1^2}\Delta_1(\vec{k}_1)e^{i\phi(\vec{k}_1)}\left[\left\{\dot{\Delta}(\vec{k}-\vec{k}_1) + i\Delta(\vec{k}-\vec{k}_1)\dot{\phi}(\vec{k}-\vec{k}_1)\right\}\right. \\ & \left.\times e^{i\phi(\vec{k}-\vec{k}_1)-i\phi(\vec{k})} - \left\{\dot{\Delta}(\vec{k}) + i\Delta(\vec{k})\dot{\phi}(\vec{k})\right\}\right].\end{aligned} \tag{4.37}$$

The leading order terms on the right-hand side above are the two terms with $\dot{\phi}$: they are at least of $O(\alpha^2)$. However, by substituting $\dot{\phi} = \dot{a}\tilde{\alpha}$ into equation (4.37), and comparing with the expression for $\bar{E}$ that follows from equation (4.36), it can be seen that these leading order terms exactly cancel the contribution from $i\dot{a}\tilde{\alpha}\bar{E}$ in equation (4.33). Thus the surviving terms in the second part of equation (4.33) are all of lower order than $O(\alpha^2)$ — therefore they can be neglected in comparison to the first part of the equation which was used to get the solution for ϕ of equation (4.35). This establishes the consistency of the approximations used to obtain this solution.

The variance of the phase shift given by equation (4.35) is:

$$\left\langle\left[\delta\phi(\vec{k},\tau)\right]^2\right\rangle = a(\tau)^2\,k^2\int d^3k_1\,\frac{(\hat{k}\cdot\hat{k}_1)^2}{k_1^2}\,P_{11}(k_1), \tag{4.38}$$

where $\delta\phi(\vec{k},\tau) \equiv \phi(\vec{k},\tau) - \phi_i(\vec{k})$, and $\hat{k}$ and $\hat{k}_1$ are unit vectors. Since $\vec{k}$ is a fixed

external vector the angular integral can be performed so that the final result depends only on the magnitude of $\vec{k}$:

$$\left\langle \left[\delta\phi(\vec{k},\tau)\right]^2 \right\rangle = \frac{4\pi}{3} a(\tau)^2 \, k^2 \int dk_1 \, P_{11}(k_1) \, . \tag{4.39}$$

Thus the leading order solution for $\delta(\vec{k})$ involves a growing (divergent) phase shift, but there are no contributions to the amplitude at this order. The above analysis can be repeated for the velocity divergence $\theta(\vec{k})$ to verify that the leading order result for $\theta(\vec{k})$ is the same, with equation (4.35) giving the solution for its phase as well. These results were obtained by retaining terms of $O(\alpha^2)$. Since divergent terms of $O(\alpha)$ are also present in the equations we cannot say anything conclusive about the degree of (possible) divergence of the amplitude $\Delta(\vec{k})$. In the following section we shall address this question by expanding the equations to next order in α with some additional assumptions.

The solution (4.35) for the phase shift has a simple physical interpretation. As noted in Section 4.2, the linear bulk velocity v_b diverges due to contributions from long wave modes (equation (4.8)). The limiting form of the integral given in equation (4.8) for v_b^2, and that of equation (4.39), is the same. This connection can be made more precise by imagining a single sine-wave density perturbation in real space: $\delta(\vec{x},\tau) = \delta_o \sin(\vec{k}\cdot\vec{x})$. Now suppose that the fluid in which this perturbation is made is moved with a uniform translational velocity of magnitude $v_b(\tau)$ given by (4.8) (the scale x in equation (4.8) has no connection to the spatial variable $\vec{x}$ used here). The distance moved by each fluid element is $\int d\tau \, v_b(\tau) = v_b(\tau)\, a(\tau)/\dot{a}(\tau)$, where we have used $v_b(\tau) \propto \dot{a}(\tau)$. If the coordinate frame is kept fixed relative to this translational motion, then the density perturbation will acquire the following time dependence due to the bulk velocity: $\delta(\vec{x},\tau) = \delta_o \sin[\vec{k}\cdot(\vec{x} - \hat{e}\, v_b a/\dot{a})]$, where $\hat{e}$ is the direction of the bulk velocity. Therefore δ acquires a phase shift: $\delta\phi(\vec{k}) = \vec{k}\cdot\hat{e}\, a/\dot{a}\, v_b$. On squaring, and averaging over angles between $\vec{k}$ and $\hat{e}$, this gives:

$$\left\langle \left[\delta\phi(\vec{k},\tau)\right]^2 \right\rangle = \frac{1}{3}\frac{a^2}{\dot{a}^2} k^2 \, v_b^2(\tau) \, . \tag{4.40}$$

Note that the averaging over angles is consistent with the angular integral done to get equation (4.39), and amounts to estimating the typical phase shift due to a superposition of bulk flows of magnitude v_b directed randomly with respect to $\vec{k}$. Substituting for v_b^2 from equation (4.8) and assuming it is dominated by the contribution from low k, we recover the result in equation (4.39). Thus we have shown that for $n < -1$ the dominant phase shift is due to the kinematical effect of the bulk motion on small scales imparted by long wave modes. This is consistent with the connection between divergences in the nonlinear terms in the fluid equations and v_b made in Section 4.2.

4.4.2 Taylor Series Expansion

In this section we make an additional assumption about the $\vec{k}$-dependence of $\delta(\vec{k})$ and $\theta(\vec{k})$: we assume that at small k, δ and θ are smooth functions of $\vec{k}$ with a well defined derivative with respect to $\vec{k}$. With this assumption we expand the nonlinear integrals in equations (4.3) in a Taylor series in (k_1/k) about 0 and restrict the range of integration to small k_1. Thus we write: $\delta(\vec{k}-\vec{k}_1) \simeq \delta(\vec{k}) - \vec{k}_1 \cdot \partial\delta/\partial\vec{k}$, and likewise for $\theta(\vec{k}-\vec{k}_1)$. Unfortunately, the standard assumption about δ and θ in cosmology is that they are Gaussian random fields at the initial time. Thus at each value of $\vec{k}$ they are given by a random number drawn from a probability distribution. The distribution of δ or θ with respect to $\vec{k}$ is quite the opposite of a smooth function, because its values at any two $\vec{k}$ are uncorrelated. We return to this point later in this section and in Section 4.6, but here we proceed with the Taylor series approach.

With the Taylor expansion described above, the right-hand sides of equations (4.3), denoted by $C(\vec{k})$ and $D(\vec{k})$, take the form:

$$C(\vec{k}) = -\int d^3k_1 \left[\theta(\vec{k}_1)\frac{\vec{k}_1\cdot\vec{k}}{k_1^2}\left(\delta(\vec{k}) - \vec{k}_1\cdot\frac{\partial\delta(\vec{k})}{\partial\vec{k}}\right) + \theta(\vec{k})\delta(\vec{k}_1) + \ldots\right], \quad (4.41a)$$

$$D(\vec{k}) = -\int d^3k_1\,\theta(\vec{k}_1)\left[\frac{\vec{k}_1\cdot\vec{k}}{k_1^2}\theta(\vec{k}) + \left(\frac{2(\vec{k}_1\cdot\vec{k})^2}{k_1^2k^2} - 1\right)\theta(\vec{k}) - \frac{\vec{k}_1\cdot\vec{k}}{k_1^2}\vec{k}_1\cdot\frac{\partial\theta(\vec{k})}{\partial\vec{k}} + \ldots\right], \quad (4.41b)$$

where both equations have been expanded to the same order. In equations (4.41) we

have included the contributions from $(\vec{k}-\vec{k}_1)\to 0$ as well. We now write equations (4.41) at the order shown as linear equations by approximating δ and θ at small k_1 by the linear solutions δ_1 and θ_1. Recall that we had obtained one linear term on the right-hand side of each equation in the previous section by introducing the integral $\vec{\alpha}$. Here we introduce three new integrals: η, γ and g_{ij},

$$\eta=\int d^3k_1\delta(\vec{k}_1)\ ;\ \gamma=\int d^3k_1[2(\hat{k}\cdot\hat{k}_1)^2-1]\delta(\vec{k}_1)\ ;\ g_{ij}=\int d^3k_1\hat{k}_{1i}\hat{k}_{1j}\delta(\vec{k}_1)\,, \quad (4.42)$$

where k_{1i} and k_{1j} denote the ith and jth components of the vector $\vec{k}_1$, so that g_{ij} is a tensor. Note that aside from the dependence of γ on the direction of $\vec{k}$, all the integrals in equation (4.42) are independent of $\vec{k}$ and τ. In addition, all the integrals are convergent in an rms sense for $n>-3$.

We proceed by writing down a second order differential equation for δ in terms of C and D:

$$\ddot{\delta}+\frac{\dot{a}}{a}\dot{\delta}-\frac{6}{\tau^2}\delta=\dot{C}+\frac{\dot{a}}{a}C+D. \quad (4.43)$$

We then use the definitions of equation (4.42) to rewrite equations (4.41) as:

$$C(\vec{k})=i\dot{a}\vec{k}\cdot\vec{\alpha}\,\delta+\dot{a}[k_ig_{ij}\partial_j]\delta-a\eta\theta\,, \quad (4.44)$$

and

$$D(\vec{k})=-i\dot{a}\vec{k}\cdot\vec{\alpha}\,\theta-\dot{a}[k_ig_{ij}\partial_j]\theta-\dot{a}\gamma\theta\,, \quad (4.45)$$

where $\partial_j\equiv\partial/\partial k_j$, and the repeated indices i and j are summed over. We will now attempt to solve these equations for the amplitude and phase of δ to a given order in α. We begin by using equations (4.44) and (4.45) to eliminate θ in the terms on the right-hand side of equation (4.43) (we will also need to use the left-hand sides of equations (4.3)). Some algebra yields the following equation for δ:

$$\ddot{\delta}+\frac{\dot{a}}{a}\left[\frac{1}{1+a\eta}-\gamma a-2ia\vec{k}\cdot\vec{\alpha}-2a(k_ig_{ij}\partial_j)\right]\dot{\delta}-\frac{6}{\tau^2}(1+a\eta)\delta$$
$$-\dot{a}^2\left[\vec{k}\cdot\vec{\alpha}-i(k_ig_{ij}\partial_j\ln\delta)\right]^2\delta-i\dot{a}^2\left[-k_ig_{ij}\alpha_j+i(k_ig_{ij}\partial_j)^2\ln\delta\right]\delta$$

$$-i\frac{\dot{a}^2}{a}\left[\vec{k}\cdot\vec{\alpha}-i(k_i g_{ij}\partial_j \ln\delta)\right]\left[\frac{1}{1+a\eta}-\gamma a+\frac{\ddot{a}a}{\dot{a}^2}\right]\delta=0. \tag{4.46}$$

We now make a WKB analysis, which relies on taking the phase to be more rapidly varying than the amplitude, to obtain self-consistent equations for the amplitude and phase. After some algebra we get the following relation for $\dot{\phi}$ by solving equation (4.46) at $O(\alpha^2)$:

$$\dot{\phi}=\dot{a}(\vec{k}\cdot\alpha+k_i g_{ij}\partial_j\phi). \tag{4.47}$$

This yields the solution,

$$\phi=k^T F\alpha+\phi_i\ ;\ F=e^{ag}g^{-1}(I-e^{-ag}), \tag{4.48}$$

where $\vec{\alpha}$ has been represented as a column vector, k^T denotes a row vector representing $\vec{k}$, and g and F are 3 by 3 matrices, with I being the identity matrix. This solution can be verified by substitution using equation (4.46). Note that for $ag<1$, F can be expanded as a Taylor series: $F\simeq a+a^2g/2+a^3g^2/6+....$ For $ag\ll 1$ the leading order solution is $\phi=a\vec{k}\cdot\vec{\alpha}+\phi_i$, in agreement with (4.35). The solution for ϕ in equation (4.48) can be used in equation (4.46) to obtain an equation for Δ only. After some algebra, this equation simplifies to:

$$\ddot{\Delta}+\frac{\dot{a}}{a}\left[\frac{1}{1+a\eta}-\gamma a--2a(k_i g_{ij}\partial_j)\right]\dot{\Delta}-\frac{6}{\tau^2}(1+a\eta)\Delta+\dot{a}^2\Delta(k_i g_{ij}\partial_j\ln\Delta)^2$$
$$+\dot{a}^2\Delta(k_i g_{ij}\partial_j)^2\ln\Delta-\frac{\dot{a}^2}{a}(k_i g_{ij}\partial_j\ln\Delta)\left[\frac{1}{1+a\eta}-\gamma a+\frac{\ddot{a}a}{\dot{a}^2}\right]\Delta=0. \tag{4.49}$$

Note that in this equation for Δ, all terms involving i and the divergent integral α have cancelled out exactly! Hence the solution for Δ has no dependence on α, the only divergent integral in equation (4.46). Obtaining the full solution for Δ is still not possible as it requires solving equation (4.49), a nonlinear partial differential equation; however, for our purpose the key goal was the assessment of the α-dependence of Δ. Thus the Taylor series approach leads to two striking results: the solution for the phase given by equation (4.48), and the result that the evolution of the amplitude is

not influenced by any divergent integrals.

The above conclusions thus support the interpretation discussed in Section 4.2 that for $-3 < n < -1$, there is no dynamically relevant divergence. Hence the evolution of scale free spectra will obey the standard self-similar scaling provided the statistics used are relevant to the growth of density perturbations. The divergent growth of the phase is not a measure of perturbation growth as it arises from bulk motions. However these conclusions rest on the assumption of a valid Taylor series approximation for δ and θ. This assumption cannot be justified in the cosmological context for random-phase Gaussian initial conditions. Hence we must still regard the conclusions of this section as being suggestive of the answer, but not as proven results.

4.5 Self-Similar Scaling in N-body Simulations

N-body simulations provide a powerful means for testing the self-similar scaling of scale free spectra. The deeply nonlinear regime is accessible in these simulations, thus offering the possibility of measuring the complete similarity solution. N-body simulations have limited dynamic range, but they do not rely on any approximations of the kind made in Sections 4.3 and 4.4. Therefore they provide a complementary technique to the analytic approaches of previous sections. In this section we study two scale free N-body simulations, $n = 0$ and $n = -2$, in order to measure their scaling properties.

The $n = -2$ simulation was performed by Ed Bertschinger. It is a particle-particle/particle-mesh simulation with 128^3 particles. Data from 21 time outputs of this simulation were analyzed, with the scale factor $a(\tau)$ increasing by a factor of $2^{1/4}$ between successive outputs. The $n = 0$ simulation was performed by Simon White. It is also a particle-particle/particle-mesh simulation done with 100^3 particles. Data were available for 9 time outputs, with the scale factor increasing by a factor of $\simeq 1.6$ between successive outputs (except for the first two). This simulation is used as a control case to test the accuracy of the results for the $n = -2$ simulation. Since

$n = 0$ does not suffer from potential long wave divergences, the standard self-similar scaling is expected to hold, and has in fact been convincingly demonstrated in earlier work. Hence the results of this simulation provide a good indication of the degree of accuracy with which the N-body simulations show the similarity solution (though the differences in the number of particles and other parameters in the two simulations complicate such a comparison).

Here we briefly outline the N-body calculation; many relevant details are provided by Gelb (1992). The particle-mesh calculation of the simulation is done by solving Poisson's equation on a cubical grid using the fast Fourier transform (FFT). In Fourier space Poisson's equation is:

$$\Phi(\vec{k},\tau) = -\frac{4\pi G\rho_b(\tau)a^2}{k^2}\delta(\vec{k},\tau), \tag{4.50}$$

where $\Phi(\vec{k},\tau)$ is the Fourier transform of the perturbed gravitational potential. In an N-body simulation the density is computed using the number density of a finite number of particles. The real space density is computed on a cubical, three dimensional grid by interpolating from the particle positions. This density is then Fourier transformed using the FFT algorithm, and then $\Phi(\vec{k},\tau)$ is computed using equation (4.50). Multiplying $\Phi(\vec{k},\tau)$ by $-i\vec{k}$ (which corresponds to taking a gradient in real space) gives the Fourier transform of the gravitational force vector. This is transformed back to real space with three FFTs for each component. The real space forces are then used to move the particles using the equation of motion in comoving coordinates. This procedure is interated to continue the simulation. To increase the resolution of the forces, the force on each particle due to its nearest neighbors is computed by direct summation using a Plummer model for the force law: $\vec{F}(r) = -Gm^2\vec{r}/(r^2+\epsilon^2)^{3/2}$, where ϵ is known as the Plummer softening parameter. It is $(1/2560)L$ for the $n = -2$ simulation, where L denotes the size of the box.

Thus in the N-body simulations there are many departures from the idealization of an infinite, continuous fluid. The limitations common to any N-body simulation are the finite size of the box and the discrete nature of particles. Additional scales

are introduced into the system due to the finite PM mesh and the Plummer softening parameter. The limitations introduced due to the presence of these length scales must be kept in mind while evaluating the accuracy of N-body results. As described in Section 4.1, the presence of these scales is not a fundamental drawback; it only means that one must be careful to ensure that the range of scales used to study the scaling in time are such that they allow for intermediate asymptotic self-similarity to set in.

The simulation data at chosen output times is stored in the form of particle positions. These were interpolated onto a 512^3 grid to get the real space density, which was fast Fourier transformed to get the Fourier transform of the density, $\delta(\vec{k}, a)$. For the $n = 0$ simulation the grid used for interpolating the density was 128^3: the relative coarseness of this grid led to some numberical suppression of the power at high-k as evident in Figure 4-9. $\delta(\vec{k}, a)$ is a complex number at each $\vec{k}$, and is therefore represented by a real and imaginary part. The values of $\vec{k}$ are represented by a three dimensional vector (k_x, k_y, k_z), with each of k_x, k_y and k_z being integers ranging from -63 to 64. Thus the magnitude of $\vec{k}$ is the wavenumber in units of $\Delta k = 2\pi/L$, with the longest wave in the box being of magnitude $k = 1$. Since $\delta(\vec{k}) = \delta^*(-\vec{k})$, only one half of the values of $\delta(\vec{k})$ are independent; thus, for example, the half of Fourier space with $k_z < 0$ does not contain any independent values of $\delta(\vec{k})$ if all the values for $k_z > 0$ are known.

We use the data for $\delta(\vec{k}, a)$ to compute the amplitude Δ and phase ϕ given by,

$$\delta(\vec{k}, a) = \Delta(\vec{k}, a) e^{i\phi(\vec{k}, a)}. \tag{4.51}$$

Δ and ϕ are the basic variables used for our self-similar scaling analysis. In Figures 4-1 to 4-3 the trajectories of the phase and amplitude of individual Fourier modes as a function of time are shown for the $n = -2$ simulation. Each of these figures has four panels, and each panel shows the evolution of five modes, chosen so that they represent a large range in k. These figures give an idea of how individual modes evolve, in contrast to the regular behavior shown by the statistics computed from

them. Thus even at relatively early times when most statistics obey linear behavior, the amplitudes and phases can be seen to follow quite jagged paths.

A technical problem in the measurement of the phase arises because conventionally the phases are defined modulo (2π). The phase trajectories that follow are shown in Figure 4-1, where all the phases lie between $-\pi$ and π. This is how the phases from N-body data have been computed in previous studies (Ryden & Gramann 1991; Scherrer et al. 1991; Suto & Suginohara 1991). However, a glance at the phase trajectories in Figure 4-1 makes it clear that this will have the effect of randomizing the phases at late times relative to their initial values, even if the growth were monotonic. This is because even a small change in the phase, $\delta\phi$, could cause it to be mapped to a value indicating a change of $(2\pi - |\delta\phi|)$. If the trajectories could be obtained with arbitrarily small increments in a then such artificial mappings could be un-done, and the phases plotted without constraining them between $-\pi$ and π. Since outputs are available only at discrete values of a, there is a two-fold ambiguity in defining the phase. Consider the phase values at two successive a's for a given $\vec{k}$: $\phi(\vec{k}, a_j)$ and $\phi(\vec{k}, a_{j+1})$, defined in the usual way to lie between $-\pi$ and π. Let $\delta\phi_j = \phi(\vec{k}, a_{j+1}) - \phi(\vec{k}, a_j)$. An alternate value for the phase at a_{j+1} is $\phi'(\vec{k}, a_{j+1}) = \phi(\vec{k}, a_j) \pm (2\pi - |\delta\phi_j|)$, where the sign in positive if $\delta\phi_j < 0$ and vice versa. To choose between ϕ and ϕ', we follow the trajectory of each mode, and at each successive value of a, we define the phase by taking the magnitude of the change in phase to be the smaller of $|\delta\phi_j|$ and $(2\pi - |\delta\phi_j|)$. The result is shown in Figure 4-2. As long as the typical changes in phase at successive times are less than π, this procedure is a reasonable way of extending the range of ϕ. As we shall see, this considerably extends the degree of phase nonlinearity accessible to our analysis.

Following Ryden & Gramann (1991) and Gramann (1992), we define the following statistics as a measure of the degree of nonlinear evolution. For the phase we define the mean deviation from the initial phase, $\overline{\delta\phi}(k, a) \equiv \langle |\delta\phi(\vec{k}, a)| \rangle = \langle \phi(\vec{k}, a) - \phi(\vec{k}, a_i) \rangle$, where a_i is the initial value of a. The averages indicated are performed over the different modes within a shell in $k-$space whose wavenumbers lie between $(k-0.5)$ and $(k+0.5)$. For the amplitude we simply measure the mean amplitude $\langle \Delta(\vec{k}, a) \rangle$ within

each shell in $k-$space. The results are plotted in Figures 4-4 and 4-5 for $n = -2$, and Figures 4-8 and 4-9 for $n = 0$. These results are interesting in themselves, but here we limit ourselves to using them to define characteristic wavenumber scales, which are then used to test for self-similar scaling. For Figures 4-4 and 4-8, if we had used the phase trajectories as shown in Figure 4-1 (i.e., defined to lie between $-\pi$ and π), then all the late time curves for $\langle \delta\phi(\vec{k}, a) \rangle$ would have reached a maximum of $(2\pi/3)$ — this corresponds to a distribution of $\phi(\vec{k}, a)$ that is uncorrelated with $\phi(\vec{k}, a_i)$. However, it is clear from Figure 4-4 that $\overline{\delta\phi}$ shows systematic growth well beyond $2\pi/3$. Thus with the phase information that we have generated, previously unexplored aspects of phase evolution in the deeply nonlinear regime can be addressed.

To analyze self-similar scaling, we define two characteristic wavenumbers. The first, denoted $k_c(a, \phi_c)$, is defined by setting $\overline{\delta\phi}(k, a) = \phi_c$, where ϕ_c is a constant. The second, denoted $k_c(a, \Delta_c)$ is defined using the amplitude as follows:

$$\left\langle \frac{|\Delta(\vec{k}, a) - \Delta_1(\vec{k}, a)|}{\Delta_1(\vec{k}, a)} \right\rangle = \Delta_c \,, \tag{4.52}$$

where $\Delta_1(\vec{k}, a)$ is the linear solution for Δ, and Δ_c is a dimensionless constant. Thus $k_c(a, \Delta_c)$ is the wavenumber at which the fractional departure of the amplitude from the linear solution is Δ_c. These statistics involve summing the magnitudes of the departures from linear behavior for each mode within a given $k-$shell; hence they probe the degree of nonlinearity more directly than if a statistic was computed first, and then its departure from the linear solution was calculated.

Figure 4-6 is a plot of $\log[k_c(a, \phi_c)]$ vs. a with $n = -2$, for 4 different values of ϕ_c. Also shown in the plot are the scalings expected from the standard self-similar behavior, $k \propto a^{-2/(3+n)} \propto a^{-2}$ for $n = -2$, and the scaling resulting from the solution for $\delta\phi$ given by equation (4.35), $k \propto a^{-1}$. The plots show that for $\phi_c = \pi$ and $\pi/2$, the latter scaling is closely followed; but for the lower values $\phi_c = \pi/4$ and $\pi/8$, the former scaling is more closely followed. We verified that the trends did reflect a gradual transition in the scaling of $k_c(a, \phi_c)$ by plotting a larger range of ϕ_c down to $\phi_c = \pi/20$. This can be interpreted as follows. For a given k, at early times as the

phase just begins to depart from the linear solution (in which ϕ remains constant in time), its evolution is dominated by perturbative or other weakly nonlinear effects. These effects in general involve the coupling of a range of values of k', mostly in the vicinity of $k' = k$, and obey the standard self-similar scaling. However at late times the phase shift is dominated by the bulk flow due to the longest waves in the box. The resulting phase change is given by equation (4.35) — it is a smooth function of a and k, and therefore dominates the other, more stochastic components of the phase change at late times. Thus the phase shows behavior that we can interpret as arising from a combination of the kinematical divergence described in previous sections, and a dynamical, nonlinear component which obeys the standard self-similar scaling. The results for $n = 0$ shown in Figure 4-10 show only one behavior, the self-similar scaling, $k \propto a^{-2/3}$. This is expected as the linear bulk velocity does not diverge, therefore the longest waves in the box do not dominate the phase shift.

For the amplitude scaling, Figure 4-7 shows a plot of $\log[k_c(a, \Delta_c)]$ vs. a with $n = -2$, for $\Delta_c = 0.25, 0.5, 1, 2$. For sufficiently high k, all four curves closely follow the standard self-similar scaling, $k \propto a^{-2}$. This is consistent with the indications from previous sections that the divergence from long waves does not affect the amplitude. All the curves show a consistent departure from the $k \propto a^{-2}$ behavior at low k, roughly for $k < 10$. This most likely indicates that the absence of power on modes with wavelengths larger than the box-size has slowed the growth of modes which would otherwise be enhanced by the former. Thus the standard self-similar solution for $n = -2$ is obtained only on scales significantly smaller than the box-size. For $n = 0$ the self-similar scaling $k \propto a^{-2/3}$ is again shown convincingly.

Our results are in partial disagreement with those of Gramann (1992). She found that for $n = -1$ in two dimensions (the analog of $n = -2$ in three dimensions), the standard self-similar scaling is broken for both the phase and amplitude. Our results for the phase scaling are consistent with hers, but the amplitude scalings are quite different: our results show good agreement with the scaling $k_c \propto a^{-2}$, whereas hers agree with $k_c \propto a^{-1}$. Since the statistics that we have measured were chosen to agree with her definitions, it is difficult to explain the origin of the disagreement.

It is conceivable that there are basic differences in the dynamics in two and three dimensions, but this is not reflected in the analytical results of Section 4.4.

4.6 Conclusion

In Sections 4.1 and 4.2 we presented arguments outlining the need to examine the self-similar scaling of scale free spectra, $P(k) \propto k^n$, for $-3 < n < -1$. It was shown that terms diverging due to the contribution from long wave modes were present in the cosmological fluid equations, but that it needed to be determined whether they had any dynamical influence on the growth of density perturbations.

We have examined this issue through analytical and N-body techniques in Sections 4.3–4.5. Our conclusions can be summarized as follows:

(i) In Section 4.3.2 we examined perturbative contributions to the power spectrum to examine the possibility of long wave divergences in these contributions for $-3 < n < -1$. We found that divergent terms were indeed present, but that the leading order divergences cancelled out at each order in perturbation theory. Terms which diverged less strongly are also present, but due to the computational complexity involved we were unable to analyze them.

(ii) In Section 4.4 we developed a non-perturbative approximation to study the non-linear coupling of long wave modes. We obtained a solution for the phase shift whose variance is divergent for $-3 < n < -1$. This divergence was interpreted to arise from the kinematical effect of the bulk flows induced by long wave modes. With additional assumptions requiring that the Fourier space density be amenable to a Taylor series expansion around $\vec{k}$, we showed that the evolution of the amplitude of $\delta(\vec{k}, a)$ is not influenced by the divergent terms. It was emphasised that the Taylor series expansion cannot be justified for Gaussian random fields, and therefore the final conclusion cannot be regarded as a proof.

(iii) In Section 4.5 we studied the self-similar scaling of an $n = -2$ scale free simulations, and used an $n = 0$ simulation as a control case. It was demonstrated numerically that for $n = -2$ the phase shift indeed obeys a scaling consistent with

the solution found in Section 4.4 at sufficiently late times. At early times the evolution of the phase shift was consistent with the standard self-similar scaling. Thus the phase shift arises from a combination of kinematical effects due to large scale flows which dominate at late times, as well as genuine dynamical effects which dominate at early times in the weakly nonlinear stage of its evolution. With some further analysis it may be possible to construct a concrete analytical model to support this interpretation.

(iv) The scaling of the amplitude followed the standard self-similar form, except at wavenumbers $k \lesssim 10$ (in units of $2\pi/L$). This is consistent with the results of Sections 4.3 and 4.4, and the interpretation that dynamical measures of perturbation growth preserve self-similar scaling for $-3 < n < -1$.

It was disappointing that neither of our analytical approaches led to a rigorous result regarding self-similar scaling of the amplitude of the density. However, in combination with the N-body results they lead us to conclude with some confidence that the self-similar evolution of the density contrast is preserved for $-3 < n < -1$. The kinematical interpretation for the scaling of the phase shift provides a useful guide to identifying statistics susceptible to such effects. The rms displacement of particle postions is another statistic which would be dominated by the bulk motions from long wave modes for $n < -1$, and must therefore be used with caution as a measure of nonlinear evolution.

It is a pleasure to thank Alan Guth for many stimulating discussions which helped to clarify and sharpen our arguments. We thank Simon White for providing the results of his scale free simulations, his hospitality at the Institute of Astronomy, and for several useful suggestions. We also acknowledge useful discussions with Shep Doeleman, Mirt Gramann, Ofer Lahav, Samir Mathur, Adi Nusser and, especially, David Weinberg.

REFERENCES

Barenblatt, G. I. 1979, Similarity, Self-Similarity, and Intermediate Asymptotics (New York: Consultants Bureau)

Bertschinger, E. 1992, in New Insights into the Universe, ed. Martinez, V. J., Portilla, M. & Saez, D. (Berlin: Springer-Verlag), p. 65

Bertschinger, E. & Gelb, J. 1991, Comp. in Physics, 5, 164

Davis, M. & Peebles, P. J. E. 1977, ApJS, 34, 425

Efstathiou, G. 1990, in Physics of the Early Universe, , ed. Peacock, J. A., Heavens, A. F. & Davies, A. T. (Bristol: IOP), p. 361

Efstathiou, G. & Eastwood, J. W. 1981, MNRAS, 194, 503

Efstathiou, G., Frenk, C. S., White, S. D. M., & Davis, M. 1988, MNRAS, 235, 715

Gelb, J. M. 1992, PhD. Thesis, M.I.T.

Goroff, M. H., Grinstein, B., Rey, S.-J. & Wise, M. B. 1986, ApJ, 311, 6

Gramann, M. 1992, ApJ, 401, 19

Klypin, A. A. & Melott, A. A. 1992, ApJ, 399, 397

Makino, N., Sasaki, M. & Suto, Y. 1992, Phys.Rev.D, 46, 585

Peebles, P. J. E. 1974, A&A, 32, 391

Peebles, P. J. E. 1980, The Large-Scale Structure of the Universe (Princeton: Princeton University Press)

Peebles, P. J. E. 1993, Principles of Physical Cosmology (Princeton: Princeton University Press)

Press, W. H. & Schechter, P. 1974, ApJ, 187, 425

Ryden, B. S. & Gramann, M. 1991, ApJ, 383, L33

Scherrer, R. J., Melott, A. L. & Shandarin, S. F. 1991, ApJ, 377, 29

Suginohara, T. & Suto, Y. 1991, ApJ, 371, 470

Vishniac, E. T. 1983, MNRAS, 203, 345

Zel'dovich, Ya. B. 1965, Adv. Astron. Ap., 3, 352

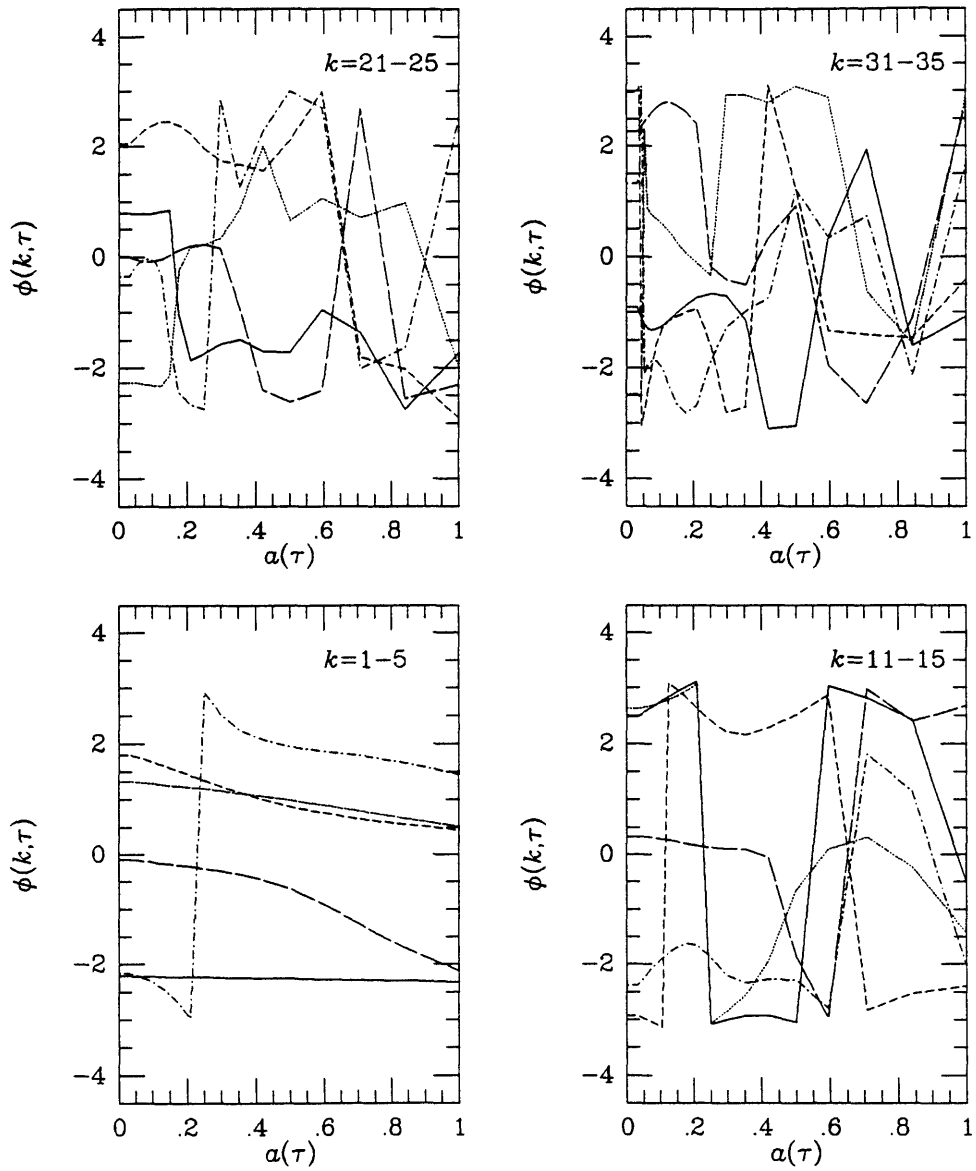

Figure 4-1 The trajectories of the phases $\phi(\vec{k},\tau)$ of individual Fourier modes for $n = -2$ are plotted vs. $a(\tau)$. The magnitudes, k, of the wavevectors are labeled in each panel; the full vectors were chosen as $\vec{k} = (0, 0, k)$. Within each panel k increases in the following order: solid, dotted, dashed, long-dashed, dashed-dotted curves. The phase is defined modulo 2π, and is therefore constrained to lie between $-\pi$ and π. Outputs at 21 values of a have been used to plot each trajectory. At $a = 0$, the value of ϕ at the earliest time has been plotted again to show the expected linear behavior.

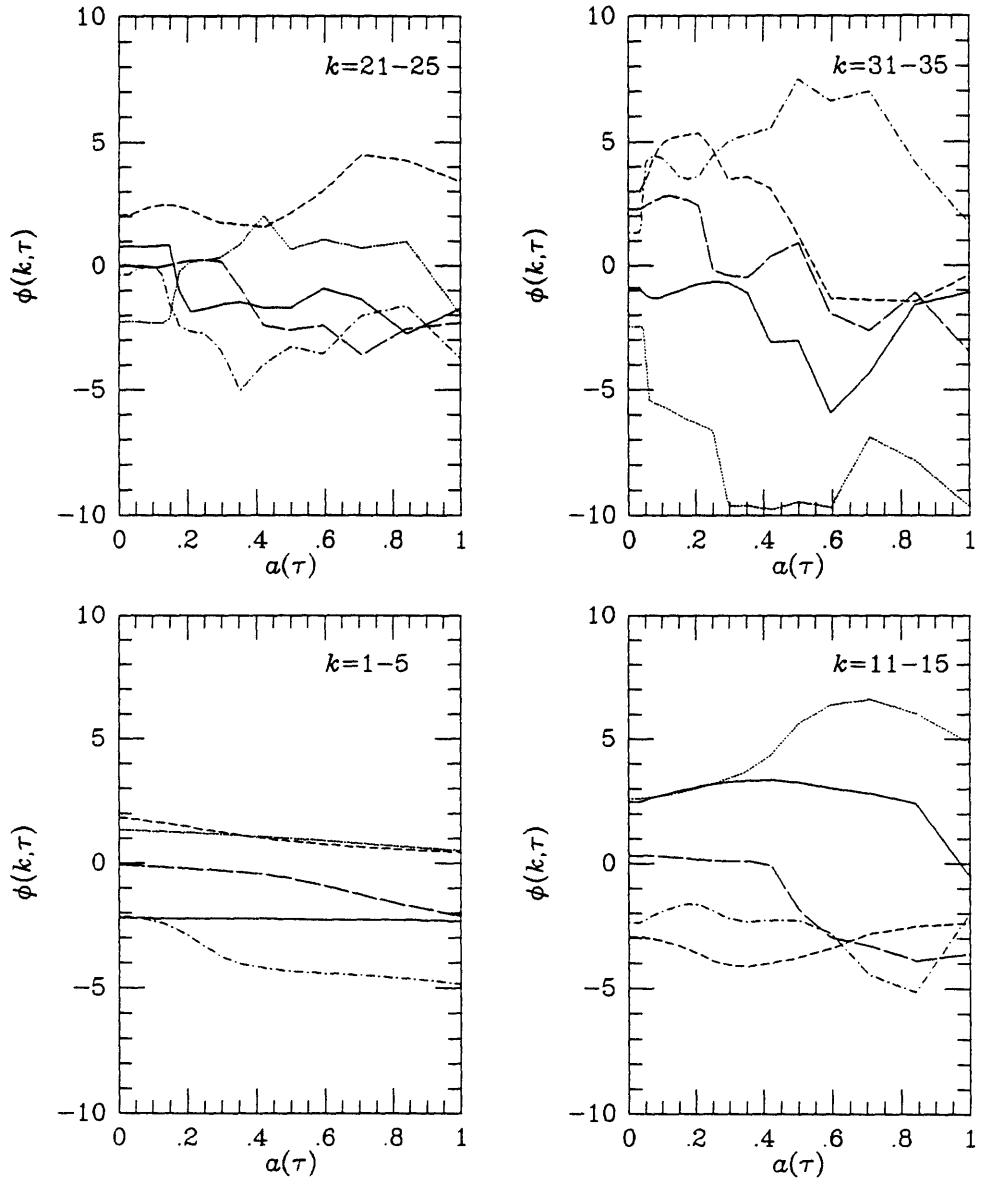

Figure 4-2 The same trajectories as in Figure 4-1 are plotted, but ϕ has been redefined so that it is no longer constrained between $-\pi$ and π (notice the limits on the y-axis). To overcome the modulo 2π constraint, the phase at each time output is defined by adding to the previous value of the phase the change in phase which is the smaller of two choices as described in Section 4.5. In linear theory the phases do not change with time; significant departures from this can be seen in all but the lowest k modes.

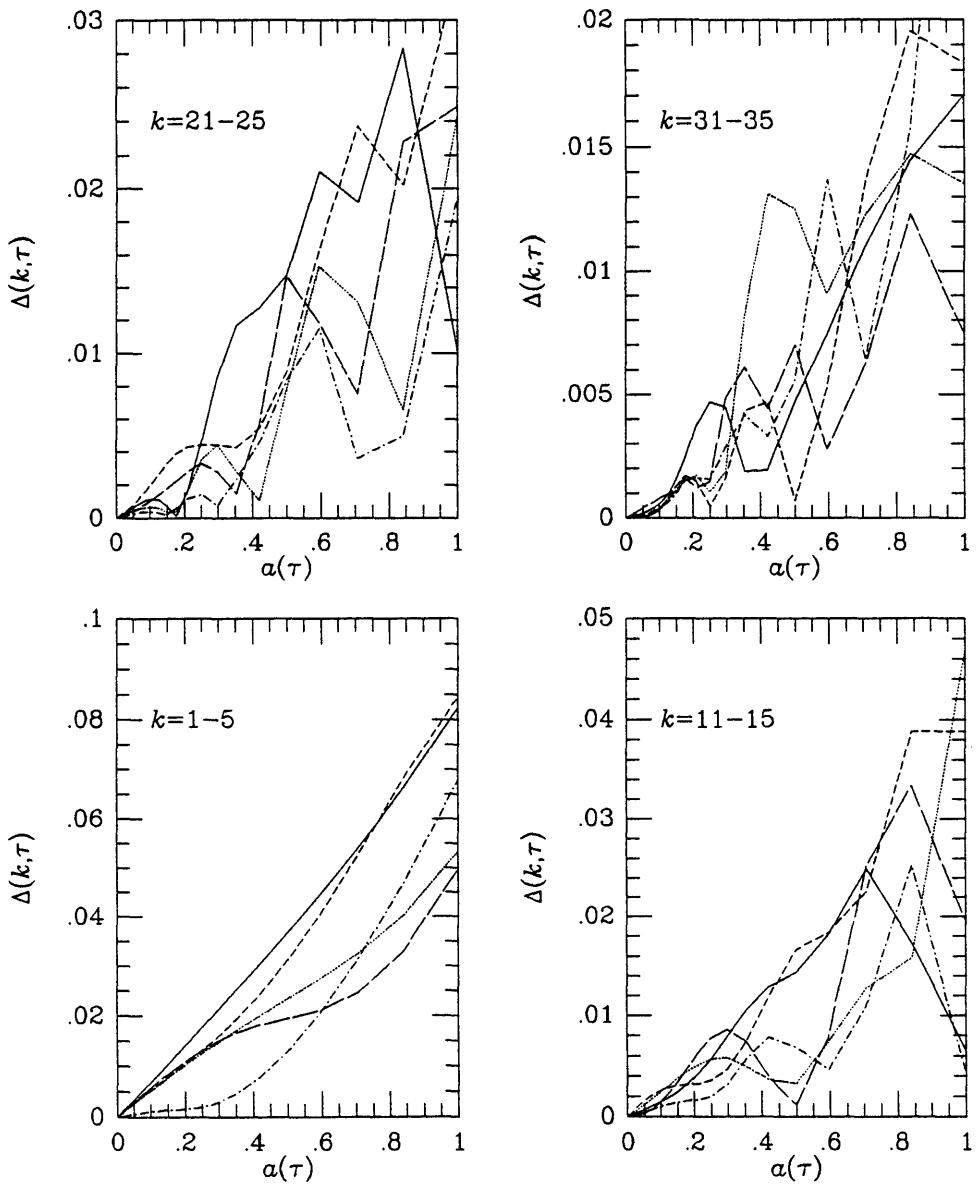

Figure 4-3 The trajectories of the amplitudes $\Delta(\vec{k},\tau)$ of individual Fourier modes for $n = -2$ are plotted vs. a, as in Figure 4-1 for the phase. Note that at early times $\Delta \propto a$: to check this all the curves have been joined to $\Delta = 0$ at $a = 0$. Therefore the lowest value of a at which departures from a straight line occur shows nonlinear behavior.

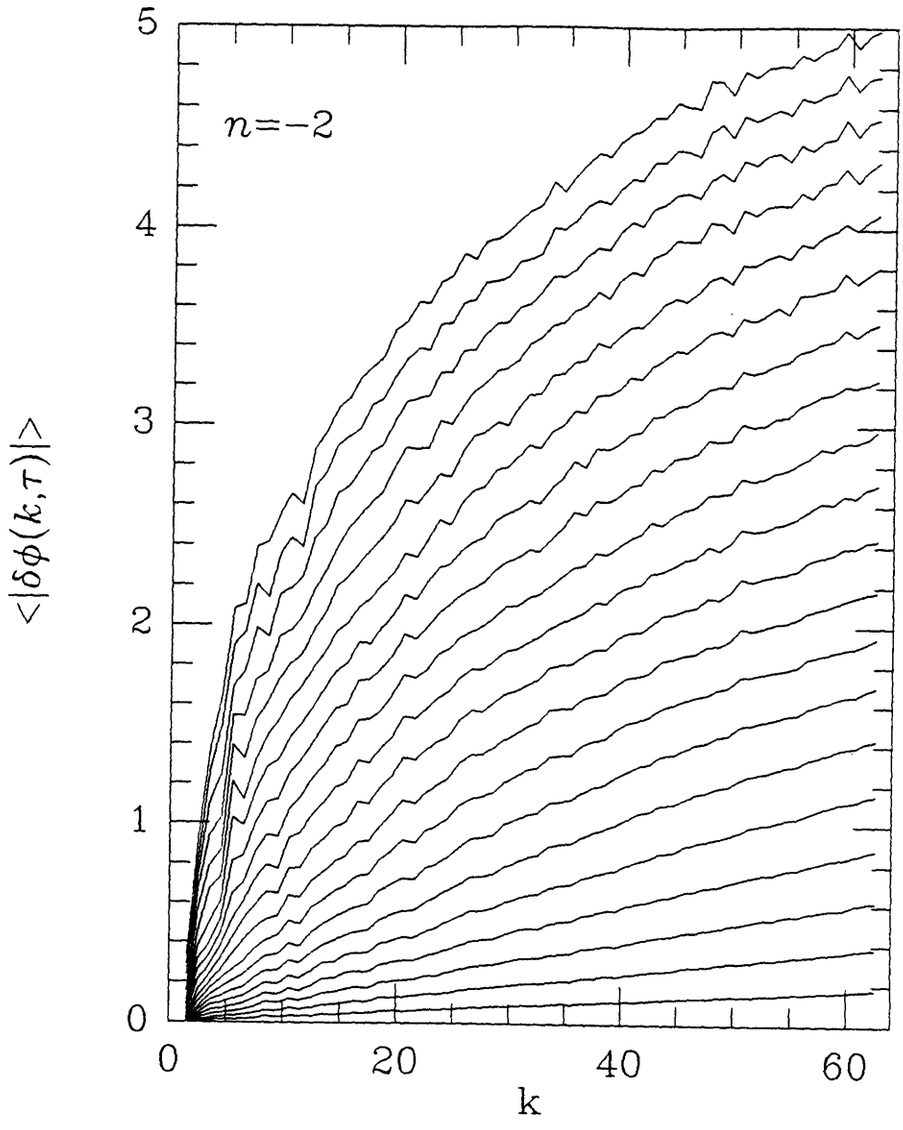

Figure 4-4 For $n = -2$, the mean magnitude of the phase deviation is plotted vs. k for 20 values of a. This is defined as $\langle|\delta\phi(\vec{k},a)|\rangle$, where $\delta\phi(\vec{k},a) = \phi(\vec{k},a) - \phi(\vec{k},a_i)$, with a_i being the initial value of a. The averaging is performed over all the modes in shells in k-space of width $\Delta k = 1$. This is the statistic used to study the scaling properties of the phase. The plots of characteristic scales, $k_c(a)$ vs. a in Figure 4-6 is obtained by setting $\langle|\delta\phi(\vec{k},a)|\rangle = \phi_c$, where ϕ_c is a constant. Hence they are obtained by reading off the values of k and a at which a horizontal line drawn at the chosen value of the ϕ_c intersects these curves.

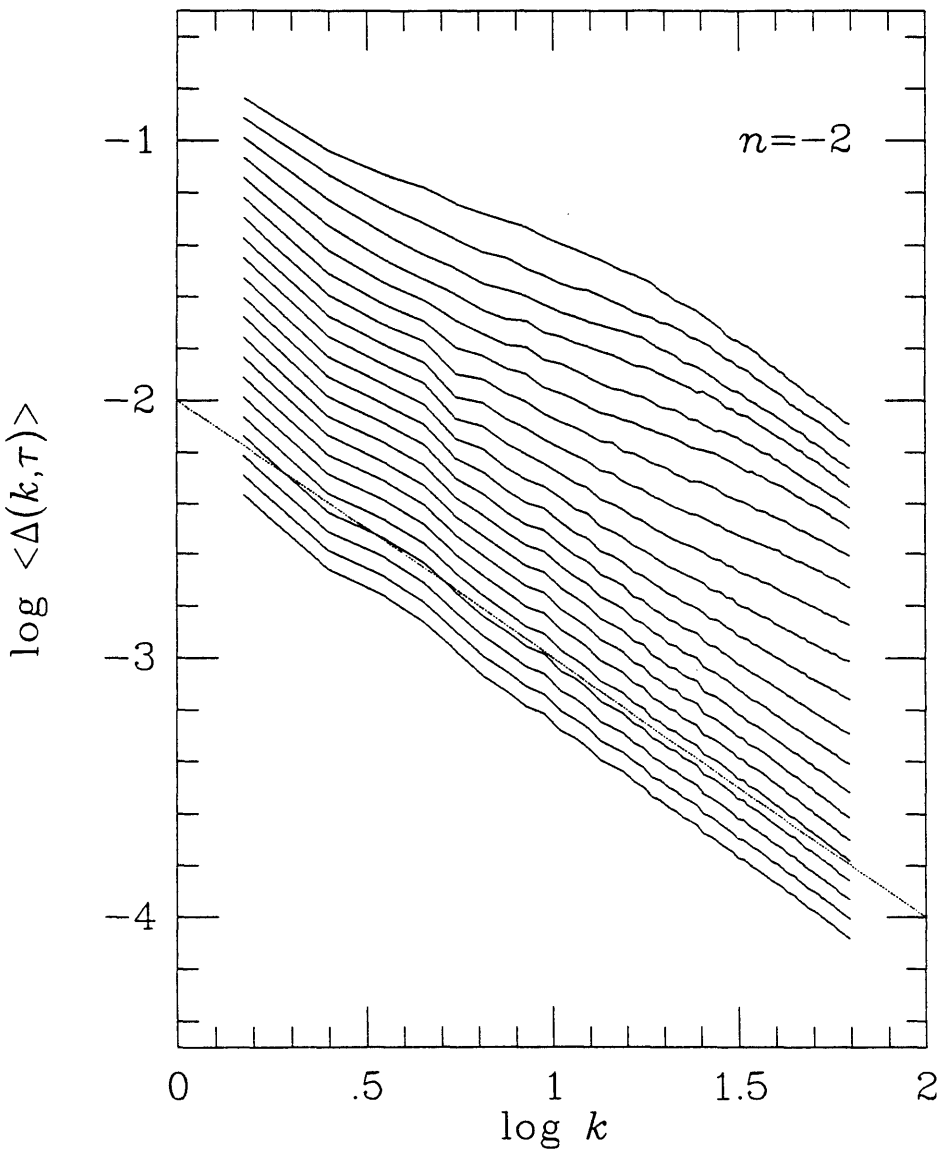

Figure 4-5 For $n = -2$, the mean amplitude $\langle\Delta(\vec{k}, a)\rangle$ is plotted vs. k, as in Figure 4-4 for the phase. The dotted line has a slope of -1 as expected in linear theory for $\langle\Delta(k)\rangle$.

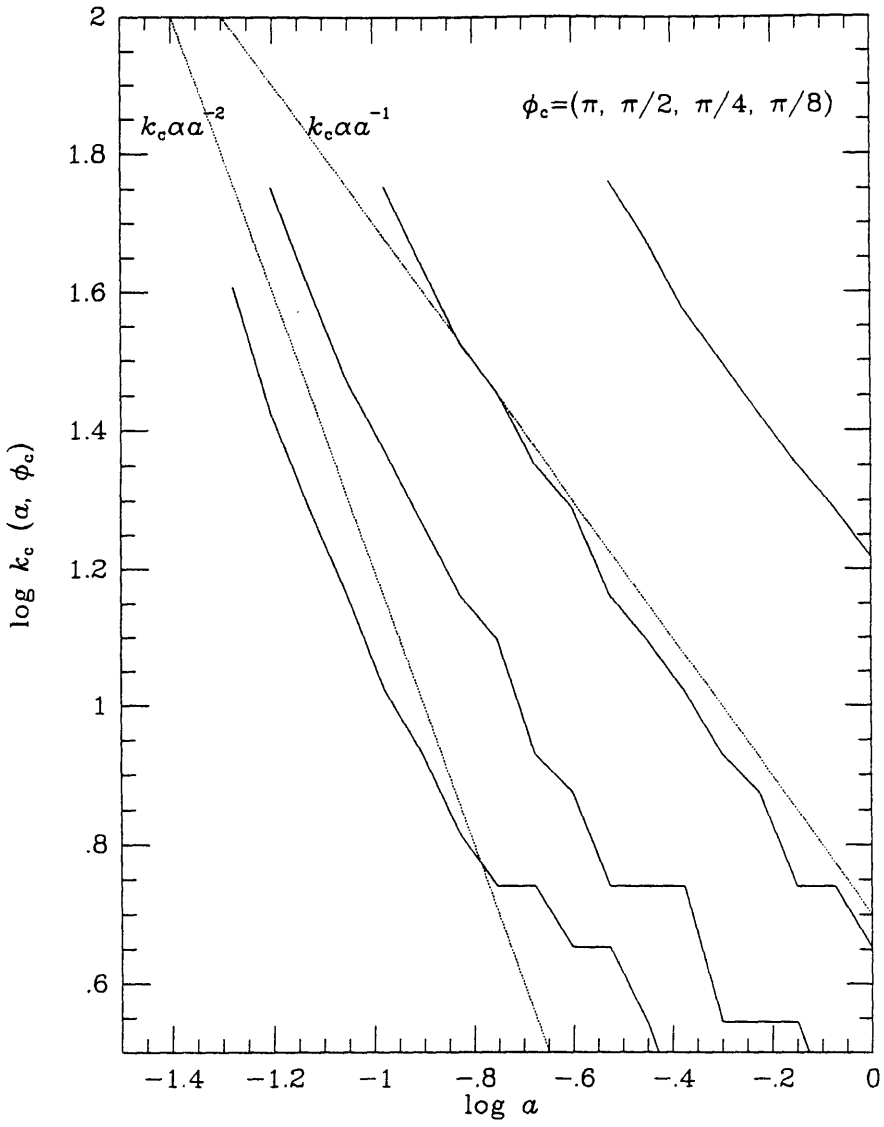

Figure 4-6 For the $n = -2$ spectrum, the scaling of characteristic wavenumber scales, k_c vs. a is shown, as derived from the mean phase deviation. As described earlier in Figure 4-4, $k_c(a, \phi_c)$ is the value of k and a at which $\langle|\delta\phi(\vec{k}, a)|\rangle = \phi_c$. The four solid curves correspond (from top to bottom) to the values of ϕ_c labelled at the top of the plot. Note that for high values of ϕ_c (the top 2 curves), the scaling closely agrees with that derived from equation (4.35): $k_c \propto a^{-1}$, which is shown by the upper dotted line. A transition towards the standard self-similar scaling $k_c \propto a^{-2}$, shown by the lower dotted line, occurs for the 2 lower values of ϕ_c.

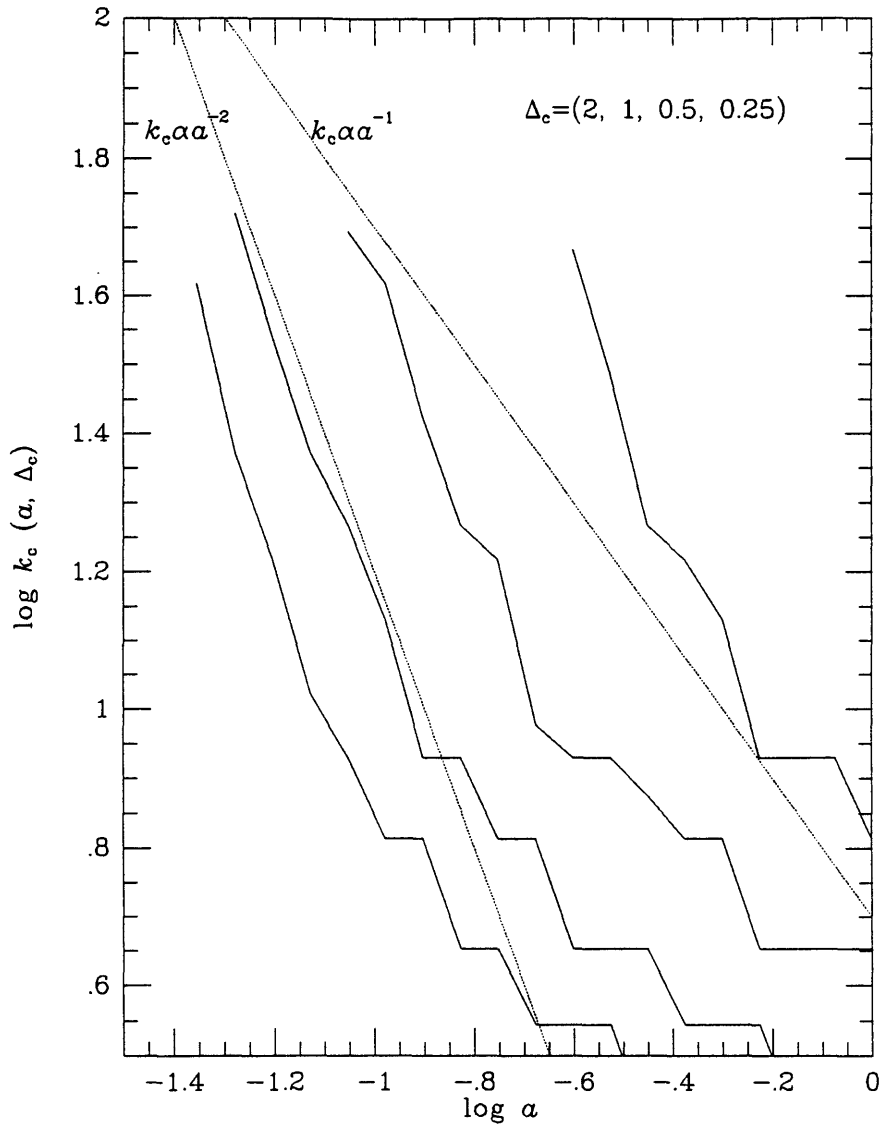

Figure 4-7 For the $n = -2$ spectrum, the scaling of characteristic wavenumber scales derived from the departure of the amplitude from linear growth, $k_c(a, \Delta_c)$ vs. a is shown for 4 different values of Δ_c (see equation (4.52) for the definition of $k_c(a, \Delta_c)$). All the curves have a slope close to the standard self-similar scaling, $k_c \propto a^{-2}$ at high k. For k below about 10 the slope becomes shallower, probably due to the limitation of a finite box.

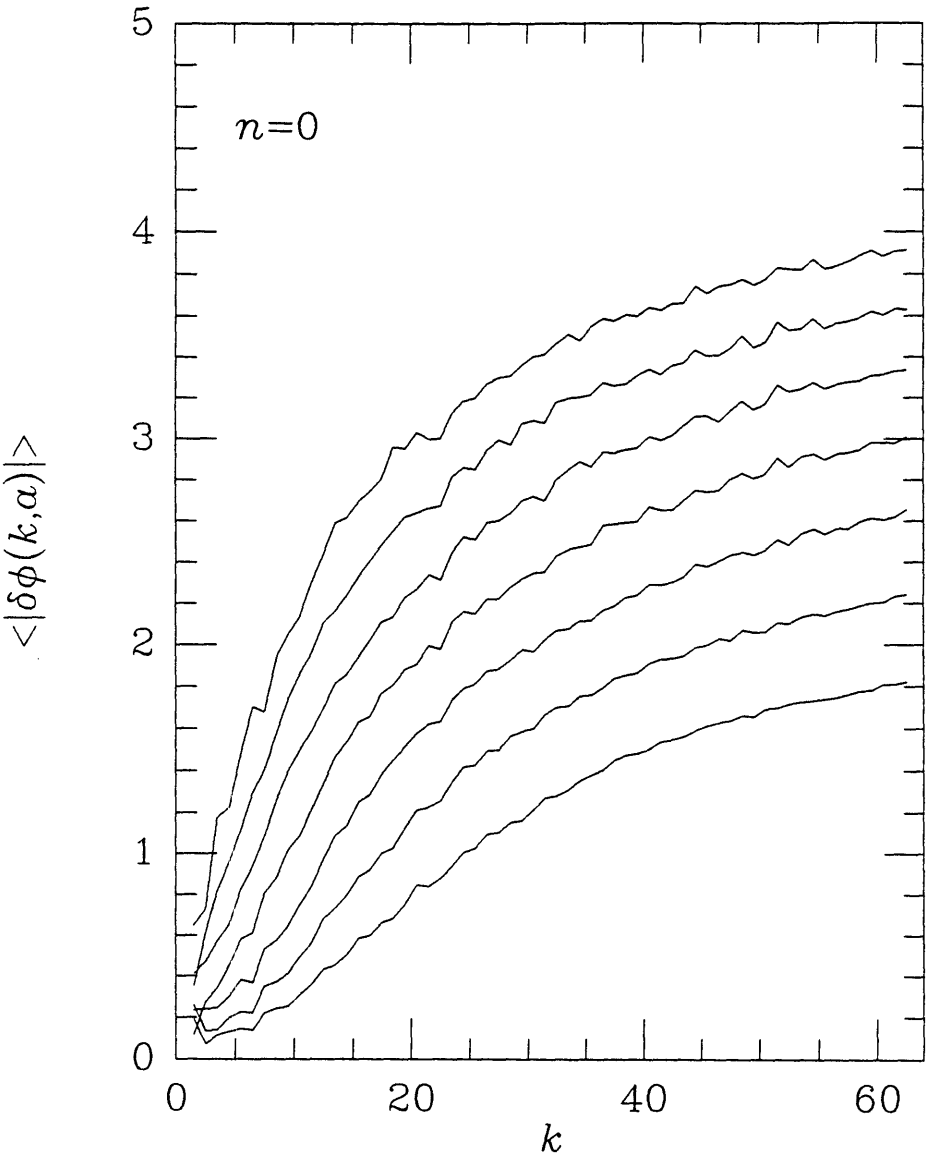

Figure 4-8 Mean phase deviation for $n = 0$: this is the counterpart of Figure 4-4 for $n = 0$.

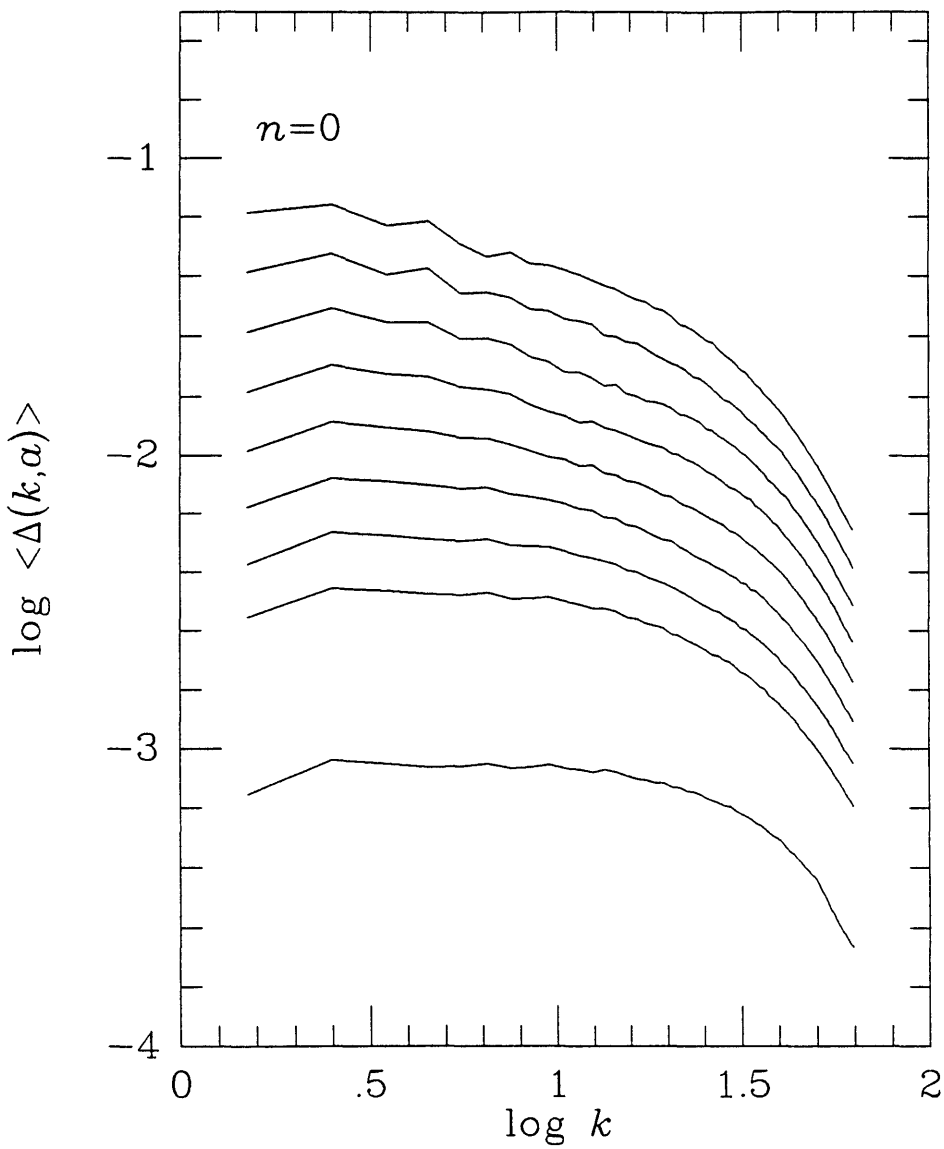

Figure 4-9 Mean amplitude for $n = 0$: this is the counterpart of Figure 4-5 for $n = 0$.

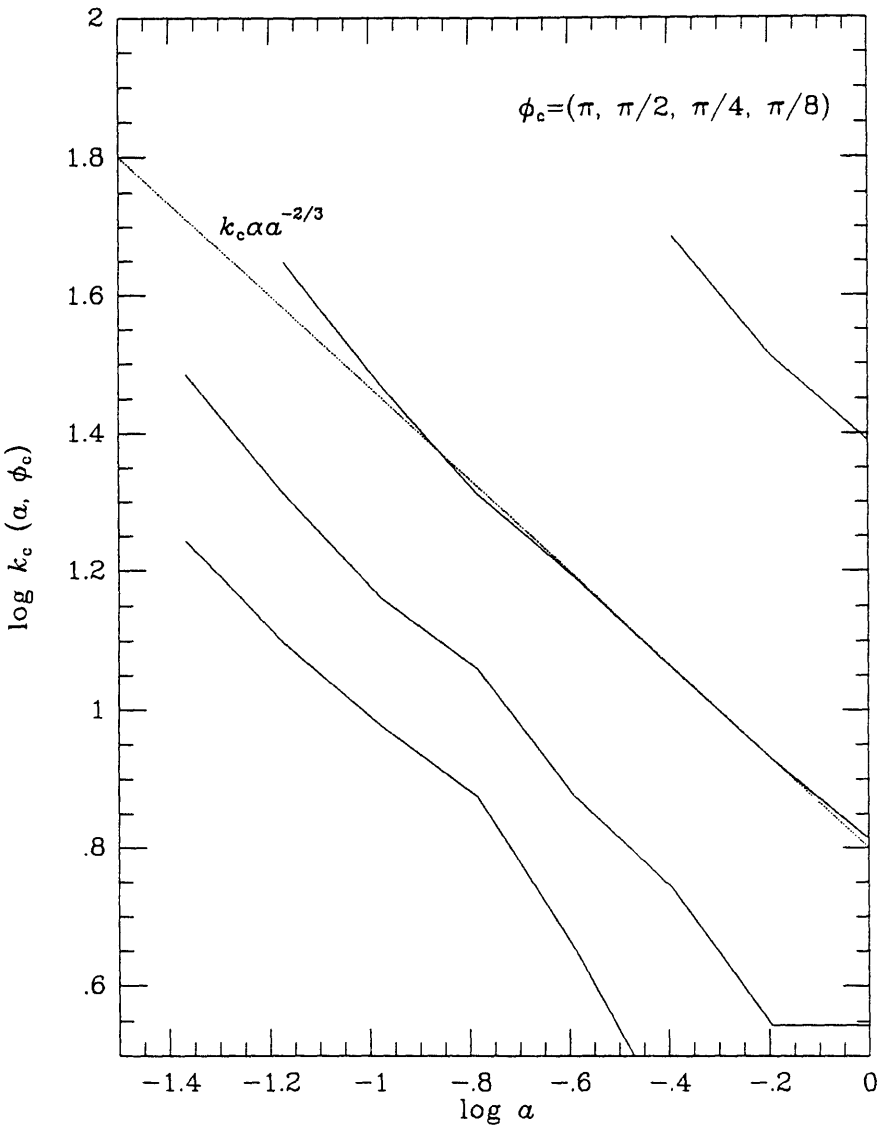

Figure 4-10 For $n = 0$ the scaling k_c vs. a is shown using the mean phase deviation. Notice that in contrast to the $n = -2$ case, here only one behavior for all values of ϕ_c is evident: the self-similar scaling $k_c \propto a^{-2/3}$.

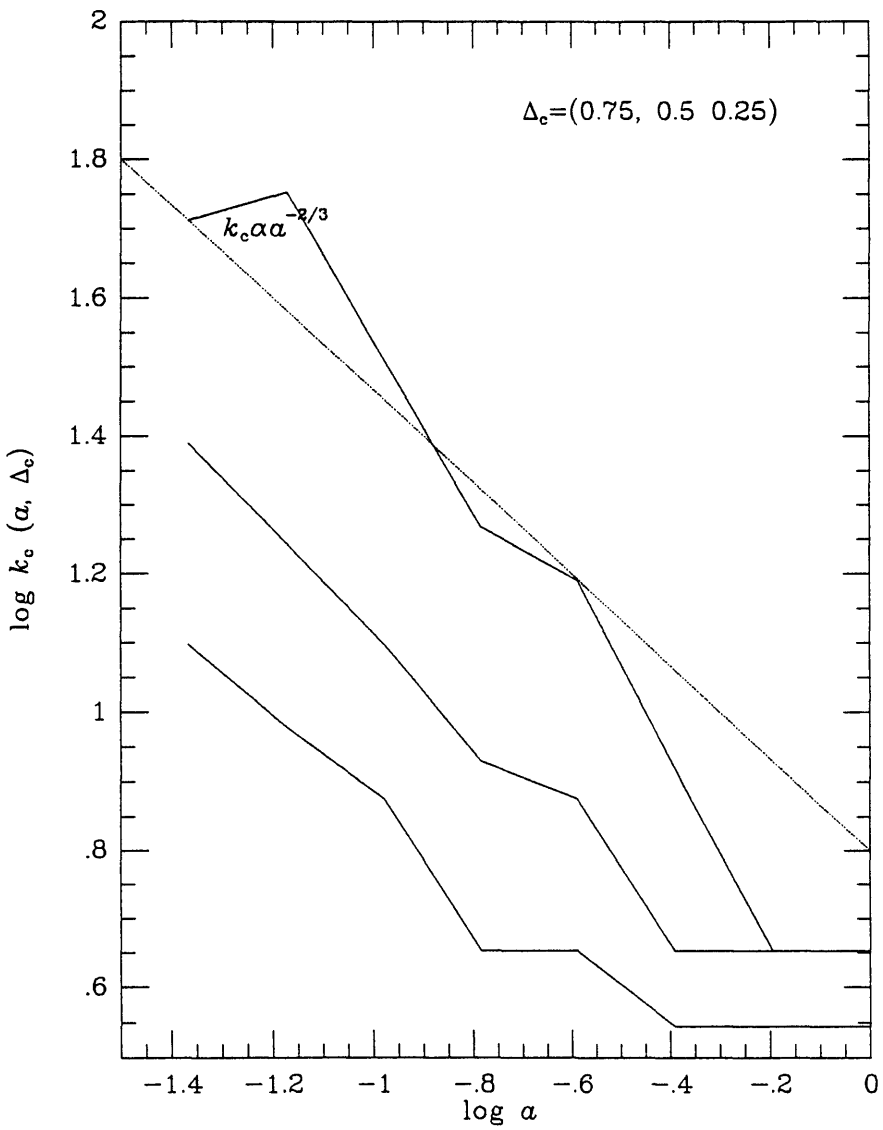

Figure 4-11 For $n = 0$ the scaling k_c vs. a is shown using the mean amplitude. Again, as in Figure 4-10, the standard self-similar scaling is recovered.

3636-9